DIAGNOZA - GENEZA - PROGNOZA => PODSTAWA KAŻDEJ DECYZJI

POLSKIE TOWARZYSTWO DIAGNOSTYKI TECHNICZNEJ
PTDT

afiliowane przy

Wydziale Nauk
Technicznych
Polskiej Akademii Nauk

Diagnostyka

ISSN 1641-6414

Nr 1(53) / 2010

WYDAWCA:
Polskie Towarzystwo Diagnostyki Technicznej
02-981 Warszawa
ul. Augustówka 5

REDAKTOR NACZELNY:
prof. dr hab. inż. **Ryszard MICHALSKI**

SEKRETARZ REDAKCJI:
dr inż. **Sławomir WIERZBICKI**

CZŁONKOWIE KOMITETU REDAKCYJNEGO:
dr inż. **Krzysztof LIGIER**
dr inż. **Paweł MIKOŁAJCZAK**

ADRES REDAKCJI:
Redakcja Diagnostyki
Katedra Budowy, Eksploatacji Pojazdów i Maszyn
UWM w Olsztynie
ul. Oczapowskiego 11
10-736 Olsztyn, Poland
tel.: 089-523-48-11, fax: 089-523-34-63
www.diagnostyka.net.pl
e-mail: redakcja@diagnostyka.net.pl

KONTO PTDT:
Bank PEKAO SA O/Warszawa
nr konta: 33 1240 5963 1111 0000 4796 8376

NAKŁAD: **500 egzemplarzy**

Wydanie dofinansowane przez Ministra Nauki i Szkolnictwa Wyższego

Spis treści / Contents

DOUBLE SINGULAR VALUE DECOMPOSITION (SVD) OF SYMPTOM OBSERVATION MATRIX IN MACHINE CONDITION MONITORING

Czesław CEMPEL

Poznań University of Technology, e-mail: czeslaw.cempel@put.poznan.pl

Summary

Application of SVD to fault extraction from the machine symptom observation matrix (SOM) seems to be validated enough by means of data taken from real diagnostic cases. But sometimes the number of observations, i.e. rank of the SOM is low, what may influence obtained results and subsequent diagnostic decision. This was the reason to look for additional improvement by the second application of SVD to generalized fault matrix obtained by the first SVD. The result is strange, no accuracy increase flows from the application of the second SVD, independently of the SOM rank. This needs further deliberations and rethinking.

Keywords: multidimensionality, symptom observation matrix, singular value decomposition.

ZASTOSOWANIE PODWÓJNEGO ROZKŁADU WARTOŚCI SZCZEGÓLNYCH (SVD) DO SYMPTOMOWEJ MACIERZY OBSERWACJI W DIAGNOSTYCE MASZYN

Korzyści zastosowania SVD w wielowymiarowej diagnostyce maszyn są potwierdzone przez wielu autorów. Jednak dla małej ilości obserwacji, kiedy rząd symptomowej macierzy obserwacji jest niski, wyniki mogą wydawać się nieprecyzyjne, co może wpływać na wynikowa decyzje diagnostyczną. Zatem zastosowano podwójny rozkład SVD w skrajnych przypadkach wziętych z praktyki diagnostycznej, kilkunastu i kilkuset obserwacji. Otrzymany rezultat zaprzecza początkowej supozycji, dodatkowe zastosowanie SVD nie daje żadnego wzrostu dokładności obliczeń uogólnionych symptomów. Przy okazji tych badań podwójnego SVD łatwo było skonstruować nowy uogólniony symptom wskazujący na występowanie dwu liczących się uszkodzeń w obserwowanym obiekcie, co może być istotne w sytuacjach nadzory złożonych obiektów.

Słowa kluczowe: wielowymiarowość, macierz symptomowej obserwacji, rozkład wartości szczególnych.

1. INTRODUCTION

The idea of symptom observation matrix (SOM) in multidimensional condition monitoring of machines is well established and brings several advantages, [Cempel et al 07]. Usually it is $p>r$ rectangular matrix with (r) symptoms S_r measured along the system life θ (p *readings*) placed in separate columns. It allows placing all physically different symptoms[1] measured in a phenomenal field of the machine in a one SOM, and to process them in order to obtain projection of **observation space** to the **fault space** of machine. Of course we usually observe more symptoms (*columns of SOM*), than there is expected number of faults in a machine.

The preprocessing of SOM may be different, but for condition monitoring it was found that normalization and extraction of symptom initial value is the best solution, bringing all symptoms to their dimensionless form. Then, the application of SVD to the dimensionless form of SOM gives needed projection of observation space to the fault space. The resultant matrices of SVD decomposition allow calculating two important matrices. The first is ***SD*** matrix, which give us generalized fault symptoms $\boldsymbol{SD_i}$ of machine, and in theory they are independent each other. From this matrix we can calculate so called total damage (*generalized*) symptom, as the sum of all $\boldsymbol{SD_i}$ generalized fault symptoms. This is mainly in order to calculate the symptom limit value $\boldsymbol{S_l}$ or to make the forecast of the total damage symptom. The second ***AL*** matrix allows us to assess the contribution of primary measured symptoms to a newly formed generalized fault symptoms. In this way we can just say which of primary symptom is redundant, as it does not give substantial information contribution, and as such can be rejected from further calculations and/or future measurements.

But the column orthogonality of SD matrix is assured for sufficient size of SOM matrix; in reality the matrix of correlation coefficient of SD matrix gives sometimes quite big off-diagonal elements, some of order 0.5 and higher. So, may be some improvements in our diagnostic reasoning is possible by the application of another orthogonal decomposition to SD matrix? In reality there is no

[1] Symptom, measurable quantity covariable (*or assumed to be*) with the system condition

big choice of decomposition method; principal components analysis (PCA), which uses SVD as it can be shown [Golub et al 96], and both are well diagnostically interpretable [Tumer et al 02], [Jasinski 04], [Korbicz 04]. The well known QR decomposition seems to be not usable in diagnostics. According to unpublished study of present author, only the main diagonal of the upper triangular matrix ***R*** of this decomposition can be compared to the first generalized symptom ***SD*$_1$**, the higher upper diagonals are shortened and do not carry readable diagnostic information.

In principle, it is possible the second application of PCA to ***SD*** matrix, but as it is known eigen values of decomposition will be the squares of singular values of SVD, and singular vectors are equal to principal components. So there is no other solution like to apply SVD again, but for matrix ***SD*** only, not to ***AL*** matrix. This will transfer only part of SOM information content, but we will see the result. Such is the main idea of this paper, and as it is hope, it brings some advantages in condition assessment. It seems to, that the effect of this additional decomposition maybe data dependent and its real usability can be jugged for the given population of diagnosed objects.

2. OPTIMIZATION OF MULTI SYMPTOM MACHINE OBSERVATION

It was assumed earlier, our information about machine condition evolution is contained in p x r **SOM**, where in r columns and p rows of the successive readings of each symptom are presented. Usually they are made at equidistant system life time moments θ_n, $n=1,2,...p$. In pre-processing operation the columns of SOM are centred and normalized to the three point average of three initial readings of every symptom. This is in order to make the SOM dimensionless, and to diminish starting disturbances of symptoms. This allows also to present the evolution range of every symptom from zero up to few times of the initial symptom value S_{0r}, (*measured in the vicinity of* $\theta = 0$).

After such preprocessing we obtain the dimensionless **SOM** in the form;

$$\mathbf{SOM} = \mathbf{O}_{pr} = \left[S'_{nm}\right], \quad S'_{nm} = \frac{S_{nm}}{S_{0m}} - 1, \tag{1}$$

Now we can apply the Singular Value Decomposition (SVD) [Golub 96], [Will 05], [Kielbasiński et al 92] to our dimensionless SOM (1), to obtain singular components (*vectors*) and singular values (*numbers*) of SOM, in the form

$$\mathbf{O}_{pr} = \mathbf{U}_{pp} \cdot \mathbf{\Sigma}_{pr} \cdot \mathbf{V}_{rr}^{\ T}, \ (T - matrix\ transposition), \tag{2}$$

where; U_{pp} is p dimensional orthonormal matrix of left hand side singular vectors, V_{rr} is r dimensional orthonormal matrix of right hand side singular vectors, and the diagonal matrix of singular values $\boldsymbol{\Sigma}_{pr}$ is defined as below

$$\mathbf{\Sigma}_{pr} = diag\left(\sigma_{1,\ldots,}\sigma_{l}\right), \quad whit\ \ nonzero\ \ s.v.: \qquad \sigma_1 > \sigma_2 > \ldots > \sigma_u > 0, \tag{3}$$
$$and\ zero\ s.\ v.\ ;\ \sigma_{u+1} = \ldots\ \sigma_l = 0; \quad l = max\ (p,\ r), \quad u \le min\ (p,\ r), \quad u < r < p.$$

Going back to SVD itself it is worthwhile to say, that every non square matrix has such decomposition, and it may be interpreted also as the product of three matrices [Will 05], namely

$$\boldsymbol{O}_{pr} = (\boldsymbol{Hanger}) \times (\boldsymbol{Stretcher}) \times (\boldsymbol{Aligner}^T) \tag{4}$$

This is a very metaphorical description of SVD transformation, but it seems to be an useful analogy for the inference and decision making in condition monitoring. The diagnostic interpretation of formulae (4) can be obtained very easily. Namely, using its left hand side part, we are stretching our **SOM** over the life (*observations*) dimension, obtaining the matrix of **generalized symptoms *SD*** as the columns of the matrix . And using its right hand side part of (4) we are stretching **SOM** over the observed (*primary*) symptoms dimension, obtaining the assessment of contribution of every primary symptoms in the form of matrix ***AL***, assessing in this way the contribution of each primary symptom to the generalized fault symptom $\boldsymbol{SD}_i$,$i=1,...u$.

$$\boldsymbol{SD} = \boldsymbol{O}_{pr} \cdot \boldsymbol{V}_{rr} = \boldsymbol{U}_{pp} \cdot \boldsymbol{\Sigma}_{rr}\ ;$$
$$and; \quad \boldsymbol{AL} = \boldsymbol{U}^T_{pp} \cdot \boldsymbol{O}_{pr} = \boldsymbol{\Sigma}_{rr} \cdot \boldsymbol{V}^T_{rr} \tag{5}$$

We will calculate the above matrices and use them for better interpretation of monitoring results (***SD***) and optimization of the dimension of the observation space (***AL***).

As the rows of **SOM** matrix were formed along the machine lifetime, so the columns of **SD** matrix

have the discrete argument of life time θ, and we can write fault space interpretation as below;

$$\boldsymbol{SD}_t(\theta) \propto \boldsymbol{F}_t(\theta), \quad t=1,2,\ldots,$$

$$Norm\ (\boldsymbol{SD}_t) \equiv //\boldsymbol{SD}_t// = \sigma_t, \ t = 1, \ldots, u \tag{6}$$

And for the total damage generalized symptom

$$\mathbf{SumSD}_i(\theta) = \sum_{i=1}^{z} \mathbf{SD}_i(\theta) = \sum_{i=1}^{z} \sigma_i(\theta) \cdot \mathbf{u}_i(\theta) \propto \mathbf{F}(\theta), \tag{7}$$

where; $\mathbf{u}_i$ is a column of $\boldsymbol{U}_{pp}$.

This concept of diagnostic inference, for individual fault $\boldsymbol{F}_t$ (6), and total fault damage $\boldsymbol{F}$ (7) has been proved in several papers [Cempel 04], [Cempel at al 07], and we will use it in further consideration.

The above results, based on generalized fault symptoms, have been obtained only from the first matrix SD in (5). And the second matrix AL gives us the relative measure of information contribution to each generalized symptom given by particular primary symptom measured during the SOM gathering. This is one way of assessment of the primary symptom redundancy, but we need some other global indicators of rejection of the redundant symptom. In our previous papers we have used modified Frobenius norm of SOM and the generalized volume of the fault space created by SOM. What is important here, these two measures are based on singular values of SOM, which in turn can be treated as the fault advancement measures (*see (6)*).

$$Frob1 = \Sigma \sigma_i; \tag{8}$$
$$and; \quad Vol1 = \Pi \sigma_i, \qquad i = 1, \ldots u.$$

Looking above for the value creation method, one can say that if some primary symptom will be really redundant its rejection should change *Frob1* measure only a little (*small* σ_I), and should much increase the fault space volume *Vol1*. We will notice how it behaves with real examples of symptom rejection in diagnosed machines.

3. TOTAL DAMAGE SYMPTOM AND DOMINATING SYMPTOM OF MACHINE, EXAMPLE

As a first example of application of our idea we will take a hard diagnostic case - a huge fan for coal milling from one of Polish thermo power station. Here the root mean square vibration velocity (V_{rms}) has been used as a symptom of condition, and initially altogether 11 symptoms at different places of fan mill aggregate structure were constantly monitored over 60 weeks lifetime θ. How unstable and noisy the fan running environment is, one can notice from the left top picture of the fig.1. It is seen further (*middle left picture*), that the symptom normalization and addition of life time symptom θ (*straight line*) do not change much the noisy behaviour of primary and generalized symptoms (*bottom left picture*).

Looking at the middle right picture of Fig.1, where matrix ***AL*** is presented, one can notice that symptoms No 7,8,9,10,11 do not give substantial contribution to the three dominating generalized symptoms, and probably can be rejected as redundant at the first approach. With this respect please note the value of Frobenius modified measure *Frob1* and the volume *Vol1* of the fault space at upper right picture. One can also note here, that there are two generalized symptoms with high information contents, and due to that two symptom limit values are assessed: S_{lc} for the total damage symptom, and S_{l1} for the first generalized symptom (*bottom pictures).*

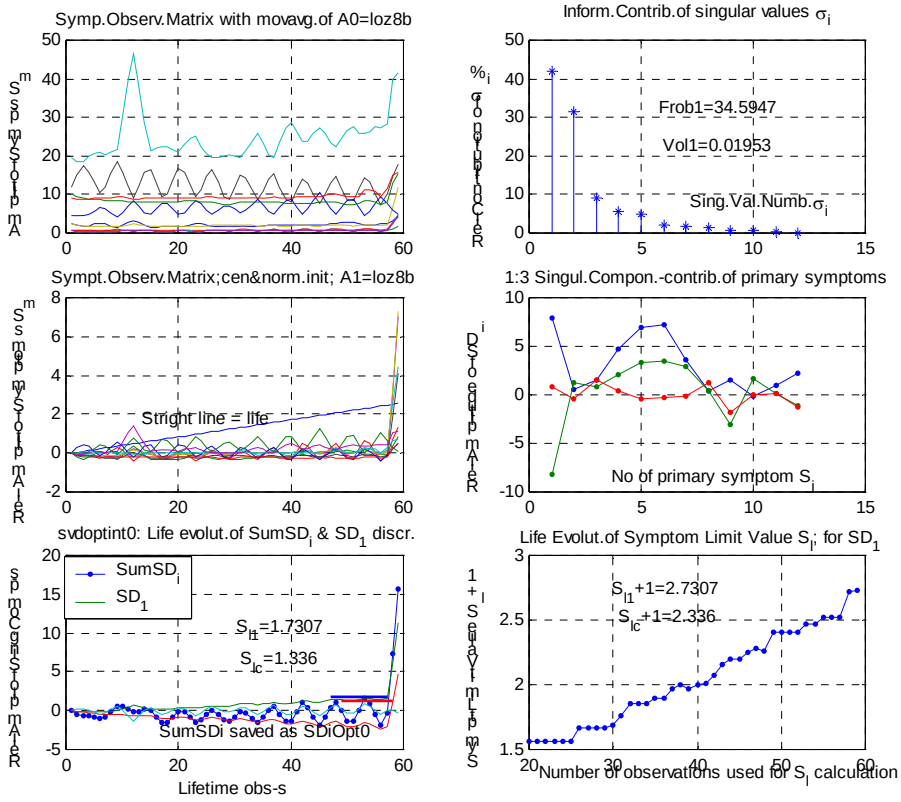

Fig. 1. Vibration condition monitoring (V_{rms}) of the coal mill fan observed at three bearings of fan and electric motor

Concerning symptom redundancy, let us look further at the Fig. 2 presenting the primary symptoms contributions measured in terms of correlation to SOM matrix, and to the total damage symptom ***SumSD**i*. Here one can come to similar conclusion for symptoms No 7, 8, 9, 10, 11 in particular. This is true with respect to the total damage symptom ***SumSD**i* at the bottom picture and also partially to the overall information resource at the upper picture.

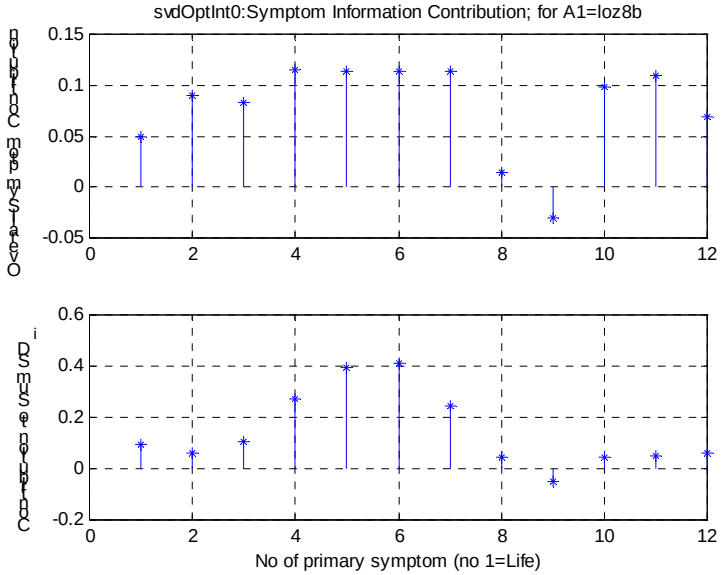

Fig. 2. Primary symptom contribution to the overall information resource and to the total damage symptom **SumSD**i, for the fan coal mill aggregate (fig.1)

Following these guidelines of Fig. 2 five symptoms have been rejected from the primary number of eleven, and the result of new SOM decomposition is seen on the Fig. 3. As can be seen from the picture top left the most of troublesome un-diagnostic symptom was rejected. Due to this one can say we have new SOM with little increase of Frobenius modified measure, and dramatic increase of the fault space volume. Comparing pictures bottom left of Fig. 1 and Fig. 3 one can notice that most of generalized symptoms oscillation has been reduces, but they are still present there. Also it is worthwhile to notice the decrease of singular values contribution in a new SOM. There are still two dominating faults but amount of information they carry is increased now.

This is the result of SOM optimization by means of symptom rejection described already in some papers [Cempel 09]. Having done this one can now proceed to condition forecast, by means of neural nets [Tabaszewski 06] or by grey system theory [Cempel et al 07]. But we are interested now in some improvements of generalised fault symptoms, possible by new SVD processing, what will be done in a next point.

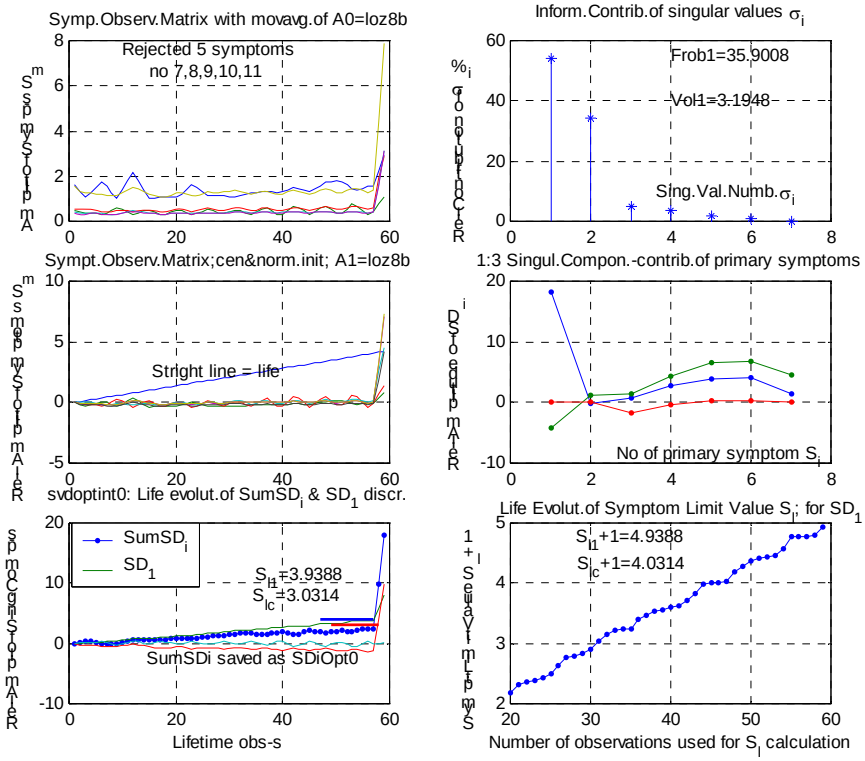

Fig. 3. Coal mill fan as on Fig.1 with five redundant symptoms rejected

4. THE SECOND DECOMPOSITION OF GENERALIZED SYMPTOM MATRIX SD

As it was said in the introduction the generalized symptoms theoretically have to be orthogonal, but usually it is not exactly true, depending on the type of SOM matrix. Hence let us recall partly the relation (5) creating the generalized symptom matrix SD

$$\boldsymbol{SD} = \boldsymbol{O}_{pr} \cdot \boldsymbol{V}_{rr} = \boldsymbol{U}_{pp} \cdot \boldsymbol{\Sigma}_{rr} .$$

As one can see this is rectangular $\boldsymbol{p} \bullet \boldsymbol{r}$ matrix, but as relation (3) indicates only $\boldsymbol{u} < \boldsymbol{r}$ of singular values are different from zero, hence we should correct above to

$$\boldsymbol{SD} = \boldsymbol{O}_{pr} \cdot \boldsymbol{V}_{uu} = \boldsymbol{U}_{pp} \cdot \boldsymbol{\Sigma}_{uu} . \qquad (9)$$

Applying now SVD again to the above, analogously to (2) we will have

$$\boldsymbol{SD} = \boldsymbol{U1}_{pp} * \boldsymbol{\Sigma 1}_{pu} * \boldsymbol{V1}^{\boldsymbol{T}}_{uu} . \qquad (10)$$

And from the last decomposition we should pass to the new generalised fault symptom matrix in the same way as in (5), let's name it ***SD1***, as below;

$$\boldsymbol{SD1} = \boldsymbol{SD} * \boldsymbol{V1}_{uu} = \boldsymbol{U1}_{pp} * \cdot \boldsymbol{\Sigma 1}_{uu} . \qquad (11)$$

It seems to, that after such double decomposition, the new generalized fault symptoms $\boldsymbol{SD1}_i$ will be much more orthogonal, this means having less disturbances in the course of system life $\boldsymbol{\theta}$.

Let us turn our attention again to Fig. 3, picture top right. As we can notice from here it seems to be two faults in our machine; with relative strength close to 60% for the first and close to 40% for the second fault. It would be interesting if the double SVD confirm the presence o two faults and repeat their internal relation. Also for the inference

process it would be helpful to create some new measure, or symptom, which confirms the presence of the second fault in a machine. This new symptom of the second fault ***(SF***) can be simply the normalized product of the two first dominating symptoms as below;

$$SF = SD_1 * SD_2 * (|SD_1|)^{-1/2}, \qquad (12)$$

where normalization is acting only with respect of first dominating symptom SD_1 .

Such calculation as sketched above has been appended to the program **svdOptInt0.m** and the result one can see and analyze looking at the Fig.4 below.

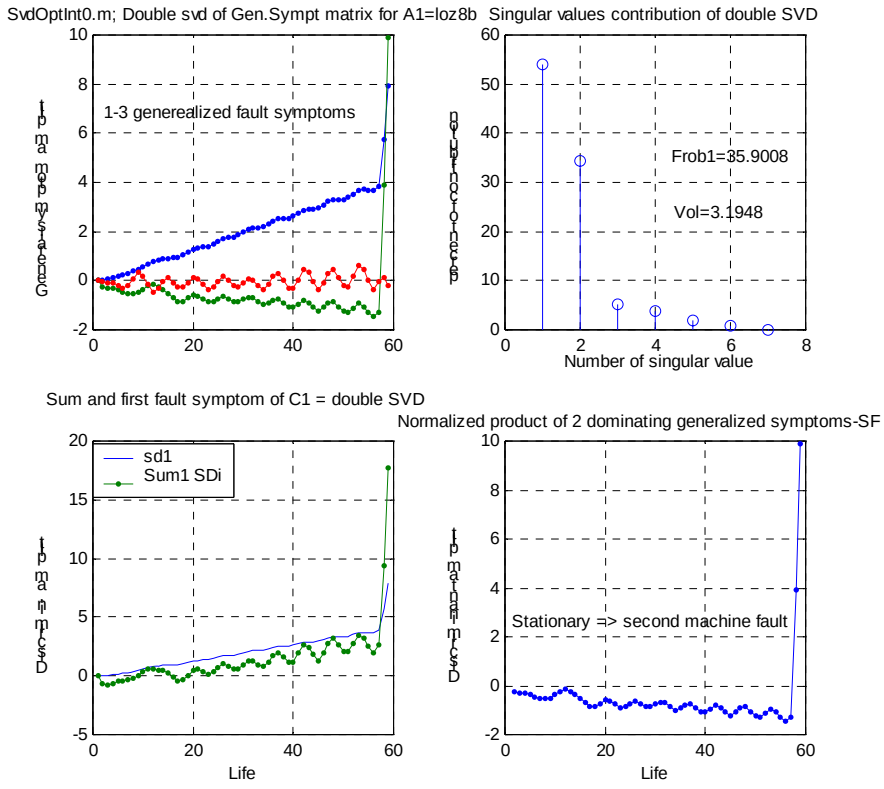

Fig. 4. The second SVD of generalized fault symptom matrix SD, and the new symptom of second fault presence, for the data of Fig.3 of a fan mill

Fig. 4 and Fig. 3 (*bottom left and top right*) we can notice their identity with the respect of shape of the curves, their values, as well as the values of Frobenius measure and Volume of the generalized fault space. This identity is shocking result. Moreover, if we calculate correlation coefficient matrix for generalized fault matrices SD and SD1 after second SVD, their results are also identical, even with respect of values of the off-diagonal elements.

What does it mean? We know that SD matrix, created according relation (5), does not carry all the information of primary SOM. The same is with SD1 matrix according to relation (10) and (11). Until now, this fact can not be interpreted correctly using author's understanding only.

But not all information contained in a Fig. 4 brings us to confusion. Looking for the picture bottom and top right, we can notice that in this case we have independent confirmation of second fault existence in our machine. So, the calculation of product of first two generalized faults (12) gives us independent confirmation of second fault existence or its not existence.

But may be this identity of results after second SVD application is data oriented? Let us take another example. This time it comes from ball bearings durability testing stand, where slowly pulsating load was applied additionally[2] and 19 symptoms has been measured initially. Fig. 5 present here optimized SOM of the ball bearing experiment, after rejection of 3 redundant symptoms, and Fig. 6 presents the results of second SVD application to the SD matrix.

And again comparing bottom left and top right pictures of Fig. 5, with the top pictures of Fig. 6 one can find their identity, the same as in previous case. So this is a rule of data processing, and identity is not data oriented. But there is a god news in Fig. 6,

[2] Author is obliged here to Dr M. Tabaszewski for providing the data.

it is confirmation of the existence of the second fault, emerging during the life testing of the bearing (*picture bottom right*). Of course there are some oscillations on the course of SF due to oscillation of bearing load, but the mean course of SF measure strictly indicate second fault presence and its evolution.

In previous examples we had rather big data base; sixty or one hundred sixty rows in SOM matrices (*readings*). Hence let us change the dimension of SOM to very short, of order of twenty symptom readings. This can be the case of railroad diesel engine condition monitoring[3], where at the top of one cylinder all vibrational quantities has been measured, each ten thousand kilometers of its mileage up to the breakdown. Figures 7 and 8 present this case in the same manner as it was done previously. Although Fig. 7 is already optimized with 3 symptoms rejected, one can see that last four singular values are very small, giving the small value of the volume of generalized fault space of order 10^{-7}. We have here situation where only one fault is developed, what is clearly seen from the pictures top right and bottom left. The rest of singular values and generalized symptoms as well, do not give substantial contribution to the total damage symptom ***Sum SD$_i$*** . And the same is seen from the Fig. 8 where the second SVD have been applied to the generalized fault symptom matrix ***SD***, picture left bottom of Fig. 7. As there is no second fault visible from the distribution of singular values (*top right pictures*), the second fault measure SF behaves quite strangely on the Fig. 8 bottom right showing us that there is no second fault. This confirms the relevance of the SF measure introduced here first time.

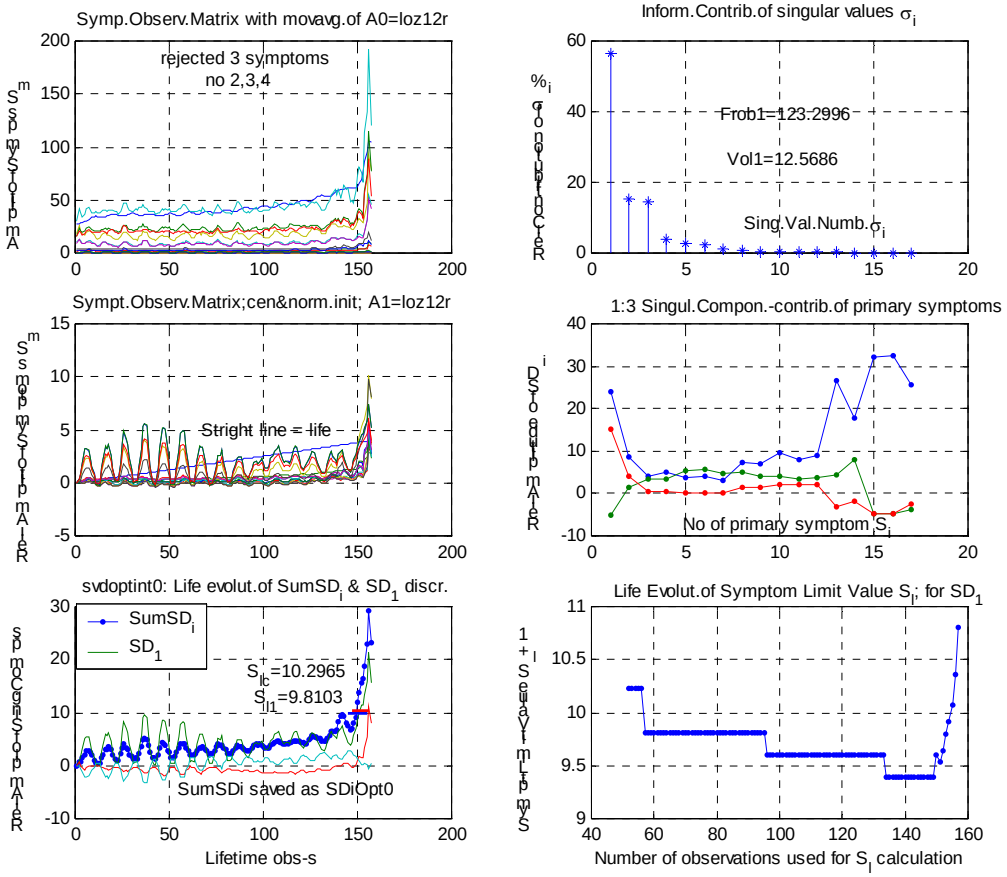

Fig. 5. Optimized SOM of ball bearing at the testing stand with slowly pulsating load

[3]This time author is obliged to Professor F. Tomaszewski for providing the data.

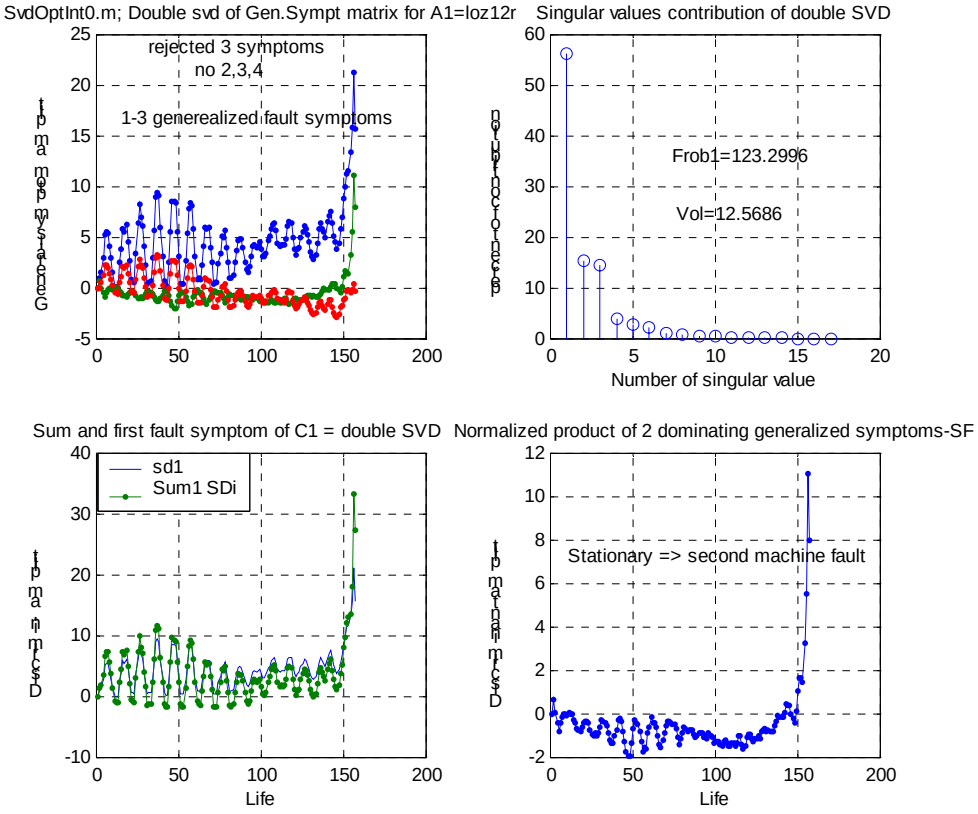

Fig. 6. Ball bearing data from the Fig5 after second SVD of generalized fault matrix SD

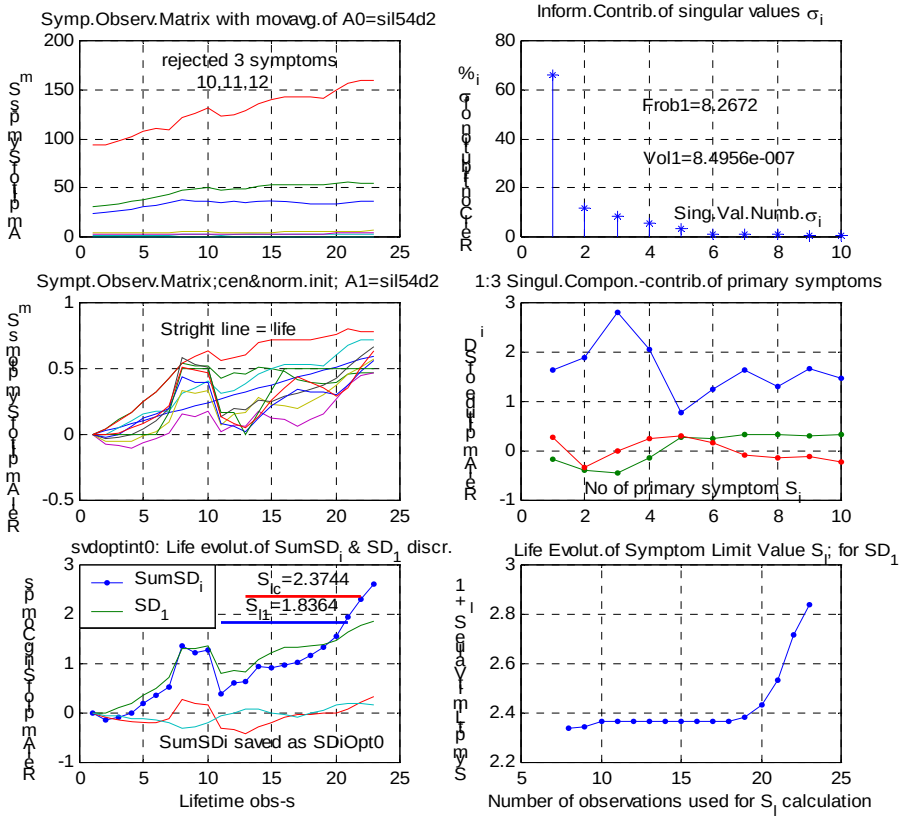

Fig. 7. Optimized SOM of railroad diesel engine diagnostically processed by SVD

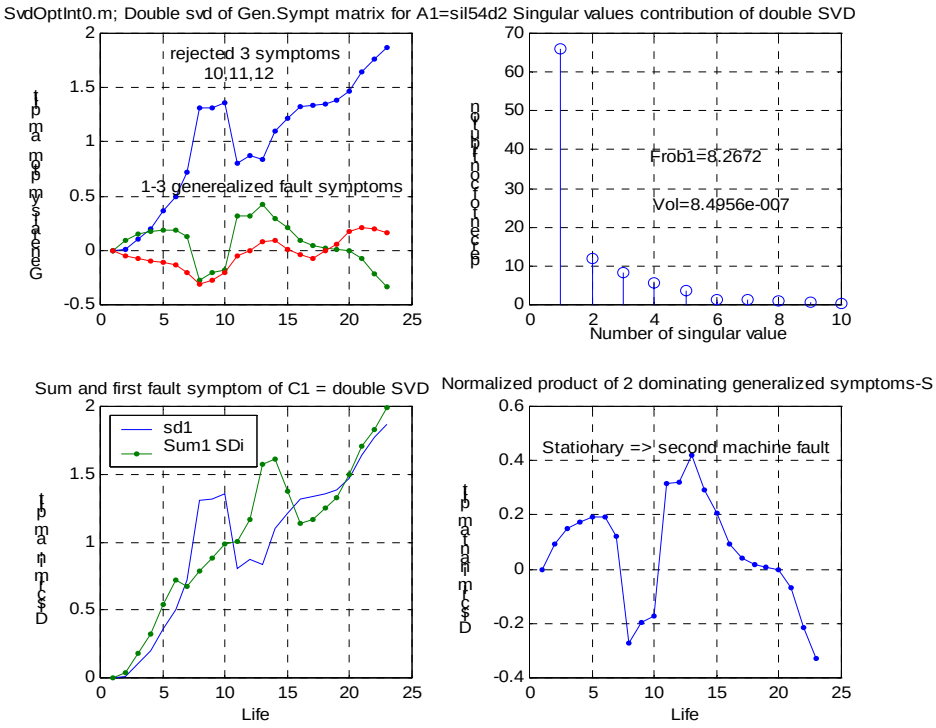

Fig. 8. Second SVD of railroad diesel generalized fault matrix, and respective SF measure life coarse

5. CONCLUSIONS

The premise for writing of this paper was unwritten assumption that singular value decomposition used in condition monitoring for fault information extraction may have some errors, in dependence of rank and the dimension of SOM of monitored object. This was amplified by the fact that correlation coefficient matrix of generalized fault symptom matrix SD has large off-diagonal elements. So, the second SVD of SD matrix of three diagnostic cases has been performed. The two of them with rather long observation history, (*60 and 160 rows of SOM as system observation*) and the last very short with 24 rows of SOM. In all three cases the results were the same, no increase in accuracy of calculation, the same singular vectors and singular values, independently of the matrix row dimension. This may be the proof of **validity of SVD use** as the method of fault information extraction, but it is not the proof of the goal of this paper.

Additionally, along this consideration some new diagnostic measure of second fault existence - SF has been introduced. In two first cases SF confirmed the existence of second fault presence, as really it was the case. This seems to be one of the concrete results of this paper

6. REFERENCES

1. Cempel C., (1999).: *Innovative developments in systems condition monitoring*, Keynote Lecture, Proceedings of DAMAS'99, Dublin, Key Engineering Materials, Vols. 167-168, Trans Tech. Publ., Switzerland, 1999, pp172-188.
2. Cempel C., Natke H. G., Yao J. P. T., (2000), *Symptom Reliability and Hazard for Systems Condition Monitoring,* Mechanical Systems and Signal Processing, Vol. 14, No 3, 2000, pp 495-505.
3. Cempel C., Tabaszewski M., (2005*), Multidimensional vibration condition monitoring of non-stationary systems in operation,* Proceedings of 12 International Congress on Sound and Vibration, (*on CD-paper No 496*), Lisbon, July 2005, (*full text in* Mechanical Systems and Signal Processing, 2007, 21 (3), pp. 1233-1241).
4. Korbicz J., et al, (*eds*.), (2004), *Fault Diagnosis – Models, Artificial Intelligence, Applications*, Springer Verlag, Berlin - Heidelberg, 2004, p828.
5. Tumer I. Y., Huff E. M., (2002), *Principal component analysis of tri-axial vibration data from helicopter transmission,* 56th Meeting of the Society of Machine Failure Prevention Technology, 2002.
6. Jasiński, M., (2004), *Empirical models in gearbox diagnostics* (in Polish), PhD Thesis, Warsaw University of Technology, Warsaw, December 2004.
7. Cempel C., (1991), *Vibroacoustic Condition Monitoring*, Ellis Horwood Press, New York, 1991, p212.

8. Cempel C.: *Simple condition forecasting techniques in vibroacoustical diagnostics*, Mechanical Systems and Signal Processing, 1987, pp 75 – 82.
9. Kielbasinski A., Schwetlik H.: *Numeric Linear Algebra*, WNT Press Warsaw, 1992, p502.
10. Golub G. H., VanLoan Ch. F.: *Matrix Computation*, III-rd edit, J Hopkins Univ. Press, Baltimore, 1996, p694.
11. Cempel C., Tabaszewski M.: *Multidimensional condition monitoring of the machines in non-stationary operation*, Mechanical Systems and Signal Processing, Vol. 21, 2007, pp 1233-1247.
12. Will T., (2005): *Hanger matrix, two-thirds theorem,* Internet: http://www.uwlax.edu/faculty/will/svd/svd/index.html , June 2005; (*see also: SVD ingredients,* Mathematica, *April 2004*).
13. Cempel C.: *Optimization of Symptom Observation Matrix in Vibration Condition Monitoring*, Proceeding of ICRMS09, Chengdu- China, July 2009, pp 944-960.
14. Tabaszewski M.: *Forecasting of residual life of the fan mill by means of neural nets* (in Polish), Diagnostyka, vol. 3, (39), 2006, pp 149-156.
15. Cempel C., Tabaszewski M.: *Application of grey system theory in multidimensional machine condition monitoring* (in Polish), Diagnostyka, No 2, (47) 2007, pp11-18.

MODERN TECHNOLOGY REVOLUTION FOR SECURITY

Pavel NECAS, Miroslav KELEMEN

The Armed Forces Academy of General Milan Rastislav Štefánik, Demänová 393,
031 01 Liptovský Mikuláš, Slovak Republic, e-mail: miroslav.kelemen@aos.sk

Summary

The global dimension of future security threats is of paramount importance. Whilst technological advancements will continue to be the basis of wealth for many nations, terrorism is likely to continue to be the harbinger of a pervasive sense of insecurity amongst populations. Increasingly, energy security will be the driver of many key strategic decisions, creating dynamic and unstable inter-state interactions in the process. With the internationalsystem itself experiencing a period of profound flux, some of the institutions that are charged with managing global problems may be overwhelmed. The likelihood of great power conflict escalating into total war is lower than at any time in the past century but weak governments, lagging economies, mass migration, WMD proliferation, religious extremism, and youth bulges, will align to generate the conditions for internal regional conflicts with global impact, backed by the Revolution in Military Affairs.

Keywords: Technology and Military Transformation, Security technology, Research and Development, Risk-Threat-Vulnerability, Life-time cycle, Afghanistan, National strategies, Emerging technology, Energy Security, Innovative approach, Revolution in Military Affairs

.

1. INTRODUCTION

Globalization and the spread of information echnology will combine to put increasing strain on the concept of state, but will not alter the geographical dimension that remains a key parameter. After due consideration of the levers impacting the future strategic environment, together an analysis of the trends of key factors such as resources, economies and populations, the resultant is likely to be a scenario of states linked by common interests, cultures, expectations and ambitions, that rotate around pivotal states acting as regional attractors. An additional level of complexity arises due to the dynamic interaction between the geographical and virtual dimensions possibly inducing centrifugal forces as individual nations cluster around pivotal states.

Technology has a range of implications for national governments: the impact that scientific and technological developments have on society, the economy and the environment; what the latest trends are; what the future might hold; and how this all affects security, both internal and external. Therefore, science and technology, research and development considerations, and others have to be included in the factors determining national strategy.

Technology has offered a high and sophisticated standard of living to societies but at the same time introduced an inherent vulnerability. Without its tools their economies can no longer be run and their infrastructure would collapse. Modern societies and their armed forces have become highly dependent on modern technology. The unarmed attacks of 9/11 clearly demonstrated this and the public is generally not aware of even larger threats, some at a nation's scale, posed by terrorists but also by accidents or natural disasters, just because of the total reliance on technology. Regarding military affairs, the Gulf Wars, the Kosovo air campaign and the war against terrorism in Afghanistan sharpened the public's interest in the military applications of high technology, through television pictures of the precision use of smart weapons and stand-off weapons platforms. The myth of the "zero-loss war" was actually born in Kosovo. Immediately deriving from this experience, the reluctance for casualties and collateral damage would have grown and influenced to some extent the political attitude of Governments in taking part into operations, eventually being able to
influence up to the nation's strategy.

2. GEO-STRATEGIC ANALYSIS

The strategic repercussions brought about by the end of the Cold War are still unfolding: emerging powers in Asia, retrenchment in Eurasia and a roiling Middle East. The very magnitude and speed of change resulting from a globalizing world will be a defining feature of the world into the 21st century. Other significant characteristics include: new challenges to governance and a more pervasive sense of insecurity due to terrorism. As one map the future, prospects for increasing global prosperity and the limited likelihood of great power conflicts provide an overall favorable environment for coping with what are otherwise daunting

challenges. Globalization, that is growing economic inter-connectedness reflected in expanded information flow, shared technology, interactive capital investment, inter-dependent markets for goods and services, and an increasingly mobile workforce throughout the world, will be an overarching mega-trend, capable of substantially influencing all parallel global forces.

3. GLOBAL DIMENSION OF CHALLENGES

An expanding global economy will increase demand for many finite raw materials e.g. oil, that is expected to become significantly scarce by the middle of the 21st century. Total global energy consumption is likely to rise by about 50 percent in the next two decades compared to a 34 percent expansion from 1980-2000. Most experts assess that, with substantial investment in new capacity, overall energy supplies will be sufficient to meet these increasing global demands. However, on the supply side, many of the areas, the Caspian/Barents Seas, Venezuela, and West Africa, that are being relied upon to provide increased output are accompanied by substantial political or economic risk. Traditional suppliers in the Middle East are also increasingly unstable. Thus sharper demand-driven competition for resources, perhaps accompanied by a major disruption of oil supplies, are among key uncertainties. Increasingly, energy security will be one of the critical elements of the security environment into the future.

Part of the pressure on governance will come from new forms of identity politics centered on religious convictions. In particular, political Islam will continue to have a significant global impact, rallying disparate ethnic and national groups and perhaps even creating an authority that transcends national boundaries. Democratization and greater pluralism could gain ground in key Middle Eastern countries that thus far have been excluded from the process by repressive regimes. Yet, the process already started in many states of the former Soviet Union and in Southeast Asia, may well prove less effective than hoped with a return to less democratic regime structures possible.

Regionally based institutions will be particularly challenged to meet the complex transnational threats posed by terrorism, organized crime and the proliferation of Weapons of Mass Destruction (WMD). Such post-World War II creations as the UN and the international financial institutions risk sliding into obsolescence unless they adjust to the profound changes taking place in the global system, including the rise of new powers (regional hegemons). A sense of insecurity will characterize public opinion based on psychological perceptions being viewed as physical threats. Even as most of the world gets richer, globalization will profoundly shake up the status quo. This generates enormous economic, cultural, and consequential political convulsions.

Current nuclear weapons states will continue to improve the survivability of their deterrent forces and almost certainly will find methods to better the reliability, accuracy, and lethality of delivery systems as well as develop capabilities to penetrate missile defenses. The active demonstration of nuclear capabilities by any state would further discredit the current nonproliferation regime, cause a possible shift in the balance of power, and increase the risk of conflicts escalating into nuclear ones. Countries without nuclear weapons, especially in the Middle East and Northeast Asia, might decide to seek them as it becomes clear that their neighbors and regional rivals are doing so. Moreover, the assistance of proliferators will reduce the time required for additional countries to develop nuclear weapons.

Information technology, allowing for instant connectivity, communication, and learning, will enable the terrorist threat to become increasingly decentralized, thus evolving into an eclectic array of groups, cells and individuals that do not need a stationary headquarters to plan and carry out their operations. Training materials, targeting guidance, weapons know-how, and fund-raising will all become virtually online.

Terrorist attacks will continue to primarily employ conventional weapons, incorporating new twists and constantly adapting to counterterrorist efforts. Terrorists probably will be most original, not in the technologies or weapons they use, but rather in their operational concepts i.e. the scope, design and support arrangements for their attacks. Strong terrorist interest in acquiring chemical, radiological, biological, and nuclear weapons increases the risk of a major terrorist attack involving WMDs. The greatest concern is that terrorists might acquire biological agents or, less likely, a nuclear device, either of which has the capacity to generate indiscriminate casualties on a huge scale. Bio-terrorism appears particularly suited to the smaller, better-informed groups. The terrorists will attempt cyber attacks to disrupt critical information networks and, even more likely, cause physical damage to information systems.

Mass migration will continue and, as a consequence of the low educational standards of most migrants, this phenomenon will continue to give rise to high levels of unemployment bringing with it the potential to generate ethnic and religious tensions. The resultant is the creation of a frustrated and disenchanted human resource 'pool' with recruitment potential for terrorism.

The difficulty for national security mechanisms is then to identify such terrorists within the state boundary and uncover the 'enemy in one's own land'. And this is vital in order to prevent terrorist activities taking place that, in turn, generate

indiscriminate victims (sometimes on a large scale but not always) within the population, instill a pervasive fear amongst populations in the process and adversely impact economic systems.

Organized crime embraces the elements of money laundering, human trafficking, smuggling, drug trafficking and corruption. Together, these elements have the potential to undermine state structures and influence the power monopoly of states.

As all developed states are dependent, and becoming increasingly dependent, on Information Technology (IT) the potential impact of cyber crime, especially as a tool of terrorism, is very likely to attain a new level of importance into the future. Already only a slight interference of these complex systems can generate damage of immense magnitude.

A large number of physical disasters are forecast, in particular, as a consequence of the melting of the polar ice caps. If this materializes widespread flooding of coastal regions will follow, necessitating migration. In addition an environmental reshaping of this magnitude is likely to be accompanied by dramatic changes to weather patterns such that an increasing number and frequency of tornados, tsunamis and storms follow. The implementation of strategies designed to counter such occurrences will demand huge national and international commitment, especially in budgetary terms and, inevitably this will divert resources from other areas, including security. The security challenge presented therefore will be to continue to provide a secure environment with diminishing resources in an increasingly natural resource scarce environment. Responsibility to counter the security challenges posed falls to the respective national security organisms, in particular intelligence services and police authorities. However, the real challenge in confronting the cause of the security risks lies hidden within democracy itself as diverting huge sums of money to environmental issues lessens the amount available for health, education, welfare. Importantly, in tandem with fractured stability issues arising within member states of NATO military capability gaps will emerge and widen as individual nations divert resources from defense to other areas as other, more pressing, difficulties arise.

4. GLOBAL VERSUS GEOGRAPHICAL APPROACH

Globalization and Revolution in Military Affairs will place enormous additional strain on governments. Growing connectivity will be accompanied by the proliferation of virtual communities of interest, complicating the ability of states to govern. The Internet, in particular, will spur the creation of even more global movements that may emerge as robust forces in international affairs.

One can rightfully ask if, in an era of globalization and 'cyberization', whether geography continues and, will continue to be a dominant value. Globalization consists largely of two aspects, one being the rise of trans-national economic actors, sometimes more powerful than states, and the other the geographical disconnection of otherwise linked economic activities, mainly between the production of goods and associated services. The 'cyberization' of communications has largely promoted the latter.

Economic activities, as they bind people and establish societies, constitute the baseline of inter-human relations. These activities are dependent on the availability of, or access to, resources (human and material) that are unevenly distributed around the globe. Geography determines the spatial pattern or distribution of these resources, be it human through living space and conditions or material through availability or, even more important, accessibility by presenting natural barriers as the mountains and deserts or natural highways like waterways and sea lanes. Of course, available technology and capital may create infrastructure that modifies these geographical features, thus influencing accessibility, but large-scale geographic barriers can rarely be completely annihilated. Geo-strategy "is not geographic determinism, but it is based on the assumption that geography defines limits and opportunities in international politics: states can realize their geopolitical opportunities or become the victims of their geopolitical situation" [4]. Even a cyber based economy will require specific human resources and infrastructure, most of the time only available in areas where other economic activities are developed.

Common economical activities shape societies and inter-societal economical exchanges are accompanied by cultural exchanges, promoting common understanding and mutual influence, the depth of which is largely dependant on the relative power balance. As geography determines spatial trade flows, it will equally influence cultural "commonality" and determine society groupings. The economical activities of a society provide the basis for its power. To determine the power distribution amongst states or regions and their evolution in the near future, it is necessary to study the building blocks constituting their power. As previously articulated, the prime power elements (or factors) constitute populations, resources in their quantitative and qualitative aspects providing a qualified labor force, availability of material resources, the capability to develop and use technology, determine the ability to change physical and human environments or to adapt to a changing environment and finally, economies in

their own right, providing capital, the ultimate means of exchange in order to acquire the resources or technology needed.

Geo-strategy is then necessarily a dynamic approach. It reflects the global constellation of power elements "arising from the interaction of geography on the one hand and technology and economic development on the other. Technology and the infusion of capital can modify, though not negate, the strategic importance of a particular geographic space".

Man-made cyber geography, the ultimate expression of globalization, is likely to exist alongside, or on top of, natural geographic features and is expected to become another example of technology modifying or reducing the influence of the natural landscape, but not reducing it to a level of inconsequent impact because that is not possible.

5. TECHNOLOGICAL DEVELOPMENT COUNTS!

A pertinent question is whether technological developments might bring Allies to the limits of interoperability. Over the last two decades the USA have been spending more money on developing technology than all the European partners spend together. One can argue that this kind of "gap" has always existed. The present problem could lie in the vanishing solidarity as the common enemy has faded away. Weaker Allies would have been backed up to avoid a breakthrough while now military and political authorities will rather question the opportunity of taking supplementary risks just for the "pleasure" of enjoying their company in the planned operations. A real technological gap may cause a shift in the threshold of interests for common action and could induce a political gap that would be much more damageable for NATO's cohesion.

The global information infrastructure enables any group, if not individuals, to have access to techniques for "home made" weaponry. Another aspect is the power acquired by major multinational armament manufacturers on governments as they detain the key technology to base military power on. On the other hand, some companies will only survive as long as public money is made available for Research and Development (R&D) and sometimes even just for running. Will modern technology become too expensive for some national defense industries in
a competitive and shrinking defense market?

Additionally, the fast development of technology could have in some nations an internal aspect as it is not sure that all top managers of the armed forces and their political masters are well aware of what is going on. This remark is not made to blame them but to stress that the technical complexity is now so high that it has become very difficult for specialists to inform thoroughly and clearly the decision makers about the possibilities but also the consequences of every technical progress. This is the open door to a lot of deleterious lobbying and potentially dangerous strategic orientations and operational choices.

6. HIGH-TECH IMPACT: IRAQ CASE STUDY

Along with the aspect of information and media, the aspect of globalization that is affecting asymmetric capabilities of our potential adversaries is that of information technology advances. Technology was once the weapon of the strong as the US with the NATO Allies demonstrated with its overwhelming defeat of the numerically superior Iraqi Army during Operation Desert Storm.

The first night of the Gulf War air campaign demonstrated that the conduct of war had changed. Well before dawn on 17 January 1991, Major Greg Biscone flew the first of two B- 52s toward Wadi Al Kirr airfield, a recently completed forward fighter base in central Iraq.

His targets were the taxiways between the runway and hardened aircraft shelters. Skimming 300 feet over the desert at 500 miles an hour it was so dark the night vision goggles and low light TV system didn't help. Iraqi early warning radars forced Biscone to drop his huge, old bomber lower, the surface-to-air missile (SAM) threat was greater than the danger of flying within a wingspan of the ground. Minutes later, Biscone and his counterparts executed a successful multi-axis attack crippling the airfield and leaving anti-aircraft artillery with nothing to fire at but the receding jet noise. Less than an hour earlier, stealthy F-117s had struck the heart of the enemy, Baghdad, in the opening minutes of the war. Tomahawk Land Attack Missiles (TLAMs) followed, striking critical electric systems and government decision-making and communications centers. F-15Es, part of an initial covert entry scheme into Iraq, attacked known SCUD launch facilities that threatened Israel and coalition nations.

Simultaneously, 13 F-117s flew against 22 separate targets including command bunkers north of Baghdad, communications exchanges in Baghdad, interceptor operations centers in Kuwait, satellite downlink facilities and vital communications nodes around the country. In western Iraq 30 aircraft attacked Saddam Hussein's chemical production facilities. Just north of Basrah, 38 fighters put Shaibah airfield out of commission and 44 others stripped away the medium altitude SAM defenses west of Baghdad near Al Taqqadum airfield, the Habanniyh oil storage area and three chemical weapons precursor facilities to clear the way for attacks the following afternoon. All suspected biological weapons storage sites were

targeted and critical oil storage facilities were hit. Conventional air launched cruise missiles (CALCMs) fired by B-52s flying from the United States reached electric facilities at Al Mawsil in Northern Iraq. By the end of the first 24 hours of the war, bombs also hit enemy bridges, military support and production factories, and naval facilities. In all, more than 1,300 offensive air sorties were flown that day. However, it was not the number of sorties that made this first day of air attacks so important, but how they were planned and co-coordinated to achieve specific effects; this represents one of the first examples of the effective implementation of the latest modern military technology assets available.

The superior defeat in less than 100 hours had forever changed the ability of modern, technologically advanced nations to wage war. The debate still spread out about whether there was or not a Revolution in Military Affairs (RMA), but what is increasingly clear is that the technology that enabled the Allies to defeat Iraq is now becoming universally available.

Technology transfer has really taken three forms. First there is almost universal access to space-based imagery, the global positioning network, and worldwide secure communications network. Second, it is now extremely easy to purchase technologically advanced weapons such as Global Positioning System (GPS), jammers, radio direction finding equipment, night vision devices and handheld radios at a fraction of the cost had paid to develop them. Finally, the cost of modern weapons has become so great, that it has increased the dependence on joint military and civilian ventures where technology transfer to the civilian community is increasingly difficult to control.

7.CONCLUSIONS AND RECOMMENDATIONS

During a fifteen minutes search on the Internet one is able to obtain high quality imagery of Washington D.C., Brussels, Pentagon, several of important nuclear facilities and almost any NATO Allies military installations. This information is available to anyone with a computer and a modem. If one is willing to pay, the information can be sent worldwide in near real time. If an adversary were planning an attack against whatever Center of Gravity (COG) as for example nuclear plant may be, this would provide an invaluable planning tool.

Access to GPS systems, satellite phones, and secure Internet communications have given criminal and terrorist networks access to the same level of information that was once available to only the most sophisticated nations. Terrorist groups and extremist organizations are making unprecedented use of this new technology as outlined in a report by the US National Infrastructure Protection Center. "Extremist groups are increasingly adopting the power of modern communications technology. An extremist organization, whose members get guidance from

e-mails or by visiting a secure web site, can operate in a coordinated fashion without its members ever having to meet face to face with other members of the organization" [5]. First, the Internet is being used to corporate new members into terrorist/extremist organizations and bombs them with a steady stream of propaganda. This propaganda indoctrination can be conducted from a safe area where the leaders are free from any threat of law enforcement. Secondly, access to online communication sources like free email accounts, chat rooms, and web-based bulletin boards, make it difficult to track where messages are coming from or going to. It provides a means for almost worldwide secure communication. The emergence of more sophisticated technology, like anonymous remailers, encryption and decryption, will only make identification and tracking more difficult.

And finally, Internet gathering points allow dispersed members to share ideological and operational information, enabling them to centralize their shared world view into independently actuated agendas in support of a common goal. Another reality of the globally connected world is the merging of defense and commercial technologies on a global scale. It is only logical that as our defense industries shrink and consolidate, they will have to produce products that have both military and civilian, dual use capabilities to survive. The ability to achieve competence in civilian production and defenseindustrial applications is becoming increasingly intertwined. At the same time, market access in the developing world (as in East Asia) increasingly requires technology sharing as an instrument of commercial competition [1].

The proliferation of weapons technology will be an increasing problem. "Technology diffusion to those few states with a motivation to arm and the economic resources to do so will accelerate as weapons and militarily relevant technologies are moved rapidly and routinely across national borders in response to increasingly commercial rather than security calculations. For such militarily related technologies as the Global Positioning System, satellite imagery, and communications, technological superiority will be difficult to maintain for very long" [2].

The greatest revolutions in military affairs are possibly more in the nature of war than in technological revolution in weapons systems, command and control devices and so on. A State is supposed to offer protection to its citizens. As for many countries the external aggressor has practically disappeared, they started concentrating

on the internal security. But the threat to internal security often comes from outside, which means that one has to go global and address the causes of the disease where they are, rather than symptoms at home. This has reoriented security policies towards more diplomacy, more co-operation and, as military forces are concerned, towards capacities of expeditionary type. This is, at least for the majority of the European Allies, such a profound change in their nature and their doctrine, their structure and their equipment that even the term "revolution" was used. NATO's success during the cold war era is undisputed. Nevertheless, after the fall of the Berlin Wall, the Alliance struggled to survive. In the security environment that follows the Balkans crisis, the concept of Collective Security emerged, thus providing grounds for the creation of an operational concept of expeditionary capability.

The tragic events of the 9/11 once again forced the Alliance into new scenarios characterized more and more by a global effect of challenges. Terrorism is more identifiable as capable of diffusing a pervasive sense of insecurity rather then defining a clear and identifiable threat, nevertheless, its global reach and effect is evident. Technological advancements, energy security issues, mass migration, proliferation of WMD, internal difficulties of international organizations with the simultaneous appearance of internal conflict in states characterized by weak governance, all serves to create a global security environment of instability.

REFERENCES

1. Center for Science and International Affairs, John F. Kennedy School of Government, Harvard University, CSIA Studies in International Security No. 4, 1994, p. 47.
2. Global Trends 2015: *A Dialogue About the Future With Nongovernmental Experts*, National Intelligence Council, NIC 2002-02, December 2000, p. 31.
3. KELEMEN M., SZABO S., SOUŠEK R.: *The development of the Slovak air forces air transport capabilities for joint logistics support operations*. In: Acta Avionica, 2006, vol. 8, number 12, pp. 114-117. ISSN 1335-9479.
4. Mackubin Thomas Owens, In Defense of Classical Geopolitics, Naval War College Review, vol. 52, no. 4 (Autumn 1999), http://www.nwc.navy.mil/press/review/1999/autumn/art3-a99.htm.
5. National Infrastructure Protection Center, Highlights 10-01, November 10, 2001, p. 2. 5 Ibid.
6. NEČAS P., SZABO S., BUČKA P.: *Crisis management and security in simulation environment*. In: Science & Military, 2006, vol. 1, number 1, pp. 33-37. ISSN 1336-8885.
7. OLEJNÍK F., NEČAS P.: *Challenges of the 21st century Global security: Reflected reforms*. Košice, Air Force Academy of General M. R. Stefanik in Kosice, 2004, 214 p. ISBN 80-7166-051-5.
8. SEDLÁK V., MESÁROŠ M., LOŠONCZI P., JAMNICKÝ O.: *GALILEO – nový globálny družicový navigačný systém a jeho perspektívy pre bezpečnosť ľudského potenciálu*. In: Security Magazín, červenec/srpen 2008, s. 23-27. ISSN 1210-8723.
9. SEDLÁK V., LOŠONCZI P., PODLESNÁ I.: *Družicové navigačné systémy*. Vysokoškolské skriptá, VŠBM Košice (vyd.), Košice, 2009, 75 s. ISBN: 978-80-89282-31-9.

TUNING OF BELIEF NETWORK-BASED DIAGNOSTIC MODEL

Wojciech CHOLEWA, Paweł CHRZANOWSKI, Tomasz ROGALA

Silesian University of Technology, Faculty of Mechanical Engineering,
Department of Fundamentals of Machinery Design
Konarskiego 18a, 44-100 Gliwice,
e-mail: wojciech.cholewa@polsl.pl, pawel.chrzanowski@polsl.pl, tomasz.rogala@polsl.pl

Summary

This paper presents a multi-stage diagnostic Belief Network Based Model (BNBM). Proposed model allows for application of acquired knowledge from data training, domain experts and domain literature. This feature is its special advantage. A general model structure, selected issues with its identification and application were shown as well. Described BNBM model consists of three stages: preliminary data processing, equalization and balance of additional variables and belief network. Tuning of BNBM model with using memetic algorithm as global optimization method with local optimization was proposed.

Keywords: belief network, model tuning, diagnostic model, memetic algorithm.

STROJENIE MODELU DIAGNOSTYCZNEGO OPARTEGO NA SIECI PRZEKONAŃ

Streszczenie

W artykule opisano wielostopniowy model diagnostyczny bazujący na sieci przekonań. Przedstawiono ogólną strukturę modelu oraz omówiono problemy związane z jego identyfikacją oraz strojeniem. Szczególną zaletą proponowanego modelu jest to, że pozwala on na stosowanie wiedzy pozyskanej zarówno z danych uczących jak i artykułowanej bezpośrednio przez specjalistów i literaturę rozpatrywanej dziedziny. Opisany model diagnostyczny składa się ze stopnia wstępnego przetwarzania, stopnia uzgadniania oraz stopnia w postaci sieci przekonań. Dla przyjętej ogólnej postaci modelu omówiono procedurę strojenia z użyciem algorytmu genetycznego. Z uwagi na wady i zalety tego algorytmu dokonano modyfikacji procedury strojenia poprzez zastosowanie algorytmu memetycznego. Określono kierunki dalszych prac badawczych.

Słowa kluczowe: sieć przekonań, strojenie modelu, model diagnostyczny, algorytm memetyczny.

1. INTRODUCTION

Wide range access to high computer technology bring a rapid growth of methods of condition monitoring. Many efforts to make diagnostic systems more efficient, which allow to early detection and isolation, fault tolerant control, state prediction ect. are still in development. One of the example is an intelligent diagnostics and process control system DiaSter [11], which combine a lot of methods from process variable selection to visualization of diagnostic results. An integral part of DiaSter system is a plugin for diagnostics with using a belief networks and multi-aspect models [3]. This model allows to apply model-based and symptom diagnostic commonly.

1.1. Model-based diagnostics

The essence of model-based diagnostics is the recognition of state class for an observed object by the analysis of generated residuals between measured values of output signals y and calculated output of model y_M. The model have to be appropriate tuned to the observed object. Such model or set of models of each state class can be used during model-based diagnostic. The main condition of using model based diagnostics is an assumption that simulation inputs and observed inputs are the same. [4].

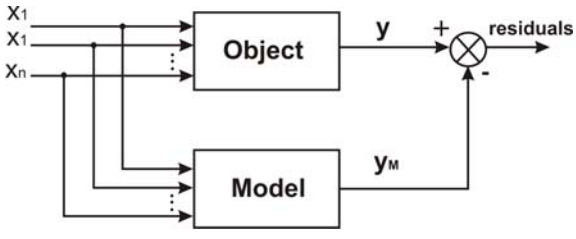

Fig. 1. Model-based diagnostics

1.2. Symptom diagnostics

Considering symptom diagnostics problems, we assume that effect of state changes of object are correlated with arising of state symptoms, which in turn indicate these faults [1]. In a case of symptom

diagnostics, the main assumption is to use domain expert knowledge which can be helpful in selection of relevant symptoms. Methods of collection, representation and notation of state-symptom relation have an essential meaning. There are many methods for gathering of state-symptom relations. In general, for symptom diagnostics, data can be collected from domain experts, passive diagnostic experiments and active diagnostic experiments.

2. BELIEF NETWORK-BASED MODEL

Considering advantages of symptom diagnostics and model-based diagnostics, a belief network-based diagnostic model (BNBM) which combine above features was proposed [3]. Let's consider model BNBM, where values of inputs and outputs are vectors x_D and y_D. Model inputs include: observed values of features, design features, parameters of operation conditions of an object. The model outputs are results of diagnostic process which can be represented as belief rate of class of state of observed object.

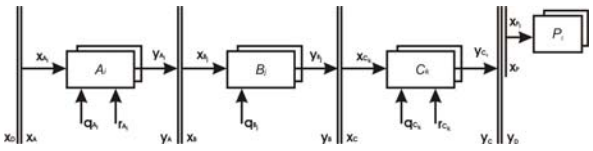

Fig. 2. Belief Network-Based Model

Multi-stage BNBM model (Fig.2.), which transforms input data x_D to output data y_D, consist of stages A_i, B_i, C_i [3], where:

- first stage A_i is a block of pre-processing of data,
- second stage B_i, which consist of blocks for equalization and balance of additional values,
- third stage C_i, which consist of a set of belief network.

Moreover, for application of BNBM model, an external module P_l for visualization of results was added.

Main task of first stage is a reduction of the number of considered features of diagnostic signals which can be obtained by: data normalization, multidimensional scaling and more complex processes of transformation input data. Transformation process can be also done with the use of a set of *One Class Classifiers* which can be interpret as a membership functions of fuzzy sets.

Equalization and balance blocks are used to incorporate constraint equations which come from domain knowledge of observed object. Lack of domain knowledge cause omitting of second stage by moving inputs to outputs without changes.

Third stage is belief networks set [10], which realize tasks coming from symptom diagnostics where knowledge is represented by descriptions state-symptom relations. Convenient representation form of approximate knowledge is a statement.

The statement is an assertion about the recognition of observed facts or assertion representing a given opinion. A statement s can be written down in the form of the pair::

$$s =< c; b > \tag{1}$$

where:

c - the statement content, and thus, e.g., an opinion on that a given object is entitled to have a given attribute, whose value is established;

b – a (logical) value of the statement of [0,1]. It is defined as the truth factor or degree of belief and concerns the content of the statement.

Bayesian Network identification is a complex process. The network structures can be defined with the use of machine learning techniques or cooperation of domain experts. The second difficult task is defining of Condition Probability Tables for each node of the network. It can be done trough identification and tuning which is directly based on the knowledge of a domain expert, intuition of knowledge engineer (a priori). Another way is to perform the process automatically with the use of learning data sets. Quality of learning is dependent on a size of data set and its quality. Some learning algorithms reduce the negative influence on small learning data sets by consideration of non-complete statements in a node. A part of data is introduced to the system manually and the rest of elements of the set can be defined in automatically way. Obtained model can be further tuned.

Statements vector of considered state classes is the result of third stage (1). The specific structure of the BNBM model allows to link selected outputs of previous blocks with the inputs of next blocks.

Each stage of BNBM (Fig.2) consists of configuration parameters. There are parameters which can not be changed $\underline{q}$ and parameters to be tuned $\underline{r}$ depending on the needs.

3. IDENTIFICATION AND TUNING OF BNBM

Identification of Belief Network-Based Model is a complex process. It requires of carefully analysis of considered problem and can be done in two steps:

- build of complete initial version of model,
- improving and tuning of model during iterative process.

It is necessary to collect and prepare data training for building the initial version of model.

3.1. Model identification

Iterative identification process of BNBM consists of the following steps:

- Defining of model input and output set, statement contents and global structure.
- Analysis of accessible model and additional variables.
- Building of equalization and balance blocks based on knowledge.
- Independent identification of each classifier on the base of prepared training data.
- Independent identification of bayesian network on the base of prepared and transformed by block A_i training data.
- Model testing.

Identified initial version of BNBM should be improved.

2.2. Tuning of BNBM

Tuning of proposed multi-stage heuristic model is difficult and complex task and requires application of method for global optimization. Genetic Algorithms meet this criteria [8]. GA are a particular class of evolutionary algorithms that use techniques inspired by evolutionary biology used in computing to find exact or approximate solutions to optimization and search problem. Typical GA can be written as follows:

```
procedure Genetic_Algorithm
{   t ← 0 ;
    P(t) ← initialization( ) ;
    while(not termination_condition)
    {   t ← t + 1 ;
        R(t) ← evaluation_and_selection( P(t − 1) ) ;
        D(t) ← reproduction( R(t) ) ;
        N(t) ← evaluation_and_selection( P(t − 1) ) ;
        P(t) ← ( P(t − 1) + D(t) − N(t) ) ;
    }
}
```

An advantage of genetic algorithm is possibility to find a global solution. Moreover, a genetic algorithm shows high resistance for extreme of criteria function. In spite of above advantages of GA for global optimization, its provide to getting individuals with limited solution cause of optimization individuals features of population. Another disadvantage of genetic algorithms is lack of individuals learning. To this end, genetic algorithm is improved by additional operations to modify elite individuals for improve themselves during the evolutionary cycle [12]. This kind of synergy of evolutionary and local improvement procedures is called Memetic Algorithm (MA). Typical procedure of MA can be written as follows:

```
procedure Memetic_Algorithm
{   t ← 0 ;
    P(t) ← initialization( ) ;
    while(not termination_condition)
    {   t ← t + 1 ;
        R(t) ← evaluation_and_selection( P(t − 1) ) ;
        D(t) ← reproduction( R(t) ) ;
        N(t) ← evaluation_and_selection( P(t − 1) ) ;
        P(t) ← ( P(t − 1) + D(t) − N(t) ) ;
        E(t) ← evaluation_and_selection( P(t) ) ;
        E(t) ← local_optimization( E(t) );
    }
}
```

Tuning of Belief Network-Based Model can be done by:

- independent improvement of stage A_i and stage C_i,
- simultaneous tuning of both considered stages A_i and C_i.

Configuration parameters $\underline{r}$ of stages A_i and C_i for considered model can be tuned (Fig. 1). They may be interpret as equivalent of genes and memes of memetic algorithm. It requires a special kind of codification of information.

The set of tuned configuration parameters for blocks of first stage may include centers location of membership function of one class classifier. Another important tuned parameter of this stage is the number of class of considered additional values. Optimal defining above parameter require detailed analysis of changes range of additional values. Small number of class of additional values lead to incorrect or weak results. However excess of class numbers increase time of calculation during the identification and tuning process.

Tuned parameters of belief network are Conditional Probability Tables (CPT) defined during identification process. Belief network tuning can be based on modification of Conditional Probability Tables for all nodes and than modification of Conditional Probability Tables for selected nodes. Expectation-maximization algorithm (EM) can be applied for tuning of CPT, where tuned parameters are number of iterations and learning error. Moreover, belief network structure can be tuned by inserting of additional weight node to clear-cut for point at searching solution.

Another difficult task of tuning process is defining of fitness function of memetic algorithm for selection of individuals and for local optimization of elite individuals. There are no clear-cut recipes for definition of feet function because it depends on the considered problem.

4. SUMMARY

Research connected with the development of identification methods and tuning of Belief Network-Based Model is still in progress. Implementation in C++ of described concept as plugin of diagnostic system framework was done. At present, a practical application and implementation of model for DiaSter system is under work.

BIBLIOGRAPHY

[1] Bargiela A. i Pedrycz W.: *Granular Computing. An Introduction*, Kluwer Academic Publishers, Boston, 2003.
[2] Cempel C.: *Fundamentals of vibroacustical condition monitoring*, WNT, Warszawa 1982 (in Polish).
[3] Cholewa W.: *Diagnostics with using a belief networks and multi-aspect models*. Project seminar, DIASTER. Szczyrk 2008, Poland. PBR-19/RMT-6/2007
[4] Cholewa W.: *Simulation diagnostics,* Problemy Eksploatacji, 1997, 27(4): 13–23 (in Polish).
[5] Cholewa W., Rogala T.: *Diagnostic modeling and inverse models*. Series: Zeszyty, Edition II, Silesian University of Technology, Department of Fundamentals of Machinery Design, 2008 (in Polish).
[6] Chrzanowski P., Rogala T.: *Comparison of belief network inference algorithms*, AIMETH Symposium, Gliwice 2007.
[7] Dawkins R.: *The selfish gene*, Oxford University Press, New York, 1976.
[8] Goldberg D. E.: *Genetic algorithms and applications*, WNT, Warszawa 1998 (in Polish).
[9] Hart W. E.: *Adaptive global optimization with local search*, Ph.d thesis, University of California, San Diego, CA, 1994.
[10] Jensen F.: *Bayesian Networks and Decision Graphs*, Springer, 2001.
[11] Kościelny J.M. (2007-2009). *Inteligentny system diagnostyki i wspomagania sterowania procesów przemysłowych „DIASTER"*. Warszawa. R01 012 02
[12] Krasnogor N. i Smith J. (2005). *A tutorial for competent memetic algorithm: model, taxonomy, and design issues*, IEEE Transactions on Evolutionary Computation 9:474–488.
[13] Moscato P. (1999). *Memetic algorithms: a short introduction*, in D. Corne, M. Dorigo i F. Glover (Red.), New ideas in optimization, McGraw-Hill, Maidenhead, pp. 219–234.
[14] Wang H., Wang D. i Yang S. (2009). *A memetic algorithm with adaptive hill climbing strategy for dynamic optimization problems*, Soft Computing 13: 763–780.

Wojciech CHOLEWA, Professor.
His research interests focus actually on the development of methods of knowledge representation for expert systems and application of belief networks.

Paweł CHRZANOWSKI, PhD Eng.
He deals mainly with issues of application and development of computer methods for diagnostic expert systems

Tomasz ROGALA, MSc. Eng. He is interested in machine learning and artificial intelligence, and applications to diagnostics.

QUALITY EVALUATION OF THE BEVEL GEAR ASSEMBLY BASED ON ANALYSIS OF THE VIBRATION SIGNAL

Łukasz JEDLIŃSKI, Józef JONAK

Lublin University of Technology, Mechanical Faculty, Department of Machine Design
36 Nadbystrzycka Street, 20-618 Lublin, Poland
tel. +4881 53-84-499, email: l.jedlinski@pollub.pl, jonak@pollub.pl

Summary

For the bevel gear assembly, the contact area is the main criterion of the assembly quality assessment. As it is obtained at a small load of the gear, it cannot fully ensure normal mating of the teeth, because under the load, the bodies, shafts, gear wheels, etc. are deformed. This paper assumes that there should be a relationship between the signal generated by the gear and the values characteristic for the contact area. Then, on the basis of vibration measurements it would be possible to evaluate the quality of assembly.

Keywords: bevel gear, assembly.

OCENAJAKOŚCI MONTAŻU PRZEKŁADNI STOŻKOWEJ NA PODSTAWIE ANALIZY SYGNAŁU DRGANIOWEGO

Streszczenie

W trakcie montażu przekładni stożkowych ślad współpracy jest głównym kryterium oceny jakości montażu. Ponieważ jest on uzyskany przy małym obciążeniu może w pełni nie gwarantować prawidłowej współpracy zębów, gdyż pod wpływem obciążenia następuje odkształcenie korpusów, wałów, kół zębatych itd. W pracy założono, że powinna zachodzić zależność między sygnałem generowanym przez przekładnię a wielkościami charakteryzującymi ślad współpracy. Wtedy na podstawie pomiarów drgań możliwa była by ocena jakości montażu.

Słowa kluczowe: przekładnia stożkowa, montaż.

1. INTRODUCTION

For a number of years engineers have tried to achieve the maximum ratio of driven power to gear weight. That is why they introduced into production special materials, heat treatment and great precision. However, even with a high manufacturing accuracy of the gear elements, assembly errors may cause greater dynamic excitation. The influence of the assembly deviations and tooth backlash on the bevel gear dynamic load has been the subject of a lot of research (e.g. Skoć [7]). For instance, it has been stated that there is no significant connection between the value of the tooth backlash and the gear's dynamics, if only it falls within the allowed limits. Yet, it affects the oil working temperature. However, as far as assembly deviations are concerned, it has been discovered that the gear dynamic load does not depend on the type and value of deviations but on the tooth contact area. This means that each of the set deviations has an equal influence on the gear's dynamic load if they cause comparable changes in the tooth contact area (the contact area was defined by a relative length).

For simple gears, composed of few elements, it is enough to prepare a general diagram of the order of assembly. For more complex gears, the assembly instructions should include a list of all assembly activities, required tools, necessary drawings and essential calculation formulas [1]. While assembling cylindrical gears, there is no possibility of improving the meshing as it is conditioned by the accuracy the gear wheels and the body were made with. In order to prevent tooth jamming during operation, the values of backlash and contact area – which confirm the quality of gear wheels and body – are checked in the first place [5]. In bevel gears, the body is designed in a way which enables shifting the wheels towards their axles. Therefore, during the assembly, it is possible to alter the size and position of the tooth contact area and the value of the backlash.

During the gear assembly, attention is focused on achieving the biggest tooth contact area. For cylindrical helical tooth gears the increase in the contact area causes a noticeable drop in the vibration speed measured on the body [8]. The factor of dynamic surpluses for bevel gears reaches the maximum value for the smallest relative length of the tooth contact area and the minimum value for the biggest [7].

The assembly is an important stage which conditions a gear's life and quietness. The tooth contact area is the main criterion of the assembly quality assessment. Obtained at a small load of the

gear, it cannot fully ensure the right mating of the teeth, because under the load, the body, shafts, bearings, gear wheels, etc. are deformed (e.g. [7]).

The article presents a quality assessment of the bevel gear assembly, made with the use of the vibration signal. Vibration-based diagnostics were performed under load, during the usability tests.

2. THE METHOD AND SUBJECT OF THE TEST

Six identical gears, which had been properly assembled and tested, were analysed. They were single-phase bevel gears with wheel-curved teeth. After assembly, the gears were subjected to usability tests, the aim of which was to run in the gears and verify the quality of their assembly. Vibration signals were registered at the maximum load. The measurement was taken with two vibration acceleration sensors. The first signal analysis included calculating the signal mean and root-mean-square values for each gear. In the second variant of the analysis the signals were subjected to a filtration process to obtain the first three harmonics. The frequency of the first harmonic was 1960 Hz, the second 3920 Hz and the third 5880 Hz. Filtration of the signals produced 1/3-octave bands with constant relative bandwidths. Middle frequencies were 2000 Hz, 4000 Hz and 6300 Hz respectively. For a signal with three mesh harmonics, mean and root-mean-square values of vibration acceleration were calculated. The diagram of the stand and the measurement path are shown in figure 1.

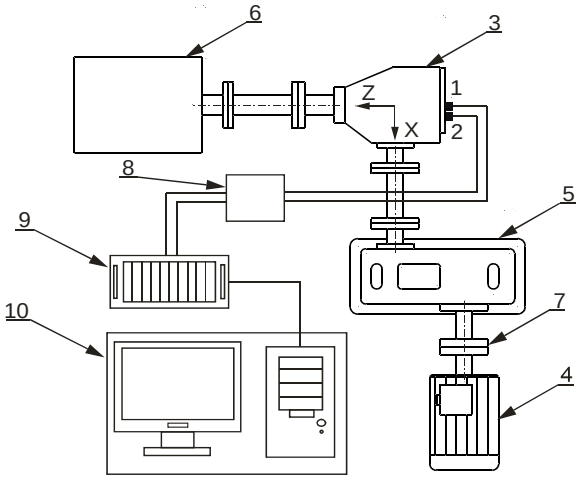

Fig. 1. Diagram of the measurement path and the test stand; 1, 2-triaxial piezoelectric vibration acceleration sensor by B&K, 4-driving motor, 5-multiplier, 6-water brake, 7-coupling, 8-signal conditioner, 9-NI measurement card, 10-PC

The correct contact area was described according to the assembly instructions. The dimensions defining the position and size of the contact area are shown in figure 2.

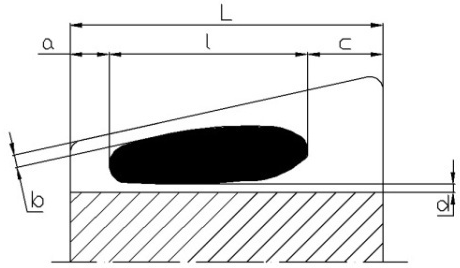

Fig. 2. The shape of the contact area with dimensions defining its position and size

The contact area was checked on three teeth spaced every 120°. Figure 3 depicts the examples of tooth contact areas with dimensions and surface areas.

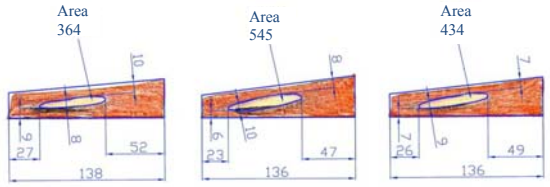

Fig. 3. Examples of the gear wheel contact areas with typical dimensions

The measure representing the contact area was its relative length L_w, specified with the dependence no. 1, and relative surface area P_w (dependence no. 2).

$$L_w = \frac{L}{L_c} \tag{1}$$

where:
L – the length of tooth contact area,
L_c – total length of tooth side surface.

$$P_w = \frac{P}{P_c} \tag{2}$$

where:
P – tooth contact surface area,
P_c – total tooth side surface area.

3. ANALYSIS OF THE RESULTS

As previously mentioned, the tooth contact area is the main criterion of the gear wheel quality assessment and the gear assembly correctness. It was assumed that there should be a relationship between the contact area and the vibration signal generated by the gear. Then, on the basis of the vibration measurements, it would be possible to judge the assembly quality. It was also accepted that the precision with which the gear wheels, bodies and other gear parts had been made had no significant influence on the generated vibrations. This project also assumes that the larger the contact area with the right position and shape, the smaller the gear vibrations should be.

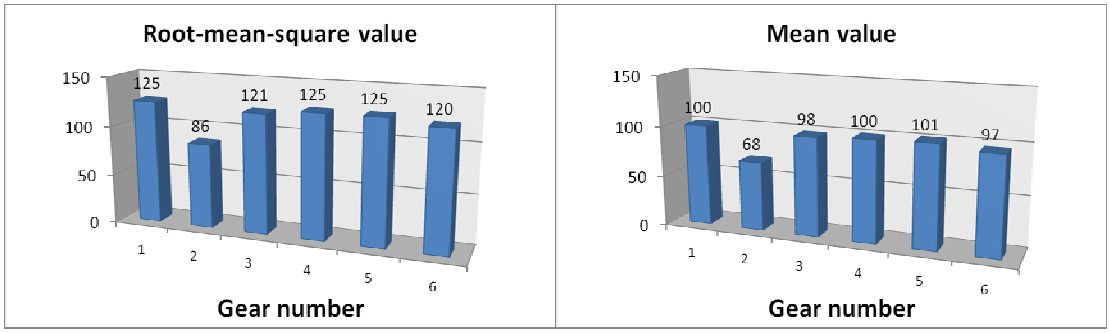

Fig. 4. Root-mean-square and mean values for non-processed signals

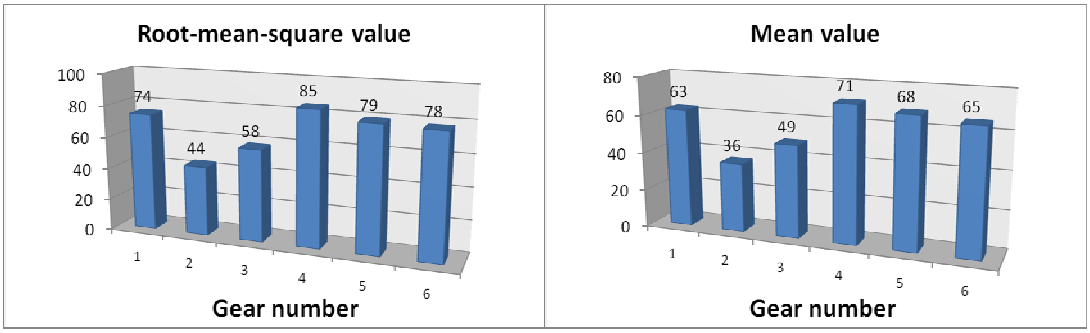

Fig. 5. Root-mean-square and mean values calculated for filtered signals

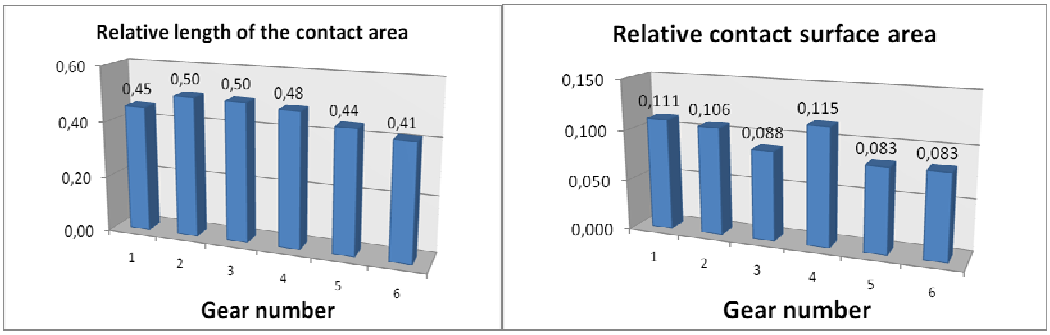

Fig. 6. Relative length of the contact area and relative contact surface areas

Comparing the root-mean-square and mean values in figure 4, we can see that the values for gear no. 6 are lower than the values for gears nos. 1, 3, 4 and 5. Similar data can be found in figure 5.

Figure 6 depicts two contact area measures, which estimate the same contact area differently, especially for gears 1 to 4. In other words, according to one measure, a particular gear was assembled in a better way compared to other gears, and according to the other measure it was not. By the words "better way" we mean higher value. Comparing the relative length and relative contact surface area with signal parameters, and remembering the earlier assumption, it should be stated that the contact area is described more appropriately by the relative contact area length. Having chosen one of the measures, we can continue further analysis. The value describing the contact area for gear no. 1 is not much bigger than for gear no. 5 (vibration parameter values should also remain at similar levels, as they do). The biggest contact area was achieved for gears nos. 2 and 3; root-mean-square and mean values should reach similar, the lowest levels. Figure 5 shows that the values are the lowest, but they are very different from one another. While in figure 4, the parameter value for gear no. 3 is at the same level as for gear no. 1. Gear no. 6 was assembled with the smallest contact area; the second in row is no. 5. Signal parameter values are not the highest for these gears but they are similar (figure 5), and the value is smaller for gear no. 6 (figure 4). The highest vibration signal parameter value is for gear no. 4, with the contact area bigger than the four other gears (figure nos. 4 and 5).

When compared to the non-processed signals, parameter values calculated for the filtered signals are closer to the contact area size. We can state this after the verification of parameter values, especially for gears 1, 3 and 5.

4. SUMMARY

The assembly of gears, especially bevel gears (with the possibility of changing the gear wheel position) is a crucial stage which influences the gear's durability. The assembly quality is also conditional on the competence of the staff. The order of the assembly and control actions is included in the assembly instructions and varies depending on the complexity of a gear [1].

The tooth contact area is the major indication of the gear assembly quality assessment. This work examines the relation between the size of the contact area and simple vibration signal measures. As a result of the research it has been shown that the size of the contact area represented by the relative length is a better measure than the relative contact trace surface area. Vibration signal parameters for filtered signals demonstrated greater compliance with the size of the contact area. The relation between the contact area size and the signal parameters was only partially confirmed. The most significant inconsistency was for gear no. 4, which, despite the third position as far as the contact area size is concerned, has the highest level of vibrations. Gears 2 and 3 (with the same contact area) also differ significantly as far as signal parameters are concerned. The reason for this may be inadequate initial signal processing or wrong signal parameters (signal analysis). In addition, defining the assembly quality only by the contact area size may not be enough. The solution to this problem may be the employment of artificial intelligence methods for the assessment of the assembly quality, and that is the direction in which further work will follow.

REFERENCE

[1] Barylski A.: *Analiza montażu stożkowo-planetarnej przekładni zębatej*. Technologia i automatyzacja montażu nr 3 i 4/2004 (s. 115-118).

[2] Czech P., Łazarz B., Wojnar G.: *Wykrywanie lokalnych uszkodzeń zębów kół przekładni z wykorzystaniem sztucznych sieci neuronowych i algorytmów genetycznych*. Wydawnictwo Instytutu Technologii Eksploatacji-PIB, Katowice-Radom 2007.

[3] Dąbrowski Z., Radkowski S., Wilk A. (redakcja naukowa): *Dynamika przekładni zębatych, Badania i symulacja w projektowaniu eksploatacyjnie zorientowanym*. Wydawnictwo i Zakład Poligrafii Instytutu Technologii Eksploatacji, Warszawa-Katowice-Radom 2000.

[4] Jasiński M., Mączak J., Radkowski S.: *Zastosowanie filtracji tercjowej sygnału wibroakustycznego w wykrywaniu błędów montażu przekładni zębatej*. Przegląd Mechaniczny 11-12/1998 (s. 20-26).

[5] Ochęduszko K.: *Koła zębate*, Tom drugi, Wykonanie i montaż. Wydawnictwo Naukowo-Techniczne, Warszawa 1976.

[6] Ochęduszko K.: *Koła zębate*, Tom trzeci, Sprawdzanie. Wydawnictwo Naukowo-Techniczne, Warszawa 1970.

[7] Skoć A.: *Prognozowanie właściwości dynamicznych przekładni zębatych stożkowych*. Wydawnictwo Politechniki Śląskiej, Gliwice 2007.

[8] Tomaszewski J.: *Diagnostyka przekładni w warunkach przemysłowych*. www.ceramizer.pl/content/view/120/65/

Łukasz JEDLIŃSKI, MSc, Eng., is a lecturer at the Department of Machine Design at the Mechanical Faculty at Lublin University of Technology. His fields are signal processing and analysis, and gear diagnostics.

Prof. **Józef JONAK**, PhD, Eng., is the Head of the Department of Machine Design at Lublin University of Technology. In his projects, he concentrates on the following issues: adaptive control of heavy-duty machines, fracture mechanics and fracture process simulation of composite materials, the construction, operation and diagnostics of mechanical gears (especially helicopter gearboxes) and computer-aided design of machines and devices.

FAULTS DETECTION IN LAYERED COMPOSITE STRUCTURES USING WAVELET TRANSFORM

Andrzej KATUNIN, Wojciech MOCZULSKI

Department of Fundamentals of Machinery Design, Faculty of Mechanical Engineering,
Silesian University of Technology, Konarskiego 18A, 44-100 Gliwice, Poland,
e-mail: andrzej.katunin@polsl.pl, wojciech.moczulski@polsl.pl

Summary

In the paper the authors present their results concerning measurements of frequency responses of cantilever rectangular GFRP plates with intentionally inserted faults of three different types (fiber discontinuities, delaminations and notches for simulating cracks). The preliminary research shows that classical methods of signal conditioning (e.g. FFT or STFT) often do not project changes between damaged and undamaged structures, when faults are inconsiderable. In the experiment the frequency responses of the investigated samples with and without faults were obtained by means of the impact test carried out using LMS SCADAS and TestXPress software. For the approximation in wavelet transform (WT) Morlet and Db8 wavelet functions were applied. The shapes of these functions give the best imitation of the measured signal shape obtained from the impact test. The obtained results allow to assert that the proposed methodology of faults detection in layered structures based on WT can be useful for fault diagnosis even in early damage phase, when other methods are insensitive. In the further work the authors will develop the proposed method for faults identification and localization in layered structures and investigate laminate behavior with faults and self-heating in fatigue processes.

Key words: GFRP laminates, faults detection, wavelet transform.

DETEKCJA USZKODZEŃ W WARSTWOWYCH STRUKTURACH KOMPOZYTOWYCH Z ZASTOSOWANIEM TRANSFORMACJI FALKOWEJ

Streszczenie

W pracy autorzy przedstawiają wyniki pomiarów odpowiedzi częstotliwościowych jednostronnie utwierdzonych prostokątnych płyt z kompozytu polimerowego zbrojonego włóknem szklanym z celowo wprowadzonymi uszkodzeniami trzech typów (nieciągłości włókien, delaminacje i karby symulujące pęknięcia). Badania wstępne pokazują, że klasyczne metody obróbki sygnałów (jak FFT czy STFT) często nie obrazują zmian pomiędzy strukturą uszkodzoną i nieuszkodzoną, gdy uszkodzenia są nieznaczne. W eksperymencie z zastosowaniem testu impulsowego były otrzymane odpowiedzi częstotliwościowe badanych próbek przy pomocy LMS SCADAS i oprogramowania TestXPress. Do aproksymacji w transformacji falkowej użyto funkcji bazowych Morleta i Db8. Kształt tych funkcji daje najlepsze przybliżenie przebiegu wartości chwilowych zmierzonego sygnału otrzymanego z testu impulsowego. Otrzymane wyniki pozwalają stwierdzić, że zaproponowana metodologia detekcji uszkodzeń w strukturach warstwowych oparta na transformacji falkowej może być użyteczne przy diagnostyce uszkodzeń nawet we wczesnych stadiach degradacji, gdy inne metody są nieczułe. W przyszłych pracach autorzy będą rozwijać zaproponowaną metodę pod kątem identyfikacji i lokalizacji uszkodzeń w strukturach warstwowych oraz badać zachowanie laminatów z uszkodzeniami i temperaturą samowzbudną w procesach zmęczeniowych.

Słowa kluczowe: laminaty polimerowe, detekcja uszkodzeń, transformacja falkowa.

1. INTRODUCTION

Layered structures, such as composite laminates, are commonly used in many responsible engineering constructions (wind turbines, turbine blades, rotors, helicopter propellers etc). Behavior and mechanisms of faults initiation and their propagation completely differ from the corresponding phenomena that occur in homogeneous materials. Moreover, there are several additional properties that influence faults and their development, such as: structure properties, fiber orientation, self-heating etc [1]. Also, the behavior must be predictable in each mode of laminate usage. Therefore, methods of diagnosing and detecting faults must be adapted to the investigated structures. There are many methods of signal analysis for detecting and diagnosing faults (e.g. DFT, STFT, cepstrum analysis, signal demodulation etc.), but only several can be applied for high precise detection of faults in early damage phase. In many cases the

standard procedure of signal analysis can be applied as well and evaluation of degradation of the structure can be carried out using Fourier Transform [2,3], but the methodology become useless when the structure condition is on early damage phase.

Therefore, the wavelet transform can be applied as well. Main advantages (in contrast of DWT or STFT) of WT (wavelet transform) are the possibility to avoid Heisenberg's indefiniteness principle and the possibility to manipulate with time-frequency window and more accurate signal approximation using different wavelet functions. Methods based on WT are widely used for analyses of non-stationary and transient signals like impacts. An additional advantage of using WT is Mallat theory, which gives an opportunity for multiresolution approximation analysis for analyzing the signal on approximation and detail part on each level of decomposition. Applications using WT were used for early detection of bearing failures [4], identifying structural defects in spindles [5], impact damages in laminates [6] and other.

2. PROBLEM DESCRIPTION

The subject of research is 24-layered GFRP laminate with epoxy matrix. Three types of faults were considered: fiber discontinuities, delaminations and notches for simulating cracks. In many situations traditional methods (e.g. DFT or STFT) do not give wide information about structure condition, especially when structure is on early damage phase. Therefore, the wavelet transform was used. Choosing the basic function for measured signal approximation it is necessary to take into consideration shape of the signal, for impact responses Morlet's and Daubechie's basic functions were applied.

The research problem, which the authors concern with is the development of sound methodology of faults detection in layered structures in an early damage phase, when other methods are insensitive. The early-stage detection has very essential meaning. Detecting faults as soon as possible is one of the most significant tasks for diagnosing laminate structures e.g. in airplanes. If some developing fault is detected early, it is very often possible to modify the schedule of usage or even the mission the airplane carries out. In the less severe cases it is possible to properly schedule the nearest repair and carefully plan its extent and duration.

Although owners and the maintenance personnel understands very well the importance of the incipient failure detection, methods and techniques used to-date quite frequently do not allow early detection of faults. This is due because of prevailing application of the symptom-based approach and employing symptoms that cannot provide any clear evidence of the incoming failure. Therefore there is the need to develop such a methodology and signal processing methods, which could help in detecting incipient faults of composite structures. To this end, patterns obtained by means of WT proved to be useful tool. The description of this approach is the main goal of the paper.

3. METHOD CONCEPTION

The research was carried out in two stages: in the first stage samples with fiber discontinuities, delaminations and undamaged samples were investigated, and in the second stage samples with notches for modeling cracks in different places were used.

The first stage concerned the preliminary analysis of faults detection in above-mentioned samples. Laminate plates with dimensions 400x50x5.28 mm were clamped on the one edge and tested in impact test using LMS SCADAS hardware with PC and TestXPress software. Measurements were processed in 2.56 seconds with sampling rate equaled to 6400 Hz. An impulse excitation was given by modal hammer PCB T086C01 and the response to the impact was measured by the shear accelerometer PCB T352C34. The number of averages was 10. The experimental stand is presented on Fig.1.

Fig. 1. Experimental stand

The collected measurements were exported to CSV format and then – to MATLAB data files (MAT). Then, signal processing was applied. Firstly, FFT analysis was processed and PSD charts were obtained, after that spectrograms of signals were made using STFT analysis and then CWT analysis was made using Morlet's basic function (Fig. 2) for obtaining scalograms. The scalograms were converted from scale representation to frequency representation using the formula (1):

$$f = \frac{5}{2\pi a}, \tag{1}$$

where a is scale coefficient. The obtained results from all the analyzes were compared with taking into consideration the damage type of samples.

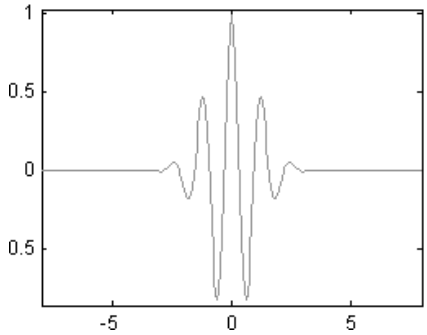

Fig. 2. Morlet basic function [7]

In the second stage samples with dimensions 250x25x5.28 mm and with intentionally inserted notches in different places were investigated. An algorithm of measurements was the same as in the first stage. After exporting measurements to MATLAB the CWT analysis was processed. The obtained scaleograms did not give clearly visible results, therefore the other approach was assumed. Each signal was approximated using Db8 (Daubechies 8) basic function (Fig.3) in DWT. Then, approximated signals were decomposed to approximate part and detail part on level of decomposition equaled to 5 with maximal decomposition level equaled to 15 (2).

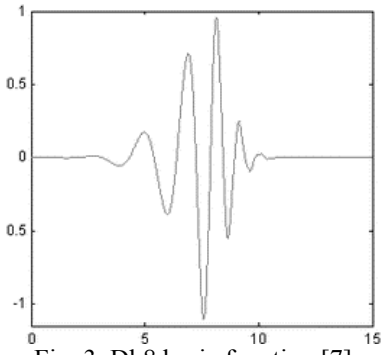

Fig. 3. Db8 basic function [7]

In theory the number of decomposition levels approaches infinity, but practically it is limited to one element of realization:

$$l = \log_2 N, \qquad (2)$$

where N is the number of elements in the realization. Higher levels of decomposition were neglected because these realizations can be considered as noised ones. In the obtained results details parts of signal were taken into consideration. Here, the statistical approach was shown: the biased autocorrelation of details on decomposition levels of undamaged sample was compared with cross-correlation between damaged and undamaged samples. For evaluation of the difference as scalar the next metric was introduced: the mean value of difference between cross-correlation value of damaged and undamaged samples divided by the peak value of the autocorrelation (3):

$$CFV = \left(\sum_{i=1}^{N} \frac{\left(R_{xx} - R_{xy,i} \right)}{N} \right) \Big/ \max\left(R_{xx} \right), \qquad (3)$$

Having done the analyzes the obtained results were compared: scalograms were compared with FFT and STFT results and finally statistical values of detail parts were confronted.

4. DETECTING THE DAMAGE TYPE

At the beginning, Fourier transform of the obtained signals took place. The results of the transform show that in cases of damaged samples the values of natural frequencies are growing, but this does not allow to clearly determine the fault occurrence and its type. The comparison of natural frequencies of the samples is presented in Table 1.

Table 1. Comparison of natural frequencies for undamaged and damaged samples

Mode number	Undamaged [Hz]	Fiber discont. [Hz]	Delamination [Hz]
1	18,36	18,75	18,75
2	114,5	116,4	116,8
3	314,8	319,1	321,5
4	598,8	616	619,5
5	991,4	1009	1017
6	2117	2172	2184

Then, STFT analysis was processed. Obtained spectrograms also do not show differences precisely (compare Fig. 4 – Fig. 6). Therefore, the CWT analysis was performed. In the algorithm, the researched frequency range was limited to 2560 Hz, because natural frequencies were excited with very low amplitudes and it did not allow to acquire any additional piece of information.

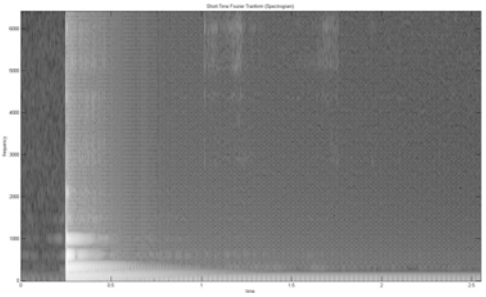
Fig. 4. STFT spectrogram of undamaged sample

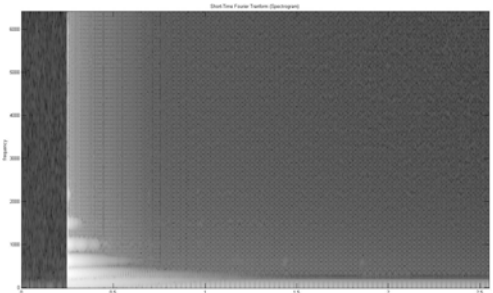
Fig. 5. STFT spectrogram of sample with fiber discontinuity

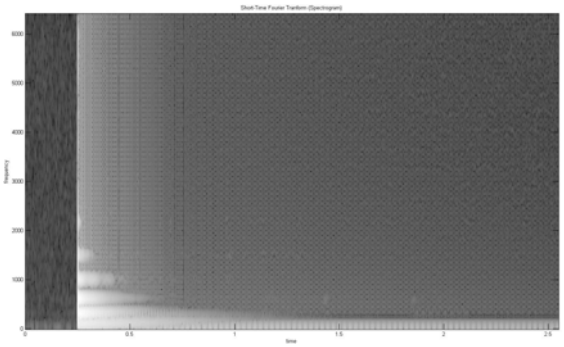

Fig. 6. STFT spectrogram of sample with delaminations

The scaleograms (Fig. 7 – Fig. 9) were prepared in direct visualization mode and transformed from scale representation to frequency representation using the formula (1). In the scaleograms the differences between undamaged and damaged samples are clearly visible. It shows that the excited natural frequencies of the damaged samples are damped lower than undamaged sample. Also, the differences can be observed in the frequency range 1000-1500 Hz. In case of the undamaged sample, frequencies in this range were excited also after impact impulse and shows alternate behavior, but in case of fiber discontinuity damage frequencies in this range were excited after pause and in case of delamination it is mostly damped.

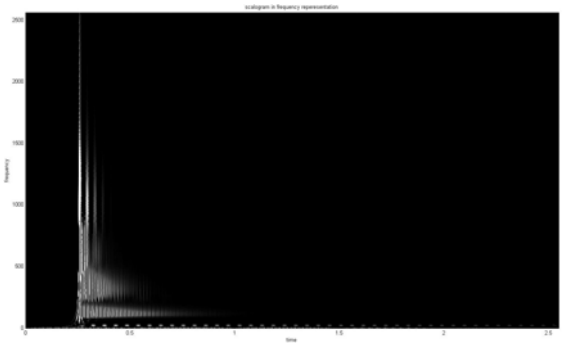

Fig. 7. CWT scalogram of undamaged sample

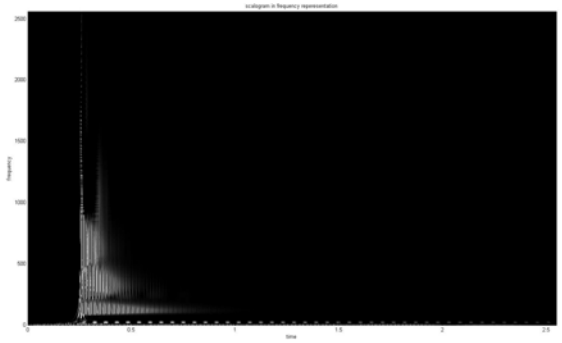

Fig. 8. CWT scaleogram of sample with fiber discontinuity

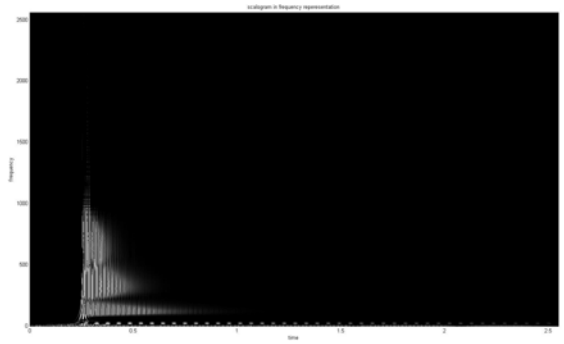

Fig. 9. CWT scaleogram of sample with delaminations

Basing on the scaleograms shown one can conclude about high sensitivity of the method and to assume the usability of the method for faults identification of the above-mentioned types. The quantitative evaluation can be calculated using degree of scaleogram concentration factor [1].

5. USABILITY OF THE METHOD FOR LIGHT-DAMAGED STRUCTURES

If the structure is on early damage phase, the scaleograms often do not show differences clearly as well. Therefore, the multilevel decomposition analysis was performed. The main idea of the analysis was presented in Fig. 10. and formula (4).

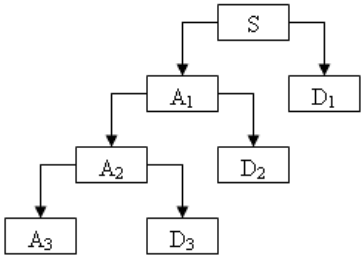

Fig. 10. Idea of multilevel decomposition [8]

$$S = A_n + \sum_{i=1}^{n} D_i \,, \tag{4}$$

In the proposed approach the detail parts of decomposition were analyzed. Five cases of faults location and two cases of notch depth were observed. In the first and second case the notch with 0,25 mm and 1 mm depth was located on XY surface at the distance 150 mm by Y, in third and fourth case notches were placed at the distance 220 mm by Y and in fifth and sixth case they were oriented angularly (60^0) starting from 207 mm to 215 mm. In other cases the notches with depths 0,5 mm and 3 mm were placed on XZ surface on distance 200 mm by X and on YZ surface on distance 12,5 mm by Y.

After decomposition of the signal of the undamaged sample the biased autocorrelation of detail parts was processed. Then, detail parts of signals wavelet spectrum of damaged samples were cross-correlated with the undamaged sample. Results

were grouped by notches location. As an example the results concerning the last two cases were shown in Fig. 11 and its detail in Fig. 12.

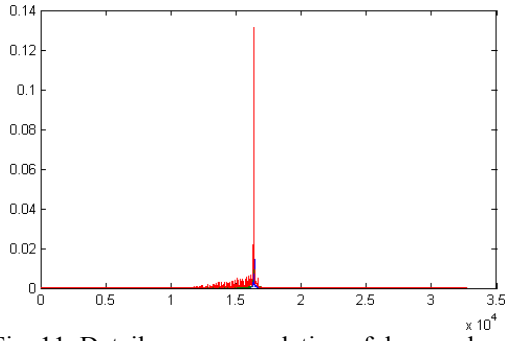

Fig. 11. Details cross-correlation of damaged and undamaged samples

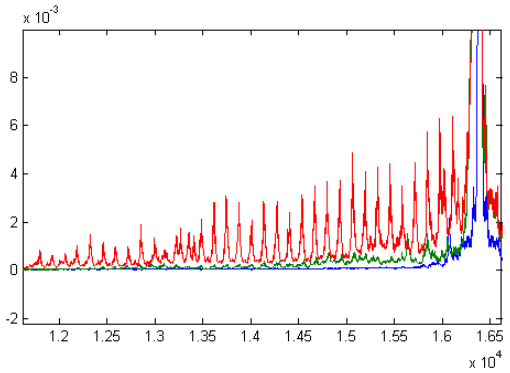

Fig. 12. Fragment of details cross-correlation from Fig.11

As the research shows, the detail parts of WT spectra damage samples have higher correlation factor, local maxima (Fig.12) near the main peak (Fig.11) and higher peak value. This regularity was confirmed in all the considered cases. For quantitative scalar evaluation CFV (correlation fault values) given by (3) were calculated and presented in Table 2. On higher levels of decomposition the CFV is quite different. Therefore the statistical normalization must be included into the algorithm.

Table 2. Correlation fault values.

Case No.	Sur-face	Fault localization [mm]	Notch depth [mm]	CFVs
1.	-	-	-	0
2.	XY	X: 150, Y: 0	0,25	$4{,}8\cdot10^{-3}$
3.	XY	X: 150, Y: 0	1	$6{,}1\cdot10^{-3}$
4.	XY	X: 220, Y: 0	0,25	$2{,}5\cdot10^{-3}$
5.	XY	X: 220, Y: 0	1	$2{,}6\cdot10^{-3}$
6.	XY	X: 207, α: 60^0	0,25	$2{,}4\cdot10^{-3}$
7.	XY	X: 207, α: 60^0	1	$7{,}6\cdot10^{-3}$
8.	XZ	X: 200, Z: 0	0,5	$7{,}8\cdot10^{-4}$
9.	XZ	X: 200, Z: 0	3	$8{,}0\cdot10^{-4}$
10.	YZ	X:250,Y:12,5	0,5	$1{,}8\cdot10^{-3}$
11.	YZ	X:250,Y:12,5	3	$3{,}2\cdot10^{-3}$

The results were presented for the first level of decomposition. On the higher levels the regularity of correlation differences was confirmed. In Figs. 13 – 16 the results of cross-correlation for higher levels of decomposition are presented.

Basing on the obtained results (Table 2.), tone can conclude about different sensitivity of the proposed fault detection algorithm with respect to the fault placement and its size. The sensitivity is good enough when the fault is placed on XY surface (compare CFV for cases 2-7 in Table 2.) and on surface YZ (cases 10, 11 in Table 2.), but poor enough when the fault is placed on XZ surface (cases 8, 9 in Table 2). In the case 8 and case 9 the algorithm is less sensitive and gives underestimated evaluation. The phenomenon can be interpreted by natural frequency shifting in frequency response of the investigated structure.

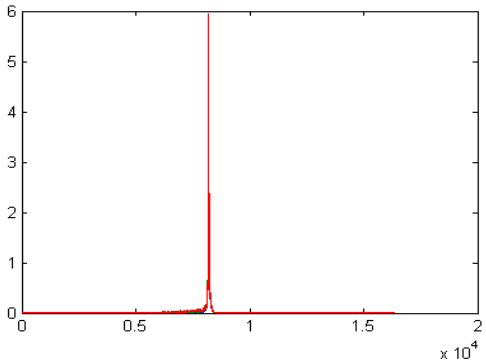

Fig. 13. Details cross-correlation of damaged and undamaged samples on 2nd decomposition level

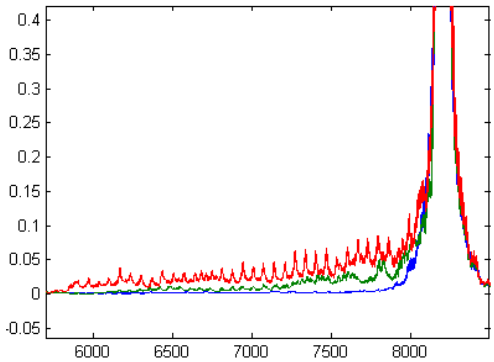

Fig. 14. Fragment of details cross-correlation on 2nd decomposition level

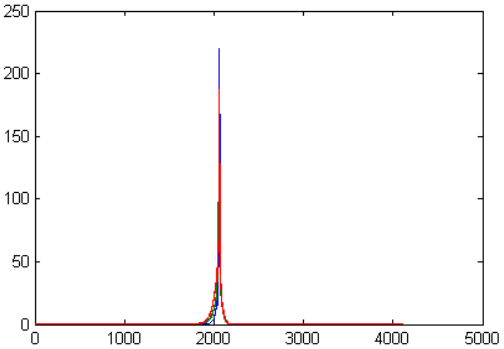

Fig. 15. Details cross-correlation of damaged and undamaged samples on 4th decomposition level

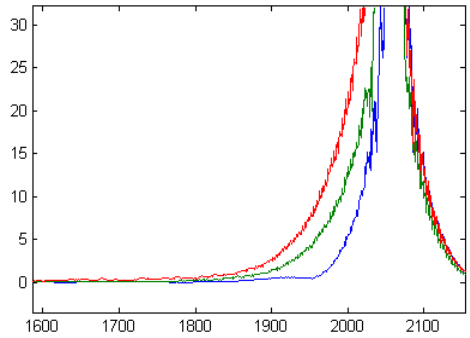

Fig. 16. Fragment of details cross-correlation on 4th decomposition level

On higher levels of the decomposition the regularity of obtained CFVs were similar. In few cases on higher levels of decomposition the CFVs for smaller faults were shown lower sensitivity of the method. After carrying out the investigation tone can conclude that the first level of decomposition gives best results for CFVs calculation. In higher levels there is a decreasing tendency of set length in detail parts and, according to this, set length in cross-correlation; the accuracy of CFVs were lower than in first level of the decomposition.

6. CONCLUSIONS AND REMARKS

The research presented in this paper proves the possibility of incipient fault detection in composite layered structures. As the results show, the proposed algorithm can be used for detection of even smallest faults, when the structure is on early damage phase in contrast to known and applied methods of signal processing. On the cross-correlation charts the faulty specimens can be recognized. For evaluating scalar values that are symptoms of faults the new metrics was introduced. The value of this metrics allows detecting faults not less than 10^{-3} CFV, so that it can be used as the lower threshold limit for faults detection.

Our next research will be targeted on the other types of faults as described in the Chapter 5. This research concerned only the surface faults, while in the future research the internal faults will be detected. Moreover, the temperature influence and structure behavior with different types of faults during fatigue processes will be detected.

REFERENCES

[1]. Katunin A., Moczulski W.: *The conception of a methodology of degradation degree evaluation of laminates*, Maintenance and Reliability, 1 (41), Warsaw 2009, pp. 33-38.
[2]. Timofiejczuk A..: *Methods of non-stationary signal analysis* (in Polish), Silesian University of Technology Publishing House, Gliwce 2004.
[3]. Katunin A., Jaroszewicz J.: *The method of faults detection in composite plates based on natural frequency of vibrations evaluation* (in Polish), VII Conference „Energy in Science and Technology", Suwalki 2008, s. 286-296.
[4]. Wysogląd B.: *The Method of Early Detection of Bearing Failures Using Wavelet Transform, Accoust*. and Vibr. Surveil. Meth. and Diagn. Tech., Compiegne, 2001, pp. 675-682.
[5]. Zhang L., Gao R. X.: *Spindle health diagnosis based on analytic wavelet enveloping*, IEEE Transactions on Instrumentation and Measurement, 55, 5, 2006, pp. 1850-1858.
[6]. Tomonori K., Sadayuki U.: *Impact Damage Evaluation of CFRP Laminate Using Discrete Wavelet Transform*, Nihon Kikai Gakkai Nenji Taikai Koen Ronbunshu, 1, 2006, pp. 591-592.
[7]. MATLAB 7.1. Wavelet Toolbox.
[8]. Misiti M., Misiti Y., Oppenheim G., Poggi J.: *Wavelet Toolbox User's Guide*. The MathWorks Inc., 2nd edition, 2002.

Andrzej KATUNIN is scientific assistant in the Department of Fundamentals of Machinery Design at the Silesian University of Technology in Gliwice His main area of interest includes FEM numerical analyses, mathematical modeling of continuum mechanics, signal processing and diagnostics of laminate composites.

Wojciech MOCZULSKI is full professor in the Department of Fundamentals of Machinery Design at the Silesian University of Technology in Gliwice, Poland. His research is focused on: design and operation of the machinery, computer science, mobile robotics, and particularly on machinery diagnostics and application of methods and means of Artificial Intelligence. He is author and co-author of over 180 publications. He has been founder and currently is a member of the Central Board of the Polish Association of Technical Diagnostics, and member of several sections of Committees of Mechanics, Mechanical Engineering, and Automatics and Robotics of the Polish Academy of Sciences.

ANALYSIS OF AE-SIGNAL GENERATED DURING THE MICROHARDNESS MEASUREMENT

Anna PIĄTKOWSKA[1], Irena POKORSKA[2]

[1]Institute of Electronic Material Technology, Wólczyńska 133, 01-191 Warsaw
e-mail: Anna.Piatkowska@itme.edu.pl
[2]Institute of Precision Mechanic, Duchnicka 3, 01-796 Warsaw

Summary

This paper presents the results of the measurements of microindentation using Vickers' indenter. The research was carried out with the system: the Cr layer layer deposited on silicon substrate and glass substrate. At the same time as the measurement of microindentation acoustic emission signals were recorded. The results of microindentation forces in the form of load-displacement curves and registered AE-time characteristics of the AE signals were compared with the SEM images of indentation. During the measurements, "burst" effects were observed as discontinuities of loading curve, that correlate with AE impulses. Rise of the maximal load resulted in the increase of damage and caused multiplication of AE pulses. Due to the fact the Cr layer was thin, most AE pulses were generated during the damaging of Si substrate. During the microindentation on Cr-glass system the transient AE signals were not registered.

Keywords: microindentation, acoustic emission, Cr layer.

ANALIZA SYGNAŁU EA GENEROWANEGO PODCZAS POMIARÓW MIKROTWARDOŚCI

Streszczenie

W pracy zostały przedstawione wyniki pomiarów mikrotwardości z zastosowaniem wgłębnika typu Vickers. Badania przeprowadzono na próbkach z warstwą Cr na podłożu krzemowym i szklanym. Podczas pomiarów mikrotwardości jednocześnie rejestrowano generowane sygnały emisji akustycznej. Następnie porównano wyniki w postaci krzywej obciążania oraz sygnały emisji akustycznej i obrazy SEM odcisków wgłębnika. Zaobserwowane na krzywej obciążania nieciągłości zostały powiązane z pojawieniem się impulsów EA. Wzrost maksymalnego obciążenia wywołał zwiększenie liczby impulsów EA, odpowiednio do stopnia uszkodzenia materiału. Z analizy wykresów wynika, iż większość rejestrowanych uszkodzeń zachodziła w podłożu krzemowym. Pomiary mikrotwardości warstwy Cr na podłożu szklanym nie wywołały impulsowych sygnałów EA.

Słowa kluczowe: mikrotwardość, emisja akustyczna, warstwa Cr.

1. INTRODUCTION

In order to decrease the length scale in technological applications, one needs to develop instruments and techniques capable to characterize mechanical properties of materials and able to register the phenomena occurring with sub-micrometrical resolution.

The microhardness is a very important property for hard thin films employed for applications in micromechanical systems.

Typically, during the microindentation the load and unload displacement curves are registered. The value of the hardness is calculated from the unload data by using the Oliver and Phar method. This calculation was developed for monolithic materials, therefore in the case of the metallic thin films the measurements of mechanical properties become more difficult. Particularly measurements of thin layers require very small depth of indentation. Sometimes it is impossible because of the technical realization or incompatibility with surface state of samples. Mismatch of the measurements conditions leads to substrate interactions on the indentation response of thin films.

The second group of problems affecting the measurement result is the existence of a number of phenomena during penetration, such as: pop-in, pile-up, cracking, delamination.

Knowledge of the presence of any of these perturbations is very helpful in assessing the value of hardness and Young's module. Print indentation imaging using SEM is not always sufficient for microhardness analysis, hence other measurement methods that can provide information on indentation data have been searched. Failure events in brittle materials are accompanied by abrupt changes in stress and strain fields, which lead to the generation of transient elastic waves in the form acoustic emission. The real time monitoring of acoustic emission can then be used as a qualitative and quantitative diagnostic method [1].

Acoustic Emission (AE) is often adopted as an indicator of on-line damage detection and

registration of AE signals can be used to evaluate the phenomena occurring during indentation. Previous studies of AE generation in the course of penetration related cracking length to the amplitude of signals and evaluated the adhesion of thin films to substrate[2, 3]. Acoustic emission during indentation loading provided essential information in predicting what mode of failure occurs, as for example: the substrate cracking, the film cracking and localized detachment, the film delamination and its propagation [4].

The aim of this study is the presentation of the AE-signals recorded in the course of the microindentation. The analysis of AE-signals can allow a detailed description of the phenomena occurring during loading and unloading of the microindenter. The collected AE-data will be compared with load-displacement curves and with the SEM images of indentation.

2. EXPERIMENTAL DETAILS

The thin film of chromium 2µm thick was deposited on Si-wafer polished substrate of 500µm thickness and on glass-substrate of 4mm thickness. The measurements of microindentation were carried by a commercial CSM Micro Hardness Tester equipped with Vickers' indenter. The maximum forces applied in the measurements were: 500mN and 1000mN. Loading and unloading times were 30s and total time of indention was 75s. The indenter approaching to the sample surface, loading with a given speed, the period of the force stabilization and unloading are automated.

AE signals were registered by AE-sensor with frequencies range of 60 – 1950 kHz. AE-sensor was fixed to the surface of the sample in 15mm distance from the zone of indentation. A detailed description of the measurement track is presented in the publication [5].

In this paper the results of values of hardness are not discussed because maximal depth of indentation is not correctly adapted for 2µm layer. With Buckle principle the maximal depth should be 1/10 of layer's thick, in this cause that is 200nm. Rise of indentation depth up to 200nm cause the influence of substrate.

The results of the AE measurements depend in the first place on the value of the maximum load and of the type and size of damages. AE signals are characterized by very small amplitudes and short duration time. In this work we propose extraction of amplitudes of AE signals whose values are above the noise level.

3. RESULTS AND DISCUSSION

Figure 1 shows the results of microindentaion and AE-signals obtained during the measurement on Cr-layer deposited on Si-substrate.

For maximal load of 500mN the 1.10µm depth of penetration was obtained. Loading-displacement curve (Fig. 1a) is almost regular. Small discontinuities are marked by circles numbered 1…5. Figure 1b shows changes of depth and the AE-impulses in time domain. It is clear that these burst 1…5 are related with registered AE-impulses. The first AE transient occur when indenter attained of 800nm depth. Next AE-impulses arose during loading and stopping stage. The last transient is related to the perturbation during the indenter removal. To summarize, during this indentation the 14 AE-count are registered. Duration time of AE-impulses is correlated with their amplitude. Typically, duration times were from ~0.1ms to ~1ms.

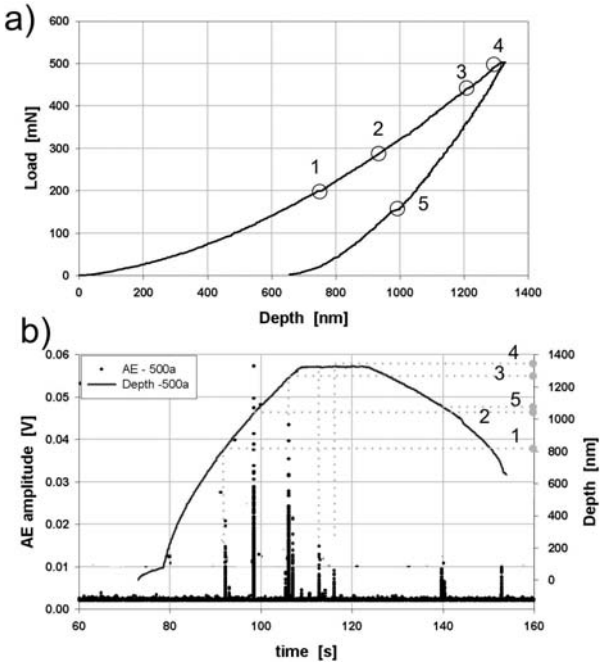

Fig. 1. The microindention results on the Cr-layer on Si-substrate for 500mN load: a) load-displacement curve, b) acoustic emission data and depth-time curve

The increasing load up to 1000mN was intended to increase the depth of penetration into the layer-substrate interface. Figure 2 shows the results of microindentation and AE-emission.

In this cause (Fig. 2a), number of discontinuities on displacement-depth curve was smaller then for 500mN load. The graph contains the zooming of the curve, with the discontinuities. First burst is registered at the depth of penetration of 550nm and is associated with first AE-transient amplitude of 0,018V. Two next discontinuities occurred at depth of 1440nm and 1800nm. Their appearance is accompanied by the maximal amplitudes of the AE pulses: 0,20V and 0,16V. During the measurement with 1000mN load we registered of 24 AE-counts, with 21 counts during loading-stage. STFT characteristics are calculated for the subsequent pulses. Figure 3 shows AE-transient with maximal amplitude in time and frequencies domain.

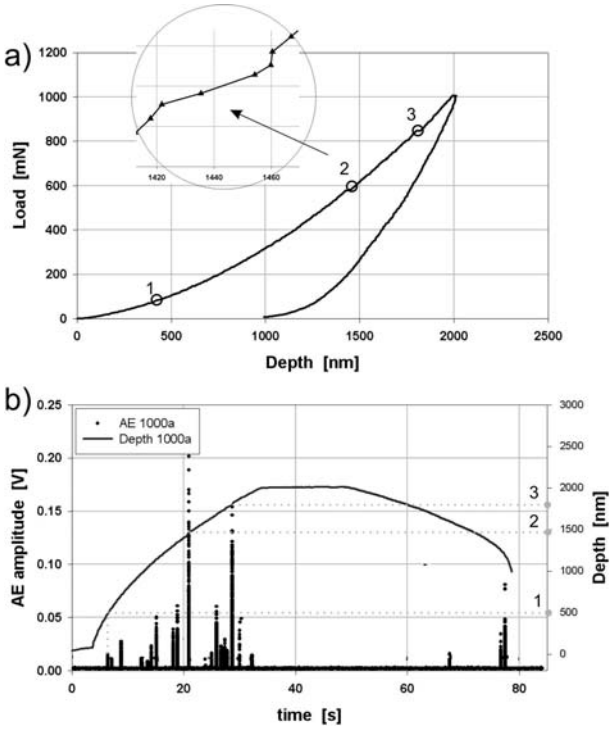

Fig. 2. The microindention results on the Cr-layer on Si-substrate for 1000mN load: a) load-displacement curve, b) acoustic emission data and depth-time curve

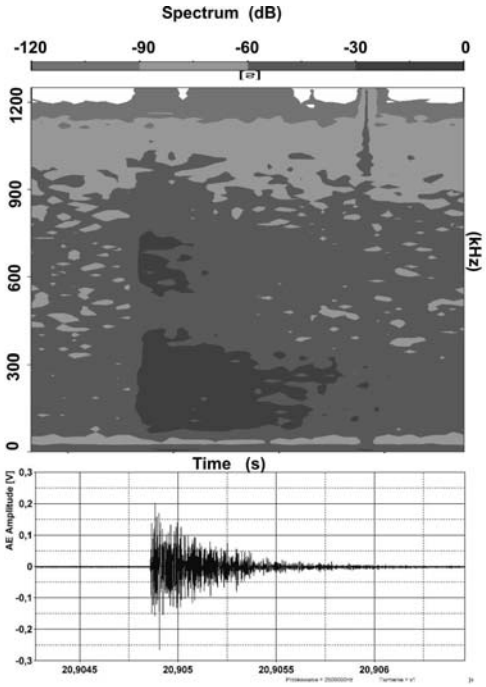

Fig. 3. The AE-transient with maximal amplitude in time and frequencies domain

This impulse time duration is 0,93ms. The STFT diagram calculated for AE-impulse shows an increase of amplification of frequencies in the range of: 150-450kHz and ~600kHz. Similar results were obtained for most impulses, regardless of the amplitude and their duration time.

The comparison of SEM images of imprints shows Figure 4.

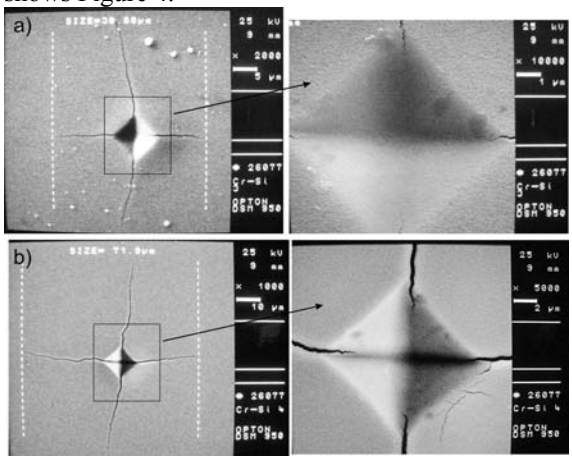

Fig. 4. SEM images of imprints for a) 500mN load, b) 1000mN load

Rise of maximal load of indentation intensified the damage of sample. The medial crack length for 500mN and 1000mN load are respectively: 30,88µm and 71,9µm. The 1000mN load causes submicrometric fissures on the outside and inside of area of indentation and the median cracks arrive on inside of imprint. In both conditions of indentation Cr-layer is not broken.

Identical indentation experiments were performed on Cr-layer on glass-substrate. Figure 5 shows the results for 500mN load.

The amplitude of AE-signal registered during indentation Cr layer deposited on glass is very small. We have not observed transient signal, only continuous signals are detected. One regularity is discovered. There is more AE activity during loading stage than unloading stage. The last impulse is related to the end of measurements and it demonstrates the correct operation of the AE-track.

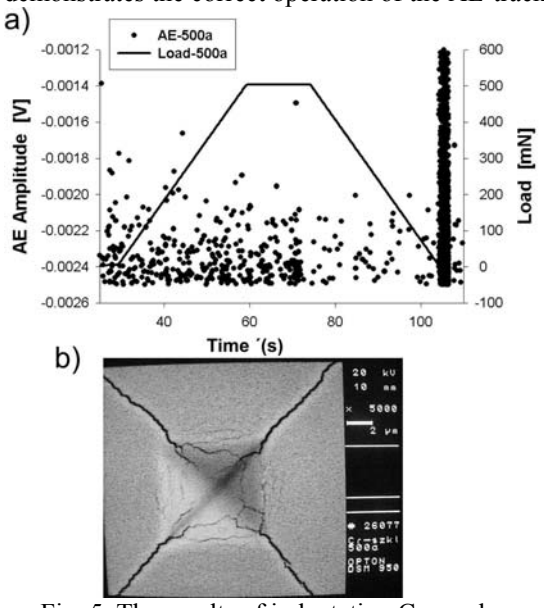

Fig. 5. The results of indentation Cr on glass, a)Load-time and AE-transient-time results for 500mN load b) SEM image of imprint

The imprint with median crack and submicrometric fissures in the penetration area presented on Fig. 5 is typical for all measurements. There is no significant difference between the effects of increased forces of indentation.

4. CONCLUSION

In microhardness studies presented on Cr layer on Si substrate we registered numerous AE impulses (transients). Amplitudes of first impulses were low or average value compared with the maximum. These transient arise at a depth of 500-800nm and can be linked to the medial crack of Cr layer. Consecutive pulses, particular those with the largest amplitudes can be linked to the destruction of Si substrate. The Si wafer is characterized by low resistance to concentrated forces and break easily along the crystallographic plane. Long and intense cracks of Si cause weakening of the material and slip of indenter with no or slight increase of loading force. It appears as the discontinuity of load-depth curve. During unloading the transfer of Si damaged fragments takes place and hence a few AE transients appear in this phase of the indentation. Note that, the damage of Si substrate does not appear in SEM images of imprints. The absence of a signal pulse for Cr layer on glass appears to be caused by a type of substrate and by an absence of glass failure. Similar AE-results have been published in the literature [4]. The medial cracks of Cr layer are not the origin of AE transient. There are sources of low increase of AE continuous signal.

Parameters such as the load size, surface condition, local pollution, the destruction of the wear products and formed cracks play a significant role especially in the emerging number of AE pulses and their amplitude. It was possible to detected the failure of substrate for presented AE set-up. It seems that placing the sensor in the head or under the sample would increase the sensitivity of AE measurements.

REFERENCES

1. Dyjak P., Singh R. P.: *Acoustic Emission analysis of nanoindentation-induced fracture events*, Experimental Mechanics 46 (2006) 333-345.
2. Belmote M., Fernandes A. J. S., Costa F.M., Oliveira F. J., Silva R.F.: *Acoustic emission detection of macro-indentation cracking of diamond coated silicon*, Diamond and related materials 12 (2003) 1744.
3. Dietiker M., Nyilas R. D., Solenthaler Ch., Spolenak R.: *Nanoindetation of single-crystalline gold thin films: Correlating hardness and the onset of plasticity*, Acta Materialia 56 (2008) 3887.
4. Qi Hua Fan, Gracio J., Nasar Ali, Pereira E.: *Comparison of the adhesion of diamond films deposited on different materials*, Diamond and related materials 10 (2001) 797-802.
5. Piatkowska A. Piatkowski T.: *Measurements and analysis of acoustic emission in the tribological system ball-on-disc,* Diagnostyka Nr4 (44) 2007

Anna PIĄTKOWSKA is a specialist in the micro- and nano-tribological research. She obtained a doctoral degree (Ph.D) from the Institute of Electronic Materials Technology, where she is an assistant professor. Her principal research subjects are: ion implantation, micro-, nano-mechanical and structural properties of implanted materials. Dr Piątkowska is a member of Polish Society of Tribology.

Irena POKORSKA is a specialist in the developing techniques for testing the mechanical properties of the surface layers and coating methods. She obtained a doctoral degree (PhD) from the Faculty of Materials Science and Ingineering. Of Warsaw Univesity of Technology.

THE MEASUREMENT OF SHELL'S ELASTIC OVALITY AS ESSENTIAL ELEMENT OF DIAGNOSTIC OF ROTARY DRUM'S TECHNICAL STATE

Maciej ŚWITALSKI

Uniwersytet Technologiczno-Przyrodniczy im. Jana i Jędrzeja Śniadeckich w Bydgoszczy,
Wydział Inżynierii Mechanicznej, Instytut Mechaniki i Konstrukcji Maszyn, Zakład Mechaniki Stosowanej
85-796 Bydgoszcz, ul. Kaliskiego 7, fax 52 340 82 50, maciej.switalski@utp.edu.pl

Summary

In the article the author carries out classification of the typical rotary drum shell's deformations. He shows the cyclic elastic distortion of shell's cross-section as one of the most essential and particularly important from the fatigue life and from the durability of plant's internal lining point of view. He describes the method and device to measurement it and he characterizes basic diagnostic parameters, such as degree of shell section's elastic ovality and curve of ovality. On example of data received from two rotary kilns' measurements, he shows possibilities and the effectiveness of the method in the range of finding the basic damages' symptoms concerning drum's main elements, i.e. its support system and its shell.

Keywords: elastic deformation, ovality, rotary drum, shell.

POMIAR SPRĘŻYSTEJ OWALIZACJI PŁASZCZA JAKO ISTOTNY ELEMENT DIAGNOSTYKI STANU TECHNICZNEGO WALCZAKA OBROTOWEGO

Streszczenie

Autor w artykule dokonuje klasyfikacji odkształceń płaszcza typowego walczaka obrotowego. Wskazuje cykliczne deformacje sprężyste przekroju płaszcza za jedne z najbardziej istotnych i szczególnie ważnych z punktu widzenia zmęczeniowej trwałości powłoki oraz z punktu widzenia trwałości wewnętrznej wykładziny obiektu. Opisuje metodę i urządzenie do ich pomiaru oraz charakteryzuje podstawowe parametry diagnostyczne, takie jak stopień sprężystej owalizacji przekroju i krzywa owalizacji. Na przykładzie danych pozyskanych z pomiarów dwóch obrotowych pieców, wskazuje możliwości i skuteczność metody w zakresie wychwytywania symptomów podstawowych uszkodzeń, dotyczących kluczowych elementów walczaka, tj. jego układu nośnego i jego płaszcza.

Słowa kluczowe: sprężyste odkształcenia, owalizacja, walczak obrotowy, płaszcz.

1. INTRODUCTION

The shell, in the form of the thin-walled steel pipe with horizontal or close to horizontal location of axis, is the basic component of typical rotary drum. The rotation is the main movement of this object, including its shell. This movement is realized thanks to the rings, which together with the pipe placed in them, roll on the pairs of rollers - subordinated to each ring. It constitutes something of the support system for the shell and simultaneously it is the stiffener of this relatively flexible construction.

The amount of the pairs of rollers equals the amount of rings and holds in the scope from 2 to 4 - the most often. The length of the pipe (shell) achieves a few dozen, and its diameter - several meters. The general scheme of this type object is presented in figure 1.

The production tasks, which rotary drums realize, were listed in the study [4]. They are very essential. In the case of many enterprises we can judge them as the core of activity.

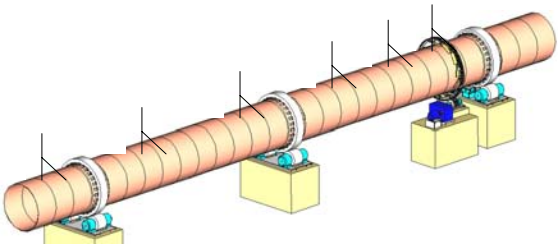

Fig. 1. General scheme of 3-piers (rings) rotary drum:
1 – support system (rings and support rollers),
2 – shell (coat),
3 – drive section (motor, reducer and open gear)

Cement plants and kilns for production of clinker situated there, are distinct example of this situation. Both, from this important reason, as well as taking the high costs of repairs into consideration, the this type machines should be subjected to increased discipline of technical supervision, and the evaluation techniques of their technical state should include as wide as possible spectrum of effective diagnostic methods and data.

Unfortunately, because of the low rotational speed (only up to several revolutions per minute), considerable dimensions and more than once very high temperature of the external surface of the drum's shell (even up to 350^0C), diagnostic tools - applied universally - have strongly limited application in this case. All activities aiming both to response.

the adaptation of classic diagnostic methods (in the field of vibro-diagnostic analysis or in the field of measurements of geometrical parameters) and to the study of completely new ways and measurement-analytic tools, are very desirable and particularly expected by operators of these big machines.

This article presents the description of the one of such innovatory methods and exactly the way, which was worked out by Swedish diagnostician - the most probably in fiftieth years the 20-th century [6]. However this method did not gain in common acceptance in the industry then. Attempts of device's implementation of prototypes basing on this way, undertook in the farther future, also in Poland [1], did not meet with the positive market

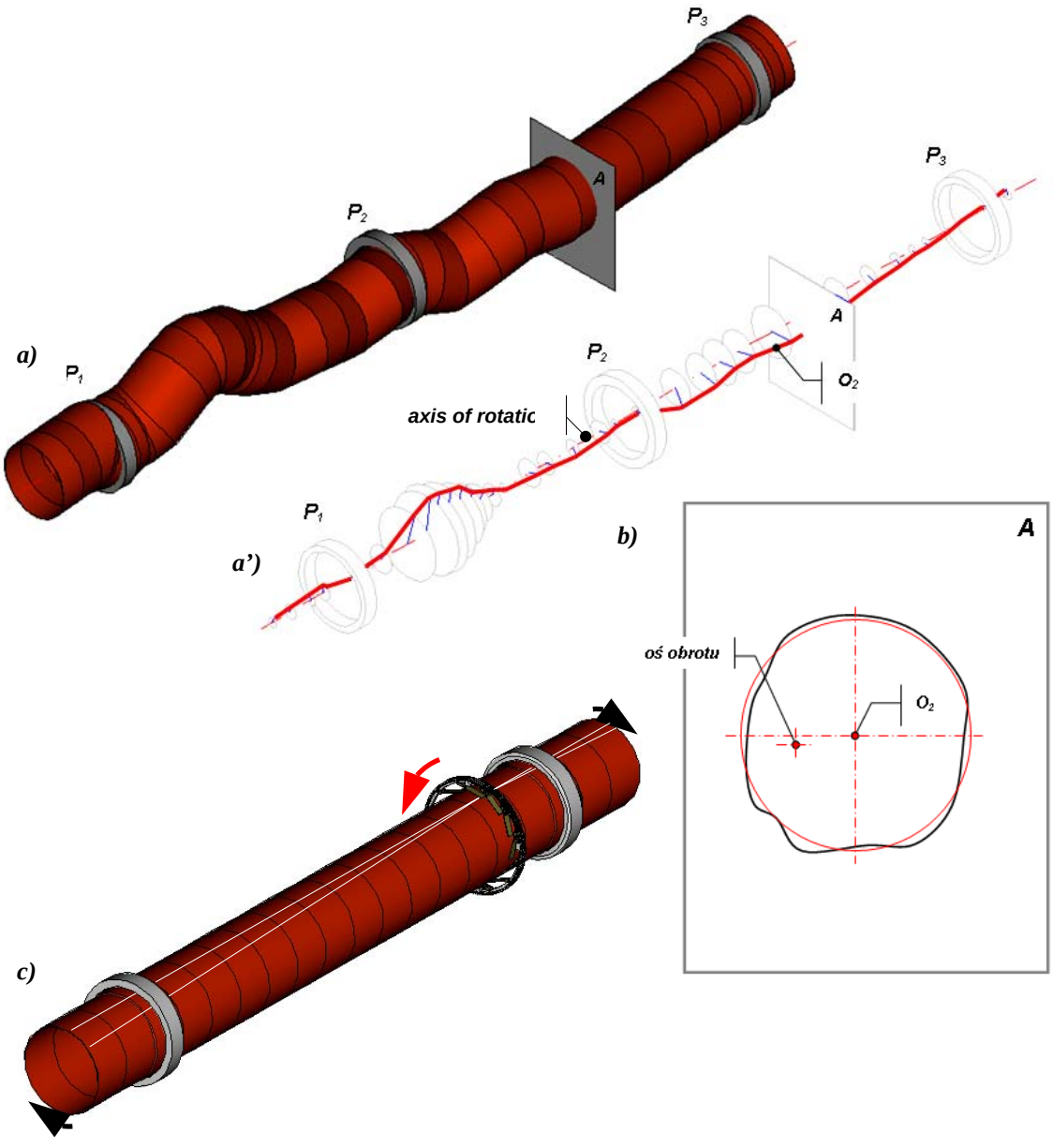

Fig. 2. Schemes of shell deformations' shapes: a) view of bended pipe, a') geometrical axis bending (scheme of O_2 pipe axis o bending of), b) deformation of selected cross-section A (sheet metal plate bending), c) torsion of pipe profile

The most probably, this fact should be connected with then technical level - limited in the relation to the present state. The current development of the technique, especially in the area of electronic devices, allows author to revive and by the way effectively enrich it by new useful possibilities.

The following contents of the article includes theoretical bases and proof of diagnostic effectiveness both the idea as well as the device. It is indispensable to understand the sense of the method
of measurement of rotary drum shell's elastic deformation during object's normal operation and to understand the idea of the instrument designed and implemented by the author to this end.

2. THE TYPES OF THE DEFORMATIONS OF THE ROTARY DRUM'S SHELL

We can classify the deformations of the typical rotary drum's shell according to the three main criterions of: form, reason and permanence of theirs appearance. According to the first of them, we can list (fig. 2):
- deformations of shell's geometrical axis O_2 (pipe's axis bending – figures: 2a and 2a'),
- deformations of cross-sections (shell's sheet metal plate bending – figure 2b),
- torsion of pipe profile (figure 2c).

Next, according to the reason criterion, we can list:
- deformations caused by mechanical factors (incorrect manufacturing of component elements, incorrect assembly, external and self-weight loads),
- deformations caused by thermal factors (e.g. by unequal distribution of temperature – no-uniform on shell's circumference).

All of these deformations, mentioned above, we can additionally classify according to permanence of theirs appearance. From this point of view we can list:
- permanent (plastic) deformations,
- temporary (elastic) deformations,

moreover elastic strains can have a cyclic (if they are synchronized with the object's rotation) or non cyclic character (if theirs values are independent on shell's turns).

3. THE ELASTIC OVALITY OF SHELL'S CROSS-SECTION AND ITS CONSEQUENCES

Deformations of shell's cross-section - elastic and periodically variable, are one of the least desirable and simultaneously the most difficult to the quantitative determination. These deformations are caused by mechanical factors the most often, less by thermal. The under-ring shell's sections are the places, where it occurs in the most intensive intensity. In these places the elastic shell, mounted with the play inside the ring, changes (self-adjust) its shape to quasi-circular inside diameter of ring. It happens under the influence of shell's self weight and the weight of the internal lining [5]. This adjustment takes place at the bottom and at the side parts of pipe profile. The shell undergoes clear flattening in its upper area and the value of its curvature radius violently grows up there. Schematically, this situation was shown on figure 3.

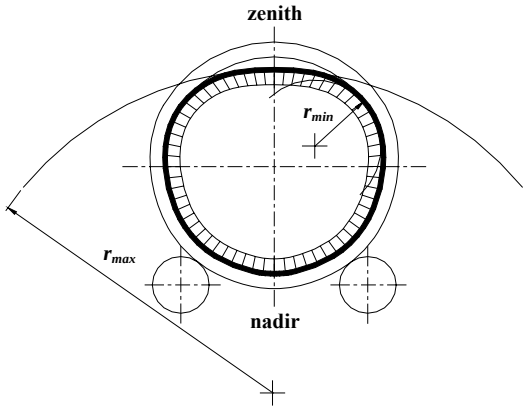

Fig. 3. Scheme of drum's shell cross-section, where shell's radius changes from minimal value r_{min} to maximal r_{max}

Thus, during the turn of the object, every point connected with the surface of the shell migrates not on the circle, but over the distorted outline, whose radius of the curvature has different value for every next circumference position of this point. The relative changes of the radius in the function of the angle of the object's rotation can be shown in the form of the graph, how this is presented on drawing 4. These changes of radius mean that the sheet metal plate of the shell undergoes cyclic bending, and this means also that shell's durability should be considered in the aspect of fatigue strength of the applied material.

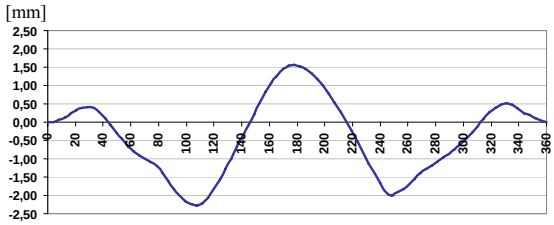

Fig. 4. The example graph of relative changes of curvature's radius as function of drum's rotation angle

The cyclic changes of the radius of the shell's sheet metal plate also have the influence on durability of the object's internal lining (if the object is equipped with such one). The best, it can be illustrated for furnace lining in the form of wedge-shaped bricks with tapers adapted to nominal - shell's inside diameter. Mainly, such brick lining is applied in rotary kilns.

In the situation when drum turns, his shell undergoes deformation and forces - tensioning and compressing - act on the lining alternately (look at figure 5).

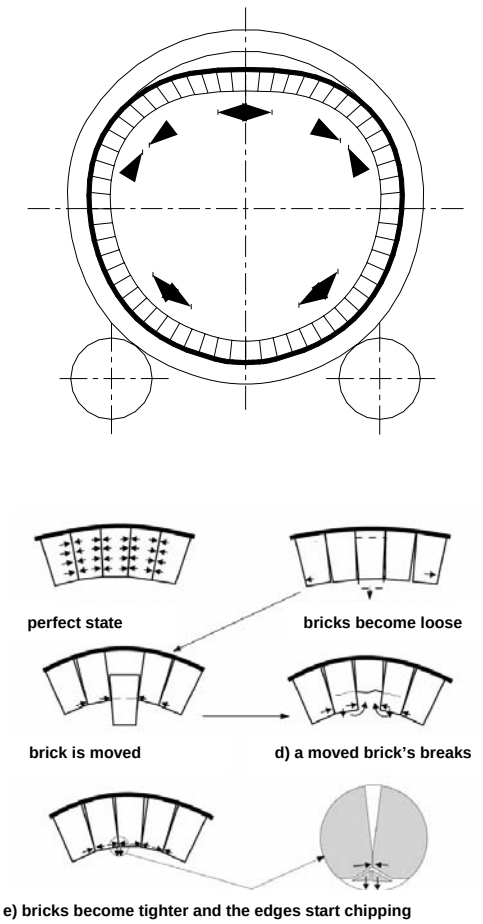

Fig. 5. Scheme of mechanical interaction on rotary kiln's brick lining - example mechanisms of lining's degradation [2]

In connection with intensity of this phenomenon, such alternating forces can lead to the brick falling out or chipping out. Typical mechanisms of lining degradation are shown in figure 5. Figure 3a represents a perfect situation, that is when the shell is not deformed and bricks correctly adjoin each other. The distribution of forces in the contact areas between the bricks is then correct. Figure 3b shows a situation when the radius of curvature increases excessively, the load on the surface of the bricks decreases, and even the gaps between them become wider. When the shell radius becomes large enough, the bricks may move /3c/ or even fall out totally. When a brick falls out, the adjacent bricks become loose, so in consequence it might lead to an extensive reduction of the lining, thus exposing the steel drum shell to high temperatures. If a loosened brick does not fall out but stays in place (fig. 3c), when the circumferential position of the facility changes then as a result of the reducing radius of curvature it will undergo compression (still look at fig. 5c). Such a situation might cause the braking of the moved brick in the cross-section compressed by the edges of adjacent bricks and the chipping out of a large portion of this one. The remaining part will resume its original position, but the lining in this area is already significantly thinner (fig. 5d). In case of smaller radius changes or better fit of the bricks (smaller initial play at installation), the movement of the bricks is limited, but chipping can also be observed. In this latter case, the chipping is caused by micro-losses in the areas of local accumulation of loads – on the edges. This situation is shown in figure 5e.

Degradation mechanisms, presented above, are chosen examples only.

To summarize, the phenomenon of cyclic change of the radius of curvature in the shell cross-section has a detrimental impact on both the life of the shell plate and on the life of drum's internal lining. The said strain is unfortunately inevitable, especially because of the frequent and necessary from the design point of view loose fit between the shell's outside diameter and the support ring's inside diameter. A periodical monitoring and keeping the strain as small as possible is consequently the only method to extend the life of trouble-free drum operation in this area.

Very useful estimator uses to evaluate the elastic strain of the shell cross-section is the parameter called in the scientific literature the elastic shell ovality ratio [3]. The definition of this parameter is based on assumption, that a deformed cross-section of the shell can be sufficiently approximated by an ellipse, i.e. a particular case of geometric figure from general collection of ovals. Then the degree of flattening (ovality) of an ellipse can be described by the following formula:

$$\omega = 2(a - b) \tag{1}$$

where:
a and b – length of ellipse semi-axes, suitably major and minor (look at fig. 6).

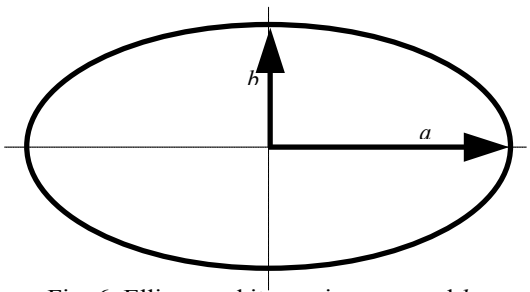

Fig. 6. Ellipse and its semi-axes a and b

In the reality, the form of the shell cross-section's deformation is more complicated, i.e. ideal symmetry between the individual half of the ellipse is not kept and the angle between the maximum and minimum position of radius doesn't equal 90^0 (go back and look at fig. 3). That is why in

reference to the section of drum's shell, generalized ovality has been assumed to present by the formula:

$$\omega = 2(r_{\max} - r_{\min}) \tag{2}$$

where:
r_{max}, r_{min} – cross-sections' radiuses, suitably maximal and minimal (look at fig. 3).

However, the diagnostic parameter, defined in a such way, is still uncomfortable for use. It doesn't give the possibilities of comparison of objects with considerably different dimensions i.e. different shell's diameters. In order to eliminate this shortcoming, parameter called ovality ratio was used [3]. This parameter presents quotient of ovality (mentioned above) and internal – nominal diameter of shell's cross-section. It is expressed by following formula:

$$\omega_0 = \frac{(r_{\max} - r_{\min})}{r} \cdot 100\% = \frac{2(r_{\max} - r_{\min})}{d} \cdot 100\% \tag{3}$$

where:
r, d – suitably, nominal radius and nominal diameter of shell's cross-section.

The measurement of elastic ovality or elastic ovality ratio is reduced to the determination of the volumes r_{max} and r_{min}, and to determination of relative difference between these radiuses - in principle. The nominal diameter of the shell is the well known value.

There are two methods of determination of difference between the maximum and the minimum radius: direct and indirect one. The direct method consists in determination of the small and large axis of the ellipse using geodesy manners. However this method is very labour-consuming, technically burdensome and sufficiently exact only for the large deformations of the cross-section. The indirect method consists in measurement of the maximum change of the deflection of the curvature - on the one meter long circumference's part - during drum's rotation. It is made using special device and calculating ovality ratio is based on simplified formula:

$$\omega_0 = \frac{4}{3} d\sigma \cdot 100\% \tag{4}$$

where:
d – inside, nominal diameter of shell's cross-section [m], σ – maximal difference of deflection of curvature [m], determined on chord 1-meter long ($L = 1m$), according to figure 7.

It is possible to find the derivation of above formula in the study [3]. The device is characterized in the next chapter, and it is the implementation of presented idea of measurement of shell's cross-section's elastic ovality.

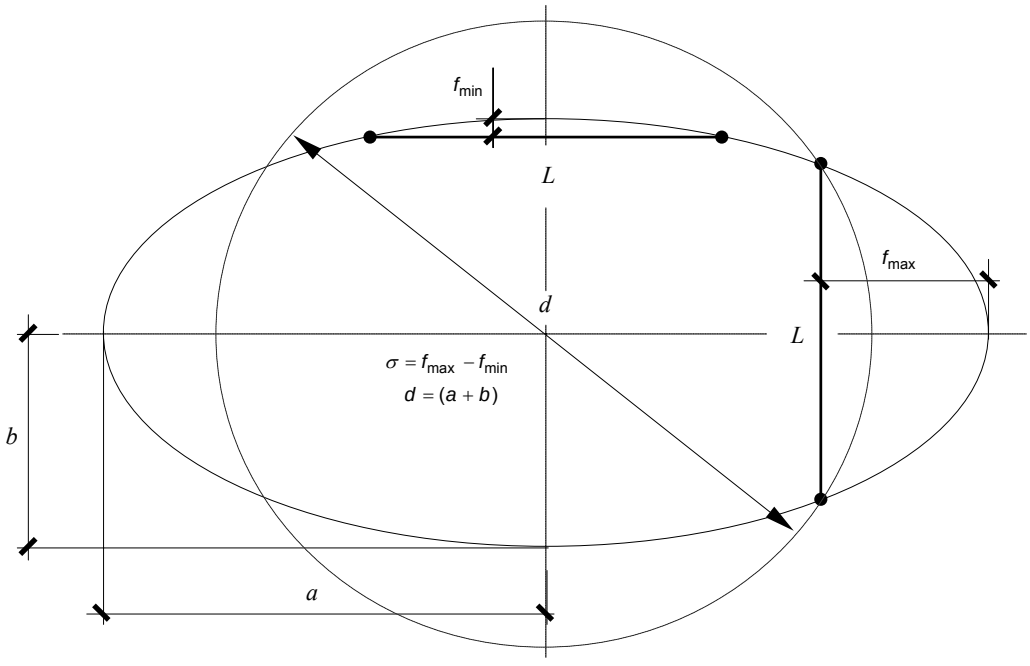

Fig. 7. Maximal deflection of curvature – example of ellipse

4. SHELLTESTER – CONSTRUCTION AND PRINCIPLE OF OPERATION

General structure of the device, called Shelltester, is presented in figure 8.

The device in the form of one-meter beam, according to measurement idea showed in figure 7, is installed by magnetic feet to the shell's external surface and it - turning with the object - measures continuously indications of electronic pin gauge, which is installed in the middle of distance between feet. These indications show relative changes of deflection *f* and are sent – with the help of radio-modem (built-in inside device's body) to radio receiver, connected to computer PC class. There, with the help of computing program – written by author – data is recorded and next is suitable processed and analyzed. Each measurement, thanks to inclination sensor - built-in device - is released and stopped in automatic mode – in the moment while device moves by so called nadir point.
Picture of device „in action" is showed in figure 9.

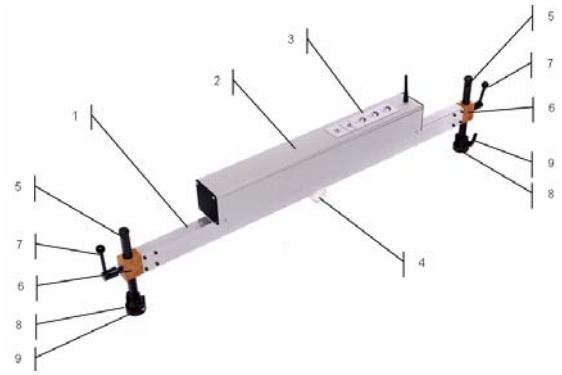

Fig. 8. Scheme of Shelltester's construction:
1 – carrying beam, 2 – body, 3 – control panel,
4 – terminal of electronic pin gauge, 5 – feet,
6 – guides of feet, 7 – clamps of feet,
8 – magnetic basis of feet,
9 – clamps of magnetic basis of feet

Fig. 9. Shelltester mounted on the rotary kiln's shell

5. SHELLTESTER – ROUTINE TESTS SCOPE, DIAGNOSTIC POSSIBILITIES

The routine test programme, assumed by author on the basis of his knowledge and experience - have been gained till now, includes installing device (measurements) on each drum's support - in two shell's cross-sections - inlet and outlet, i.e. close by front of and just behind the ring (fig. 10). In each measurement planes, the device is located in three places on the circumference (A, B and C), arranged every 120^0. Together, on every support (near every ring) it is made six measurements. This causes, that for the most typical - triple-support drum, the number of instrument's installations amount 18.

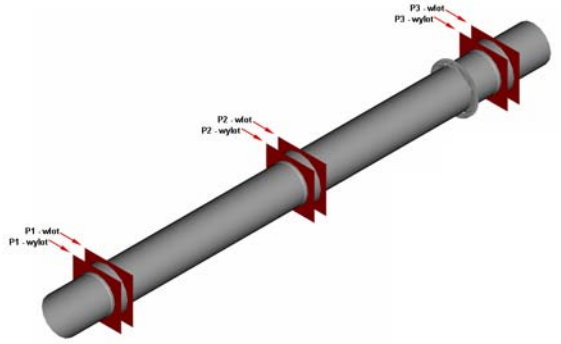

Fig. 10. Measurement planes for routine test scope for triple-support kiln

For such chose diagnostic programme, there are opportunities:

1. to determine the value of maximum degree of shell's elastic ovality ratio in every one from measured cross-sections and to compare the results to the allowable value - defined for given diameter and thickness of the sheet metal plate of the shell.
   The analysis, made by the author, shows that the ovality ratio of under-ring shell's sections should be placed below curves given on graph presented in figure 11. There, upper line is determined for minimal, and lower line for maximal values of shell's steel plate thickness – for given pipes' inside diameters, which presents domain of graph.
   The author foresaw to publish the calculation of these allowable limits, within separate article in the next future,
2. to execute the qualitative estimation (individual and comparative) of all gathered curves of deflection's changes in the function of rotation angle of the drum (for each cross-section and for each circumference position). Utilitarian example of such possibility is presented in the next chapter. There is selected results from measurements performed for: rotary lime kiln, which has been operated in Mondi Świecie S.A and rotary kiln number 4 for clinker baking, located in Rudniki Cement Plant.

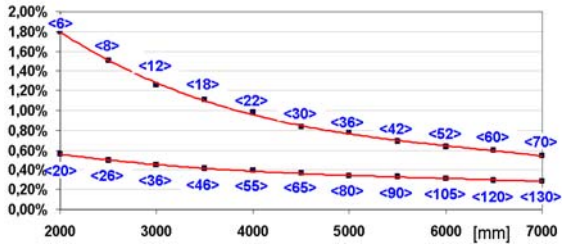

Fig. 11. The allowable limits of elastic ovality ratio of shell's cross-section in the function of inside diameter for suitable: minimal (upper curve) and maximal plate's thickness (lower curve). Plate thickness of shell are given in the brackets

6. EXAMPLE ANALYSIS OF VALUES AND OF OVALITY CHARTS

6.1. The rotary kiln (Mondi Świecie S.A.)

Measurements were executed 21st July 2009. The basic parameters of the object's shell and the conditions of the measurement are presented in table 1. The statement of got results of measurement in the form of the graph of cross-section's ovality ratio - on individual supports - is showed
in figure 12. Example ovality curves, gathered on one of the kiln supports, are presented in figure 14. The shell unit with the largest elastic deformations of its cross-sections was chosen to the analysis (i.e. the support P2).

On the basis of such selectively presented results, it can be stated (diagnosed), as it follows:

- the average ratio of the shell elastic ovality on the support P2 is close to the allowable value, and for the case of the circumference position A of device - in the inlet cross-section – it is observed even overflow of accepted limit, what threatens with appearing the fatigue cracks of the shell,
- ovality curves for measurements realized for various circumference positions don't overlap, but this situation is almost the same both for the cross-section - located on the inlet and on the outlet side. This suggests stable (plastic) deformation of under-ring shell section and/or occurrence
  of the geometrical eccentricity of the shell's axis in reference to the axis of revolution. Because of the fact, that this un-overlapping on circumference positions corresponding with positions
  of rollers (30^0 and 330^0) is only slight, it is more probable that stable - significant value - shell's deformation is the main cause of this situation,
- curves which present average graphs for measurement made on A, B and C position - for the inlet and outlet cross-sections - are almost the same, what, connected with information about clear symmetry reference to vertical plane (determined by angle 180^0), shows that rollers' position are correct (the symmetrical load distribution, the uniform thrust on both rollers, correct slope of the rollers' shafts).

6.2. The rotary kiln (Cemex Polska Sp. z o.o. – Rudniki Cement Plant)

Measurements were executed 12th August 2009. The basic parameters of the object's shell and the conditions of the measurement are presented in table 1. The statement of got results of measurement in the form of the graph of cross-section's ovality ratio - on individual supports - is showed in figure 13. Example ovality curves, gathered on one of the kiln supports, are presented in figure 15. The shell unit with very high elastic deformations and simultaneously regards by the author as the most interesting from the diagnostic point of view was chosen to the analysis (i.e. the support P5).

On the basis of such selectively presented results, it can be stated (diagnosed), as it follows:

- the average ratio of shell elastic ovality on the supports P4 and P5 significantly exceeds values accepted as allowable limits. This fact should be connected with considerable eccentricity of shell geometrical axis in reference to object's axis of rotation, and also, especially in the case of P5 support, with increased value of under-ring gap (19,7mm – look at tab. 1). Measured values give the basis to the fears, that fatigue cracks of shell plate can appear. It simultaneously arise a doubts in the range of the life time of the internal kiln lining,
- the fact, that ovality curves from A, B and C device's position don't overlap mutually (it is visible also on angular co-ordinate 30^0 and 330^0), supports opinion about existing eccentricity,
- curves which present average graphs for measurement made on A, B and C position - for the inlet and outlet cross-sections - don't overlap. It suggest wrong rollers' positions (theirs wrong slopes) or occurrence of gaps in the contact between them and ring's raceway - on the outlet side of ring. I can be effect of e.g. taper shape of ring and/or taper shapes of rollers' raceways. Curves on the outlet side show distinct change of shell's radius, as an effect of rollers' load reactions. The same symptom doesn't exist on the inlet side.

Table 1. The basic parameters and measurement conditions for:
- lime kiln (Mondi Świecie S.A.),
- clinker kiln no.4 (Cemex Polska Sp. z o.o. – Rudniki Cement Plant)

kiln - Świecie	**Support #1**	**Support #2**	**Support #3**	**Support #4**	**---**	
shell's inside diameter	3750	3750	3750	3750	---	mm
thickness of shell's plate	45	45	45	45	---	mm
* under-ring gap	4,0	4,5	6,9	3,7	---	mm
** allowable ovality ratio	0,309	0,309	0,309	0,309	---	%
kiln no.4 - Rudniki	**Support #1**	**Support #2**	**Support #3**	**Support #4**	**Support #5**	
shell's inside diameter	3750	3750	3450	3750	3750	mm
thickness of shell's plate	60	60	60	60	60	mm
* under-ring gap	lack of data	lack of data	2,5	8,9	19,7	mm
** allowable ovality ratio	0,335	0,335	0,310	0,335	0,335	%

* determined during measurement using Shelltester, as difference of mean values of ring's inside diameter and shell's outside diameter,

** given on the basis of chart from figure 11, as approximation of suitable values.

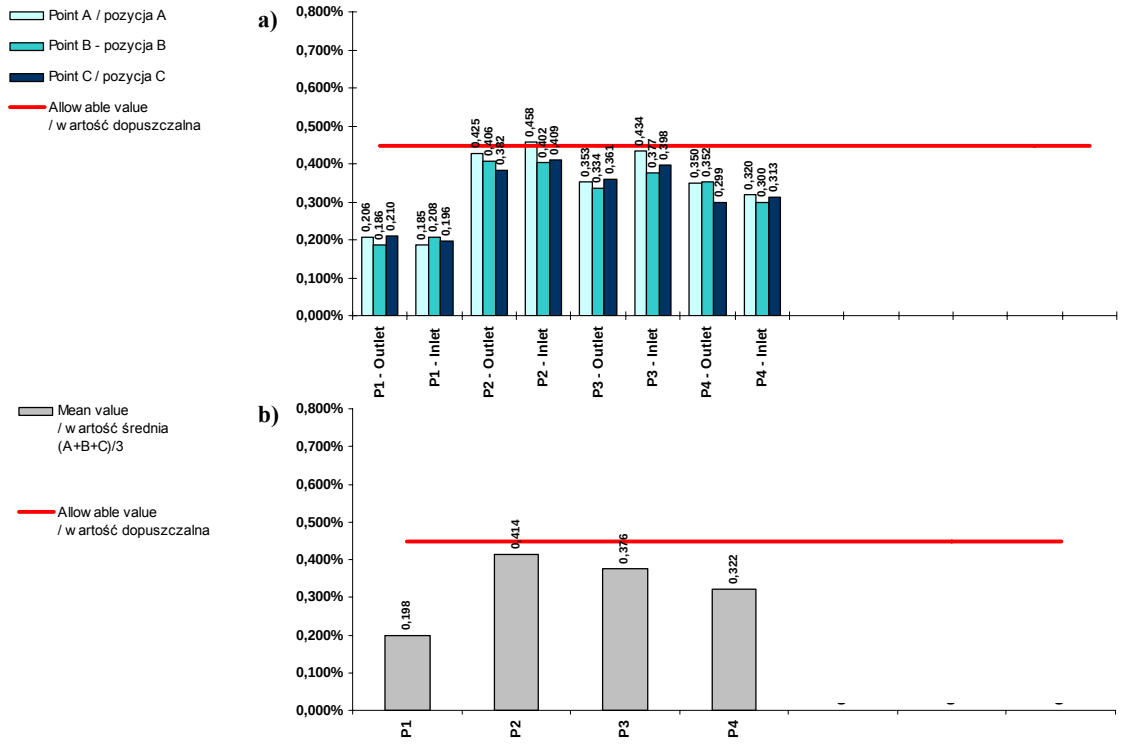

Fig. 12. Values of elastic ovality ratio of shell's cross-sections (kiln from Mondi Świecie):
a) detailed values, given for each plane and each circumference position of device,
b) mean values from particular supports

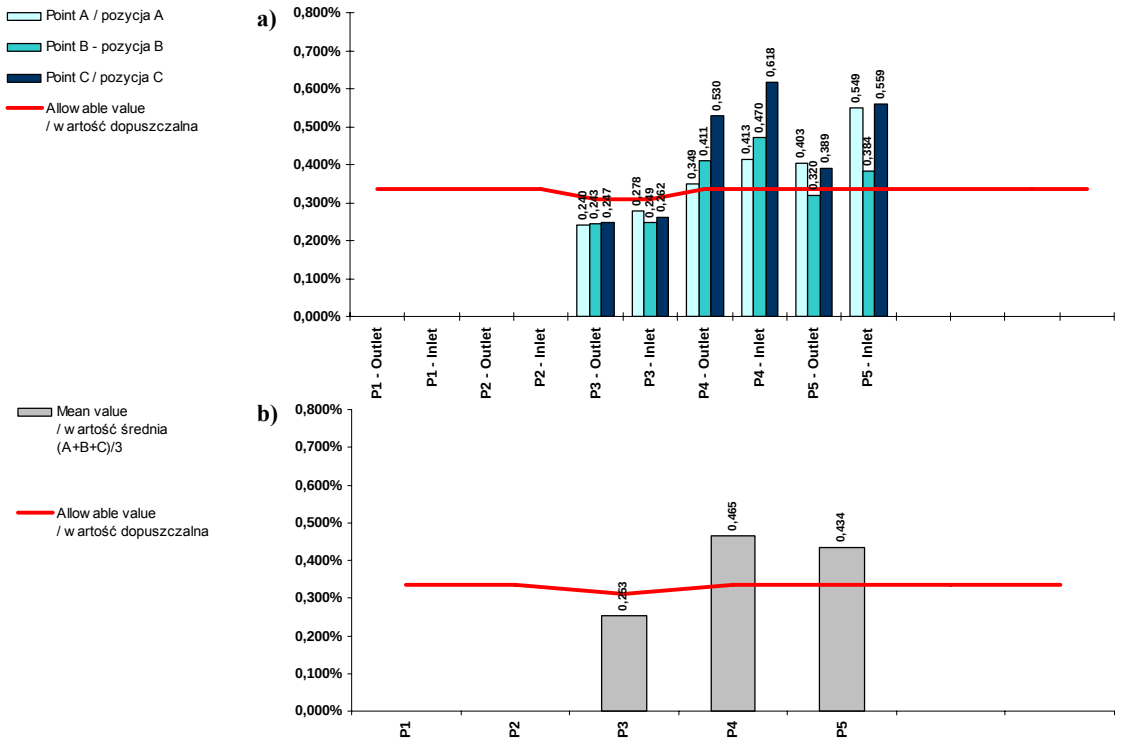

Fig. 13. Values of elastic ovality ratio of shell's cross-sections (kiln no.4 from Rudniki Cement Plant): a) detailed values, given for each plane and each circumference position of device, b) mean values from particular supports.
According to too high temperature of shell, measurements for P1 and P2 supports wasn't executed

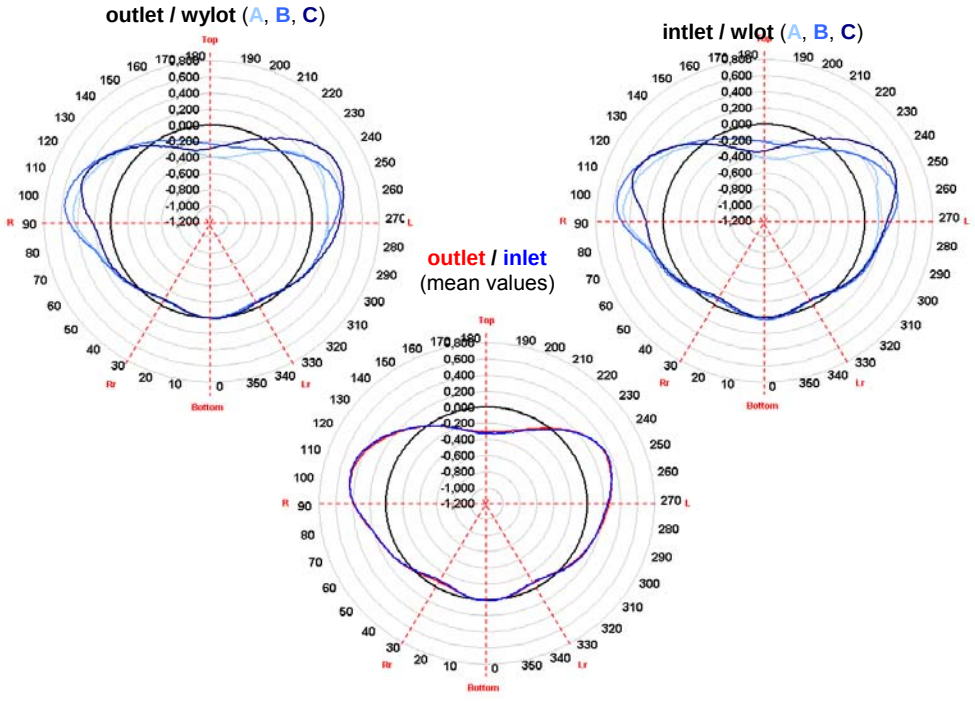

Fig. 14. Ovality curves i.e. changes of shell deflections *f* (kiln from Mondi Świecie – support P2)

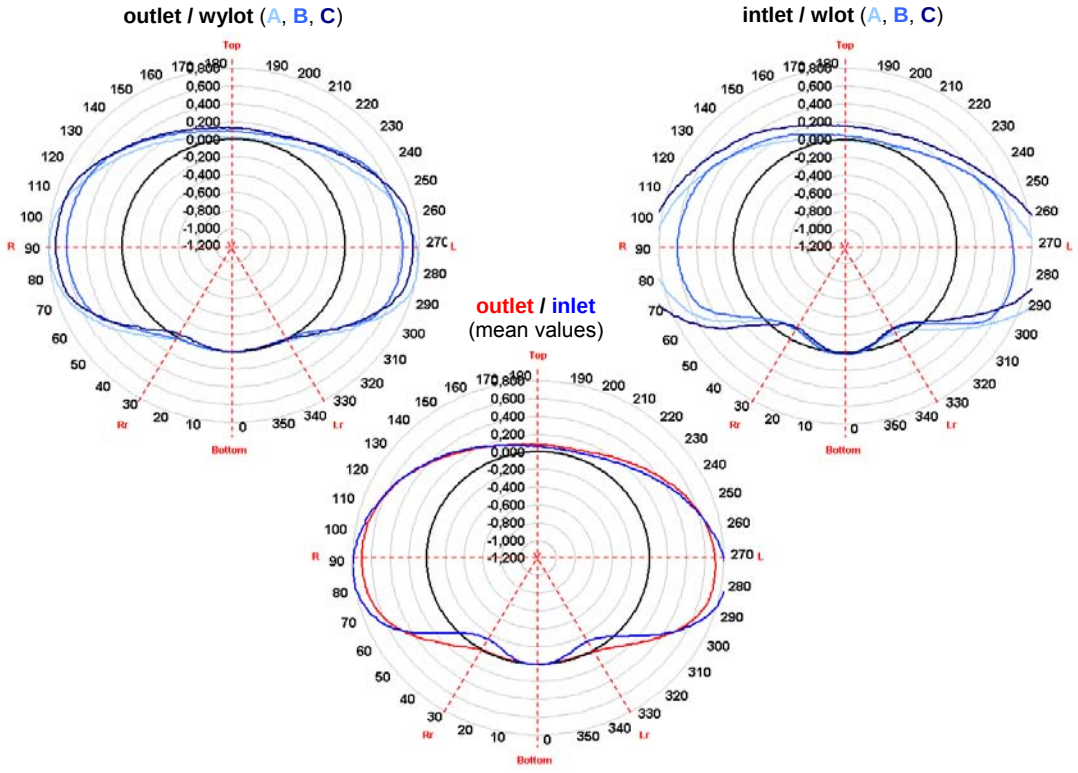

Fig. 15. Ovality curves i.e. changes of shell deflections *f* (kiln no.4 from Rudniki Cement Plant – support P5)

6.3. The comparative analysis of kiln's state

After detailed comparison of values and graphs got for both kilns, it can be established that:

- kiln located in Rudniki cement Plant is an object with clearly worse technical state. In spite, that the diameter of his shell has the same value as in the case of kiln from Świecie (except of the P3 support), elastic deformations of his shell's cross-sections are significant higher (even about 50%),
- this is particularly dangerous in the aspect of the fact that thicknesses of the shell's under-ring segments in Rudniki are indeed larger than in Świecie (60mm versus 45mm),
- un-overlapping curves got on circumference positions A, B and C is particularly visible on kiln located in Rudniki, where this situation appears on the whole kiln's circumference. In the case of kiln located in Świecie, un-overlapping exists for angles from 70^0 to 320^0, what is the natural range of circumference - if there is under-ring gap. This situation shows, that in Mondi problem of ovality comes from under-ring gaps and for kiln located in cement plant higher values of elastic shell's ovality are derivative of additional irregularities in the form of errors in shell's geometry and in the form of shortcomings in the positions of support system's components (wrong rollers' setting).

7. SUMMARY, CONCLUSIONS

Contents, given in the present publication, can be sum up, as follows:

1. method and device to the rotary drum's technical state's evaluation by measurement and analysis elastic ovality of the shell's cross-sections give very rich diagnostic information,
2. this information - first of all it is the quantitative determined value of the elastic ovality and secondly the graphs of the changeability of the shell's deflection in the function of the angle of the drum's rotation,
3. first of mentioned diagnostic parameters - after comparing to the appointed allowable limit - gives clear-cut view on the risk of appearing fatigue cracks in the drum's steel shell. Moreover this shows the danger of the lowering durability of the internal object's lining, if object is equipped in such one,
4. the graphs of the changeability of the shell's deflection are the derivative of changeability of the curvature radius during drum's rotation. The mutual comparison of these graphs - collected curves (in the range of section, support, the object, and even in the reference to different drums) gives possibilities for evaluation of their shapes and for the qualitative determination

of reasons - causing the departures from expected form,

5. these departures make up the qualitative symptoms of deviation from drum's normal mechanical conditions, and they include both basic mistakes in the geometry of the support system (including rollers positions) and more subtle irregularities, which can take place in the area
of shell,
6. thanks to such set of diagnostic information, described method and device become very valuable tool, which help to estimate the technical state of the object - rotary drum type,
7. next enrichment of the analysis may constitute described way and device in the rank of one of the most effective diagnostic performances. The author plans to do it within the next future. He intends to enrich method about the quantitative estimation of detected irregularities, which distort shapes of ovality curves.

8. LITERATURA

[1] Gocał J., Kozak S.: Patent tymczasowy nr P.183415 pt. *Urządzenie do pomiaru sprężystych deformacji bębna obrotowego*, zgłoszony dnia 18.09.1975.
[2] Piech J.: *Piece ceramiczne i szklarskie*. Wydanie II, Uczelniane Wyd. Naukowe AGH, Kraków 2001.
[3] Praca zbiorowa.: *Geodezja inżynieryjna, tom II, rozdział 7.7 – Badanie deformacji korpusu pieca obrotowego*. PPWK, Warszawa 1980.
[4] Świtalski M.: *Modelowanie i analiza zjawisk rządzących stabilnością osiowego ruchu walczaków obrotowych*. Rozprawa doktorska. ATR Bydgoszcz, 2004.
[5] Zachwieja J.: *Odkształcenia promieniowe pierścieni tocznych walczaków obrotowych*. Cement Wapno Beton, 1, 2003, 39-45.
[6] Żurakowski S., Hojarczyk S.: *Piece obrotowe - projektowanie i konstrukcje*. WNT, Warszawa 1969.

PhD Eng.. **Maciej ŚWITALSKI** – closely related to Jan & Jędrzej Śniadecki University of Technology and Life Sciences in Bydgoszcz. There he has graduated and in 2004 he has got PhD title. At present he works there in the Department of Applied Mechanics - in the Institute of Mechanics and Machinery Construction - in the Faculty of Mechanical Engineering. Since 1993 he deals with issues of diagnostic and rotary machines' maintenance, especially in the range of large dimensions rotary drums. Scientific activity in this area is supported by active co-operation with domestic and foreign industrial plants, mainly with the cement, paper and soda companies.

WIRELESS DIAGNOSTIC SYSTEM WITH USE OF THE HARMONIC POLYNOMIAL BASE

Zenon SYROKA
Uniwersytet Warmińsko – Mazurski, Wydział Nauk Technicznych
Ul. Oczapowskiego 11, 10 –717 Olsztyn

Summary

In this work were given the basics of the wireless diagnostic system which is the subject of patent application. This system is using the method of developing signals to Fourier series.

Keywords: wireless diagnostic system, sampling signal, Fourier series.

BEZPRZEWODOWY SYSTEM DIAGNOSTYCZNY
Z WYKORZYSTANIEM BAZ HARMONICZNYCH I WIELOMIANOWYCH

Streszczenie

W pracy zostały przedstawione założenia bezprzewodowego systemu diagnostycznego będącego przedmiotem zgłoszenia patentowego [1]. System ten wykorzystuje w nadajniku metodę rozwijania sygnałów w szereg Fouriera.

Słowa kluczowe: bezprzewodowe systemy diagnostyczne, próbkowanie sygnałów, szeregi Fouriera względem wielomianów ortogonalnych.

1. INTRODUCTION

The subject of this article is wireless diagnostic system being an alleged invention [1]. The sense of this patent is to spread the analog diagnostic signal – from converter, into the Fourier series due to relevant orthogonal basis and further transmission of the Fourier series components and their further processing.

Input signal (wireless diagnostic system) can be given by dismantling the electrical signal into the series according to relevant orthogonal basis (these series are called finite and infinite sampling series) on the transmission side and sending in channel information only about it's coefficient expansion and in receiver generate and sum them properly.

This system is used to wireless diagnosis of devices, mechanical machines and dangerous or inaccesible electric installations such as high voltage or high concentration of chemicals.

Mathematical basics of his system were given in these articles [2, 3, 4].

The most similar systems of data transfer are Bluetooth, IrDA and OFDM.

2. GENERAL SYSTEM DESCRIPTION

Data are delivered as non electric signal,which is turned with converter to electric. In next faze of converting, the signal is expanded into the Fourier series due to exact orthogonal basis, usually harmonic or into the series against orthogonal polynomial by Legendre, Czebyszew, Laguerre and Hermite. In radio channel are transmitted informations only about coefficient expansion of the signal. In the receiver according to received coefficients the components of the diagnostic signal are generated. These coefficients are next sum up with harmonic sampling kernels such as Dirichlet, Fejer or de la Valle Poussin kernels.

Harmonic basis will be used mostly to wireless diagnosis of devices using signals in forms of vibrations from different sources. These vibrations have harmonic pattern.

In case of diagnostic signals having non harmonic patterns - impulses, it's better to use polynomial kernels against Legendre, Czebyszew, Laguerre or Hermie polynomials, which allow to generale input signal having less coefficients in it's expansion, so it's possibile to get it's higher compression.

The radio system will be using OFDM modulation. It's more safe due to unwanted data capture in radio channel. In this channel will be transmitted infomations about signal expansion coefficients not about signal itself, so the capacity of data will be increased.

OFDM transmission technique allow to increase WLAN network discharge between dewices significantly. OFDM rely on single stream data coding in many carriers. In this system are used subcarriers in which are used BPSK, QPSK or QAM/64-QAM modulations. Maksimum speed of data transmission - 54 Mbit/s is achieved for 64-QAM (216 data bits per one OFDM symbol) modulation.

OFDM modulation is based on FDM but is used as digital modulation. Transmitted bit stream is spread to over twelve parallel streams. Available

band is spread between couple of subchannels and every smaller stream is transmitted by one subchannel modulating it's carrier with use of simple modulation, for example PSK or QAM. Subcarriers are chosen in certain way, that every modulated stream is orthogonal against the others. This way gives opportunity to eliminate the co-channel disturbances. The alignment of channel is simplified because of usage of slower narrow band channels instead of one wide band channel. The basic rule of OFDM is to get along with different, sometimes hard environment of Chanel, for example With narrow band interferencje without any filters.

This solution allowed to build wireless diagnosis system without need to switch analog signal to digital. This system is immune for interferences of radio wave propagation for unwanted data capture and gives the allegiance of receivered signal with minimum of band occupancy.

Using of that system allow for immediate diagnosis based on valuation of unwanted components of diagnostic signal. This system exclude A/C and C/A converters. The basic idea of his project is decay od signal in the transmittor and to sum the components in receiver. Precision of mapping of signal in receiver is only up to amount of components granted in sum not up to parameters of transmission channel. In radio channel are transmitted the informations about the components of series. Thsis system can be used in other purposes and in the same way in receiver use informations from expansion into series in this receiver for example to indentification, diagnosis - telemedicine.

The block scheme of the system in case of polynomial base is in Fig. 1, in case of harmonic base in Fig. 2.

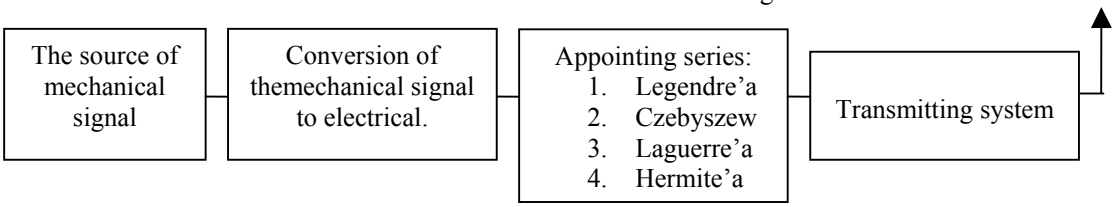

The block scheme – conversion of diagnostic signals in the transmitter

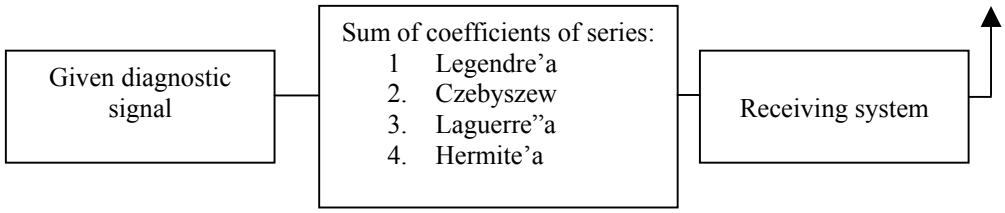

The block scheme of signal conversion in the receiver

Fig. 1 The block scheme of diagnostic system using polynomial basis

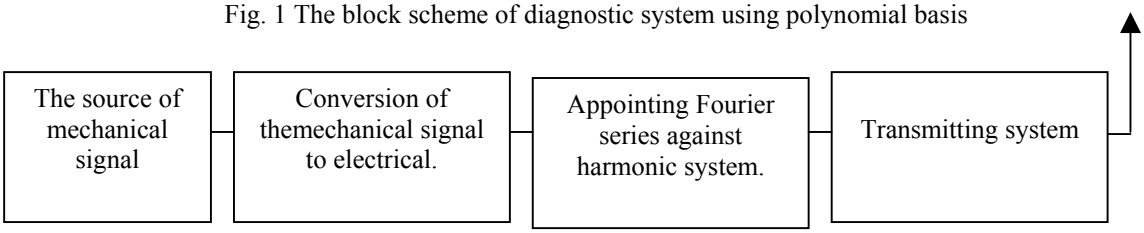

The block scheme - conversion of diagnostic signals in the transmitter

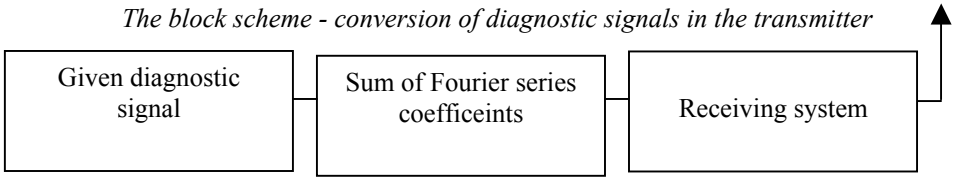

The block scheme of signal conversion in the receiver

Fig . 2 The block scheme of diagnostic system using harmonic basis

3. SIGNAL ANALYSE SYSTEMS BASED ON GENERALISED FOURIER SERIES

General block scheme of system used to define coefficeints of signal expansion into generalised Fourier series. Fig. 3.

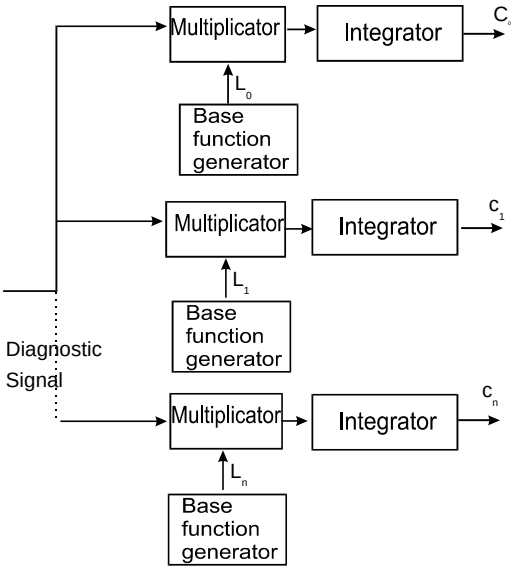

Fig. 3. Block scheme of system used to appoint Fourier coefficients of diagnostic signal

Basic elements of this system are base function genereators according to the expansion is effected.

Signal analyse – diagnosis, running in real-time.

Analysed diagnostic signal is multiplied by exact base functions and than integrated (integrating amplifier).

In the output of every integrating amplifier at the final moment of integration interval the continuous in time signal occure, which value is exact to responsive coefficient of generalized Fourier series.

On drawings 4, 5, 6, 7 are block schemes of basic function generators for eight first functions.

The base to build the electronic system generating particular basic functions are recurrence equations.

For Hermite polynomials this equation is :

$$H_{n+1}(x) = 2xH_n(x) - 2nH_{n-1}(x) \qquad (1)$$

According to this equation dependings which define the eight first Hermite polynomials are :

$$\begin{aligned} H_0 &= 1 \\ H_1 &= 2x \\ H_2 &= 2(xH_1 - H_0) \\ H_3 &= 2(xH_2 - 2H_1) \\ H_4 &= 2(xH_3 - 3H_2) \\ H_5 &= 2(xH_4 - 4H_3) \\ H_6 &= 2(xH_5 - 5H_4) \\ H_7 &= 2(H_6 - 6H_5) \end{aligned} \qquad (2)$$

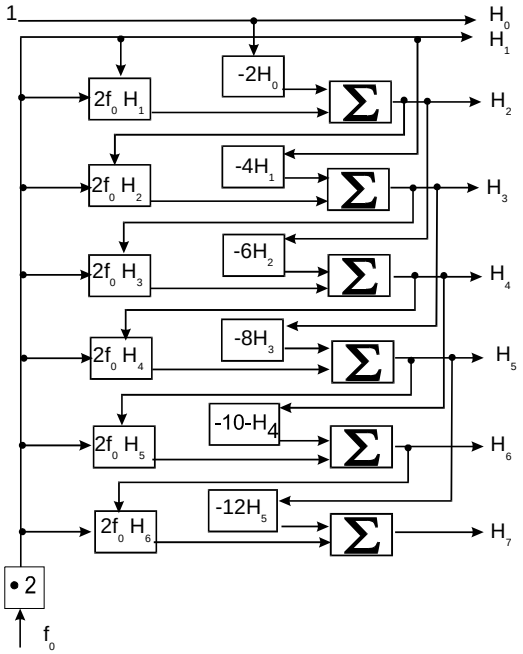

Fig. 4. Block scheme of generator of eight first Hermite polynomials

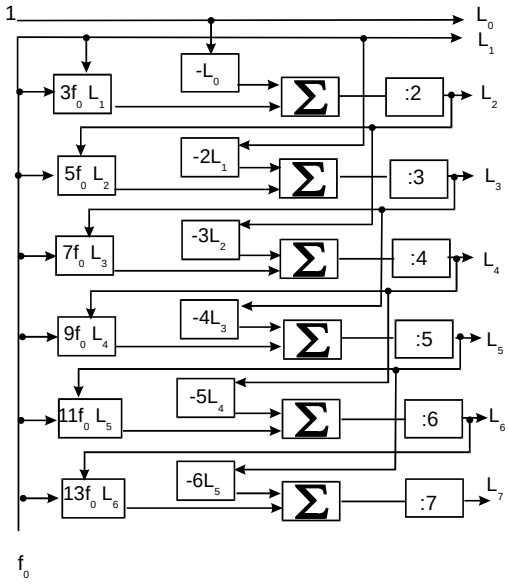

Fig. 5. Block scheme of eight first Legendre polynomials generator

For Legendre polynomials, recurrence equation is formed :

$$L_{n+1}(x) = \frac{1}{n+1}\left[(2n-1)xL_n(x) - L_{n-1}(x)\right] \qquad (3)$$

From above equation, rules defining the eight firs Legendre polynomials are consequent :

$$\begin{aligned}
L_0 &= 1\\
L_1 &= x\\
L_2 &= \frac{1}{2}\left(x3L_1 - L_0\right)\\
L_3 &= \frac{1}{3}\left(x5L_2 - 2L_1\right)\\
L_4 &= \frac{1}{4}\left(x7L_3 - 3L_2\right)\\
L_5 &= \frac{1}{5}\left(x9L_4 - 4L_3\right)\\
L_6 &= \frac{1}{6}\left(x11L_5 - 5L_4\right)\\
L_7 &= \frac{1}{7}\left(x13L_6 - 6L_5\right)
\end{aligned} \tag{4}$$

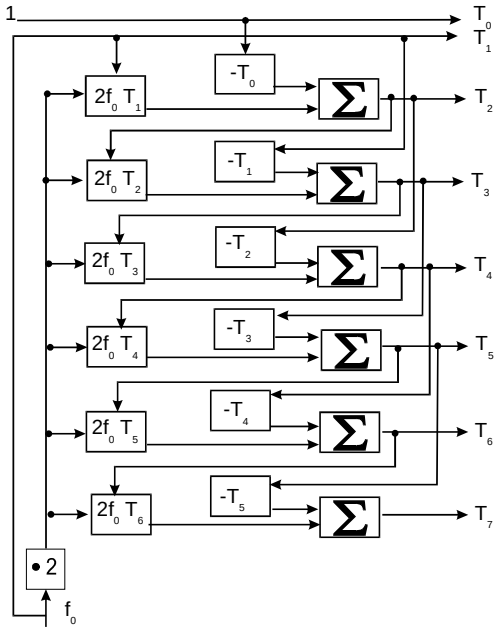

Fig. 6. Block scheme of eight first Czebyszew polynomials generator first type

For Czebyszew first type polynomials, recurrence equation is formed:

$$T_{n+1}(x) = 2xT_n(x) - T_{n-1}(x) \tag{5}$$

From above equation, rules defining the eight firs Czebyszew polynomials first type, are consequent:

$$\begin{aligned}
T_0 &= 1\\
T_1 &= x\\
T_2 &= 2xT_1 - T_0\\
T_3 &= 2xT_2 - T_1\\
T_4 &= 2xT_3 - T_2\\
T_5 &= 2xT_4 - T_3\\
T_6 &= 2xT_5 - T_4\\
T_7 &= 2xT_6 - T_5
\end{aligned} \tag{6}$$

For Laguerre polynomials, recurrence equation is formed:

$$L_{n+1}^{(a)}(x) = \frac{-\left(x-a-2n-1\right)}{n+1}L_n^{(a)}(x) - \frac{n+a}{n-1}L_{n-1}^{(a)}(x) \tag{7}$$

From above equation, rules defining the eight firs Laguerre polynomials are consequent:

$$\begin{aligned}
La_0 &= 1\\
La_1 &= \left(a+1\right) - x\\
La_2 &= \frac{\left(a+3\right)-x}{2}La_1 - \frac{a+1}{2}La_0\\
La_3 &= \frac{\left(a+5\right)-x}{3}La_2 - \frac{a+2}{3}La_1\\
La_4 &= \frac{\left(a+7\right)-x}{4}La_3 - \frac{a+3}{4}La_2\\
La_5 &= \frac{\left(a+9\right)-x}{5}La_4 - \frac{a+4}{5}La_3\\
La_6 &= \frac{\left(a+11\right)-x}{6}La_5 - \frac{a+5}{6}La_4\\
La_7 &= \frac{\left(a+13\right)-x}{7}La_6 - \frac{a+6}{7}La_5
\end{aligned} \tag{8}$$

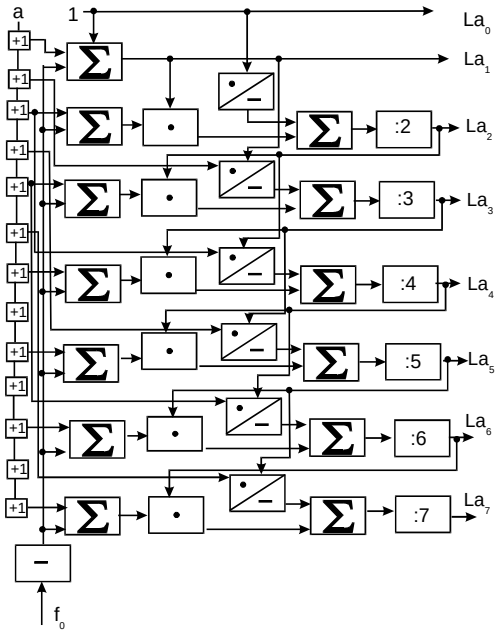

Fig. 7. Block scheme of eight first Laguerre polynomials generator

Markers are:


multiplying system


multiplying and reverse phase sys tem


turning-out phase system

The *a* prameter is being increased by 1 and than transmitted to exact adder and to multiplying and reversing system. Some parameters (*a*+8; *a*+10, *a*+12) in eight first Laguerre polynomial generator are not in use. Basicly every non even value of

coefficient $a+n$ is always used twice and even value once to generate polynomial of given order.

It's often to asume value $a=0$ because this parameter is gained by one. Only in case of fractional or irrational value of a parameter is important to grant it's value. In most cases a must be chosen experimentaly depending of analysed diagnostic signal.

4. SUMMARY

The most common solution in diagnostic technique is to change the analog signal (from converter) into digital the quickest way. Transmission of whole digital signal is made in radio channel. In the receiver of diagnostic signal is made it's analysis (usually digital signal processing).

In given solution decay of diagnostic signal into the series in the transmitter is being made. For that reason to receiver is getting information about malfunction (unwanted harmonic signal).

The reasons for designing wireless diagnostic system are:

- To build wireless diagnostic system without changing analog signal into digital.
- To ensure it's immunity for radio waves propagation decay.
- To ensure maximum immunity of system for unwanted data capture.
- To ensure maximum allegiance of received signal with minimum bundle interruption.
- To ensure the possibility of immediate diagnosis based on estimation of unwanted components of diagnostic signal (granting of the pattern spectrum of the machine).

BIBLIOGRAPHY

[1] *Bezprzewodowy system diagnostyczny* – zgłoszenie patentowe, data zgłoszenia 25.07.2007, P-382991

[2] Syroka Z.: *Próbkowanie sygnałów diagnostycznych. Cz. I. Próbkowanie w przestrzeni Hilberta z reprodukującym jądrem Shanona.* Diagnostyka Nr 2(42)/2007,s. 19-26.

[3] Syroka Z.: *Próbkowanie sygnałów diagnostycznych. Cz. II. Próbkowanie w przestrzeni Hilberta z bazami harmonicznymi za pomocą nieklasycznych jąder.* Diagnostyka Nr 2(42)/2007, s. 27-34.

[4] Syroka Z.: *Próbkowanie sygnałów diagnostycznych. CzIII. Próbkowanie w przestrzeni Hilberta z bazami wielomianowymi za pomocą nieklasycznych jąder.* Diagnostyka Nr 2(42)/2007, s. 35-41.

SPECTRUM WIDTH FACTOR AS A DIAGNOSTIC PARAMETER DETERMINING THE DEGREE OF DAMAGE OF TOOTH SURFACE

Stanisław RADKOWSKI, Robert GUMIŃSKI

Institute of Automotive Engineering, Warsaw University of Technology,
Narbutta 84, 02-524 Warsaw, Poland, fax. 022 234 8121, ras@simr.pw.edu.pl

Summary

The article discusses the issue of use of the spectrum width factor in diagnosing the development of pitting of toothed wheels. Theoretical issues have been presented related to the dependence of the level and structure of non-linear noise on the size, type and evolution phase of the process of degradation of surfaces of teeth being in contact. The paper discusses an example of diagnosis of the condition of teeth surfaces while using the data obtained during the experiment. An analysis of the relation between the spectrum width factor and the rigidity of shafts has also been conducted. The result of the analysis shows that the spectrum width factor can also be used in diagnosis of machine shafts.

Keywords: spectrum width factor, pitting, toothed gears.

WSPÓŁCZYNNIK SZEROKOŚCI WIDMA JAKO PARAMETR DIAGNOSTYCZNY STOPNIA USZKODZENIA POWIERZCHNI ZĘBÓW

Streszczenie

W artykule podjęto zagadnienie wykorzystania współczynnika szerokości widma w diagnozowaniu rozwoju pittingu kół zębatych. Przedstawiono zagadnienia teoretyczne odnośnie zależności poziomu i struktury zakłóceń nieliniowych od wielkości, rodzaju i fazy ewolucji procesu degradacji powierzchni zębów znajdujących się w przyporze. Omówiono przykład diagnozowania stanu powierzchni zębów z wykorzystaniem danych uzyskanych w trakcie eksperymentu. Przeprowadzono również analizę związku współczynnika szerokości widma ze sztywnością zastosowanych wałów. Wynik tej analizy wskazuje, że współczynnik szerokości widma może być wykorzystany również w diagnostyce wałów maszynowych.

Słowa kluczowe: współczynnik szerokości widma, pitting, przekładnie zębate.

1. INTRODUCTION – SPECTRUM WIDTH FACTOR

The publication [10] tackles the issue of origination and development of pitting in toothed wheels as well as monitoring of development of pitting with the use of spectrum width factor. The results presented therein show that the numerous factors can have influence on the intensity of the pitting process. While exploiting the possibilities offered by the test-bed, the influence of a toothed gear's operating conditions on the development of spectrum width factor has been examined.

Generally it is recognized [8, 3] that pitting is a process of wear due to fatigue which dominates in toothed gears with soft teeth which operate at average tangential velocity of below 50 m/s. A factor which leads to chipping is the variable contact stress which occurs in the area of negative slip. In addition, attention has been drawn to the fact [5, 9] that the physical and chemical properties of oil, thickness of the lubricating layer, hardness of the material and micro-geometry of surfaces will be the factors determining the intensity of the process of surface chipping. As a result of the surface wear process , pitting cavities emerge which, as the defect develops, form bigger strips of damaged surface whose width continuously increases. These strips most often occur in the area of a tooth's foot, in the area where the biggest slip occurs. This type of surface defects leads to reduction of the size of working surfaces and in the next stage of the destruction process they can become a place in which fatigue-related crack and the associated process of fatigue-related breaking of a tooth are initiated. Thus, diagnosis of emergence and development of pitting can play the role of detection of early defects during the phase of low-energy development of fatigue-related tooth breaking. Conducting of such a diagnosis means the need for developing the relevant methods of detecting diagnostic information which can be "coded" in various ways, depending on the phase of surface pitting process. The literature on the topic [7, 8] identifies three main phases of the process:

- the phase of initiation of cracks in the outer layer;

- the phase of development and propagation of cracks as a result of destructive operation of oil in the contact zones;
- the phase of development of pitting cavities, which results in removal of part of the material from the outer layer.

Description of the mechanism of emergence of fatigue-related cracks, while accounting for the fact that initiation of this process occurs in Bielayev's point, that is in the point where the stress on the material is the biggest, is presented in [5, 9].

Oil is forced into the cracks as the influence of friction forces increases in the contact zone and Bielayev's point is moved in the direction of the friction surface, which is a signal confirming the start of the second phase of the destruction process. Rolling of the elements mating in such conditions leads to variable impact on the extensive network of cracks and in the third stage it leads to chipping of further particles from the elements (profiles). Such destruction constitutes substantial disturbance of contact conditions and hence it can become a reason for changes of the frequency structure of the generated vibroacoustic signal. Generally, as pointed out in [4, 6], overall growth of the noise level, in a broad frequency band of the analyzed signal, will occur in the case of development of pitting.

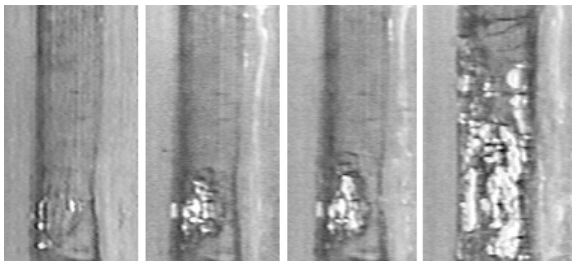

Fig. 1. Development of pitting on a tooth surface (from an experiment)

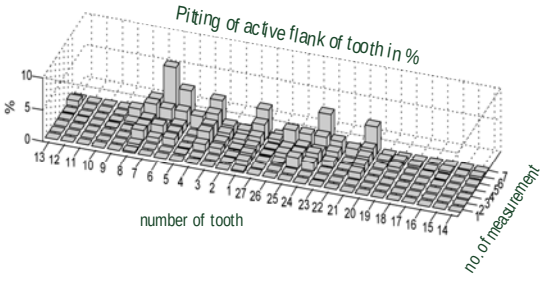

Fig. 2. Development of pitting in respective teeth of the pinion.

The method of modeling of vibroacoustic signal generation, including the impact of various methods of causing damage on a vibroacoustic signal's parameters and hence leading to change of parameters of a dynamic model, is discussed in detail in [10]. Pitting in toothed wheels was examined and the results are presented below. Fig. 1 presents an example of growth of bandwidth in the case of a surface which was chipped due to wear. In addition, during the surveys we noted that pitting could start on one or bigger number of teeth and then spread to the remaining teeth (Fig. 2).

Use of spectrum width factor has been proposed for modeling of pitting in toothed wheels. The method of calculating the spectrum width factor is presented below. Spectral moments have to be determined for this purpose according to the following formula [1]:

$$m_k = \int_{-\infty}^{\infty} \omega^k S(\omega) d\omega \tag{1}$$

and then the measure of spectrum width has to be determined in the form of spectrum width factor:

$$\nu = \frac{m_2^2}{m_0 m_4} \tag{2}$$

where:

$$m_0 = \int_{-\infty}^{\infty} S(\omega) d\omega$$

$$m_2 = \int_{-\infty}^{\infty} \omega^2 S(\omega) d\omega$$

$$m_4 = \int_{-\infty}^{\infty} \omega^4 S(\omega) d\omega$$

$S(\omega)$ - spectrum,

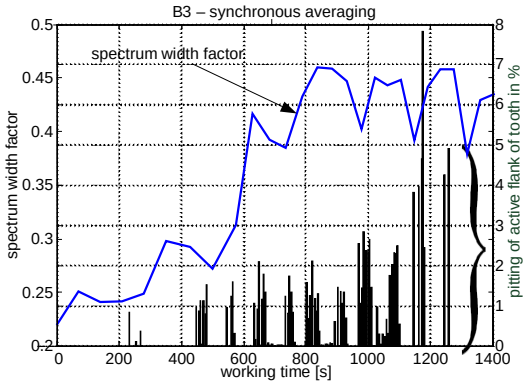

Fig. 3. Changes of the value of spectrum width factor during the time of the strength test.

Fig. 3 presents the changes of the value of the spectrum width factor in time during the strength test. In accordance with the results found in Fig. 2, as the test continues we witness increase of the number of teeth affected by the fatigue-related process of surface destruction. The aforementioned fact has been reflected accordingly by the changing width of the bar on the abscissa. The heights of respective bars correspond to the percentage of destructed surface of a tooth's side as compared to the total surface. Let us note, that it is reflected by the changes of spectrum width factor, however in addition one can note the quality change associated with damage to surfaces of further teeth. Let us note that the qualitative change is observed already in the case of destruction of only several percent of

a tooth's surface. Thus a diagnostic parameter has been obtained which is highly sensitive, especially during the initial phase of pitting.

2. DESCRIPTION OF THE EXPERIMENT

The experiment was conducted in revolving power test-bed. The test-bed consists of two toothed gears which operate in revolving power system and it enables examination of both, toothed wheels and toothed gear lubricants. The precise description of the test-bed is found in [2]. Toothed wheels made of 20H2N4A steel, carburized and hardened to hardness of 60 HRC were used in the experiment. They were subjected to accelerated fatigue testing.

The experiment was planned in such a way so as to enable analysis of the impact of various factors on the degradation process (load and gear quality).

In addition two sets of shafts were used with different torsional rigidity, which enabled examination of the impact of torsional rigidity on the conditions of mating of teeth coming into contact.

Parameters of examined toothed wheels are found in Table 1.

Table 1 Comparison of parameters of examined toothed wheels

No. of experiment	Torsional rigidity of shafts	Experiment time [s]	Input rotational speed [rev/s]	Load [Nm]
1	Two times bigger as in case of second shafts ($K_{T1}=2K_{T2}$)	10254	24	1222
2		3960		1303
3		1188		1492
4		5922		1200
5	Smaller (K_{T2})	7770		1218
6		8238		1214
7		4206		1309
8		6186		1294

The measurement system mounted in the test-bed enabled registration of five different signals:

- channel 1 – revolutions marker (one marker per revolution)
- channel 2 – signal from tensometers affixed to the shaft, proportional to the degree at which a shaft is twisted
- channel 3 – signal from tensometers affixed at the of a tooth's head, proportional to tooth deflection
- channels 4 and 5 – acceleration of vibration in the body of the examined toothed gear as measured at the body's upper part, just above the place of mounting of pinion shaft bearing, in a horizontal direction – perpendicularly to shaft axis, and in vertical direction.

Channels 2 and 3 were equipped with a telemetric system manufactured by ESA Messtechnik GmbH. The system enabled data transmission from rotating elements. Tensometers manufactured by MEASUREMENTS GROUP INC. served as the active measuring elements. The information obtained this way was used for tracking the deformations at the foot of a tooth as well as the shaft torsion angle during the experiment. The information obtained this way was used for determining the moment of crack initiation and for tracking of a crack's propagation. An inductive sensor was also installed in the examined toothed gear. It shut down the test bed at the moment when a tooth broke.

The experiments were conducted until total breaking of a tooth while at the same time conducting continuous registration (in 6-second-long modules). It is worth stressing that no artificial defects were introduced prior to starting the tests, so as not to disturb this way the course of the process of initiation of a fatigue-related breaking of a tooth. Such a method of research differs substantially from the research related to examining the development of a tooth's breaking in which artificial defects are introduced, e.g. by cutting the tooth. The adopted method of realization of the experiments resulted in a situation that in most cases the teeth which broke were not the ones for which stress measurements were carried out.

Based on the vibration signals registered in two directions, we were able to determine the diagnostic parameters in the form of width factor of power spectrum for a broadband signal of vibration acceleration as well as of signals generated by acceleration of vibration filtered off in the bands with widths of 120Hz, 400Hz, 600Hz surrounding the first eight harmonic frequencies of meshing.

Due to the fact that the time till occurrence of a defect varied for respective toothed wheels, thus to facilitate the analysis of results the time was standardized and presented in the form of percentage of time till defect occurrence.

3. MONITORING OF PITTING DEVELOPMENT

Due to the fact that during the fatigue tests there also occurred pitting-related damage of teeth's surfaces, thus it is worth analyzing the change of spectrum width factor for such a wheel and confirm its utility value in the process of monitoring of pitting development. Changes of spectrum width factors were analyzed for the wheel in which seven teeth suffered from pitting. The information on the development of pitting is found in the signal's spectrum, in direction X (horizontal-and-perpendicular to shaft axis) and it is presented in the form of a spectrum width factor for the entire frequency band (Fig. 4).

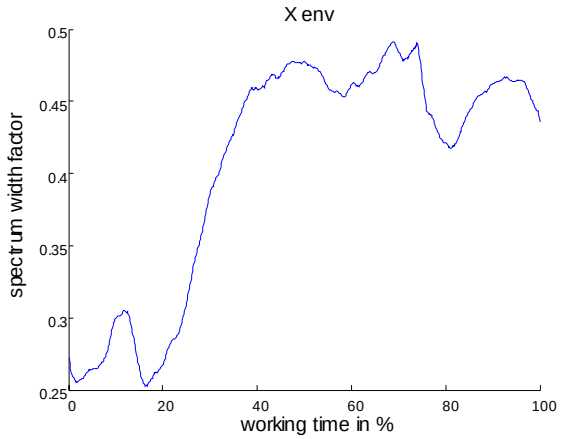

Fig. 4. Spectrum width factor of a signal's vibration acceleration in direction X

During the initial period of the test the value of spectrum width factor demonstrated no upward trend, while a distinct upward trend became visible after 20% of the test's time. This could have been associated with the phase of initiation of pitting-related defects. After some time the trend was halted, which most probably meant end of the phase of intensive development of pitting.

An interesting task is posed by determination of the frequency band in which the information on development of pitting can be found. To this end the spectrum width factor has been determined in frequency bands with the width of 120Hz around subsequent harmonics of meshing (the first eight). A similar qualitative change growth of spectrum width factor, as in the case of the whole frequency band of the analyzed signal, could be observed in the bandwidth surrounding the third harmonic of meshing, the scale of qualitative change in this case is quite different (Fig. 5).

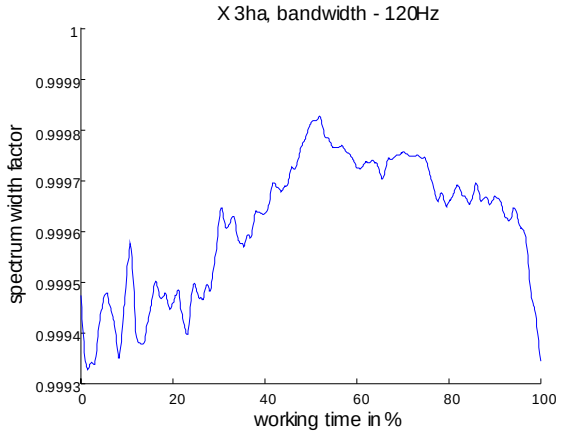

Fig. 5. Spectrum width factor of signal vibration acceleration in direction X in the bandwidth surrounding the third meshing harmonic.

Spectrum width factor, for the signal registered in direction Z (in the entire frequency band) whose run is presented in Fig. 6, also maintained an upward trend, however the level of random noise is substantially higher than in direction X.

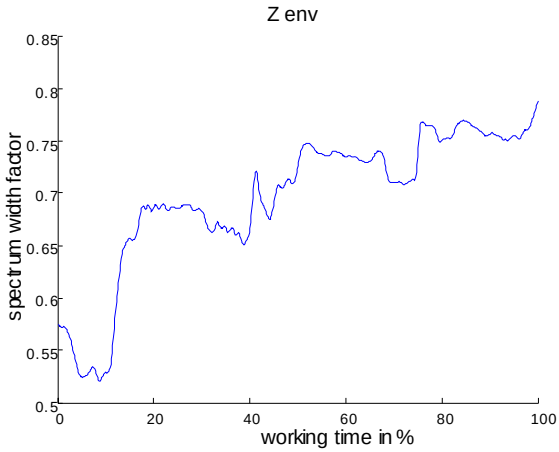

Fig. 6. Spectrum width factor of signal vibration acceleration in direction Z

In this case it is difficult to indicate the bandwidth which is characterized by particular sensitivity to the process of pitting development. The bandwidth around the 6th harmonic frequency can be considered to be the one which reflects the general trend in the biggest degree (Fig. 7).

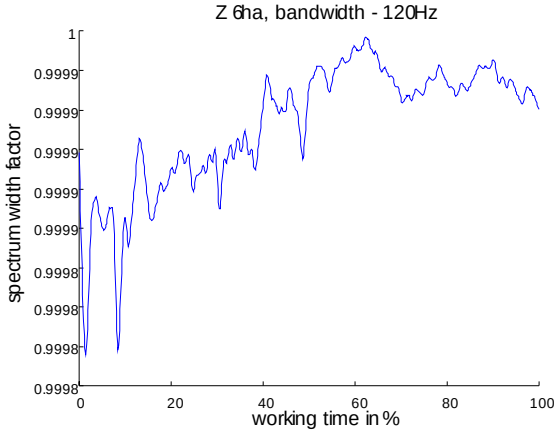

Fig. 7. Spectrum width factor of signal vibration acceleration in direction Z in the bandwidth surrounding the sixth harmonic frequency.

We also conducted the analyses in the bands with widths of 400Hz and 600Hz – the obtained results did not differ significantly. This indicates that the information on the occurrence and development of pitting is encoded in a narrow band around relevant harmonic frequencies which correspond to occurrence of amplitude modulation.

4. ANALYSIS OF THE IMPACT OF TORSIONAL RIGIDITY

The possibility of using the prepared characteristics was analyzed in order to be able to distinguish the values of individual parameters of the experiment. The results concerning the torsional rigidity of shafts are presented below. The grey color denotes the runs determined on the basis of registered signals in a situation when shafts with

higher rigidity were mounted, while the black color denotes the runs associated with shafts having smaller rigidity).

It turned out that the most useful diagnostic parameters in this task were the spectrum width factors for the following signals:

- in direction X in the bandwidth around:
  - the first harmonic frequency of meshing with bandwidth of 400Hz (Fig. 8);
  - the fifth harmonic frequency of meshing with bandwidth of 120Hz, 400Hz, 600Hz (Fig. 9);
- in direction Z in the bandwidth around:
  - the fifth harmonic frequency of meshing with bandwidth of 120Hz (Fig. 10);

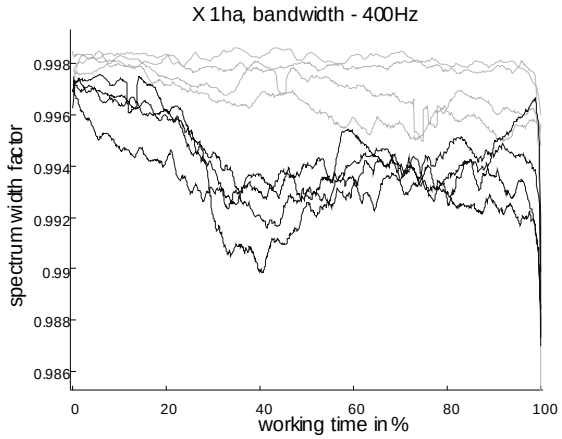

Fig. 8. Spectrum width factor of signal vibration acceleration in direction X in the bandwidth surrounding the first harmonic frequency with width of 400Hz.

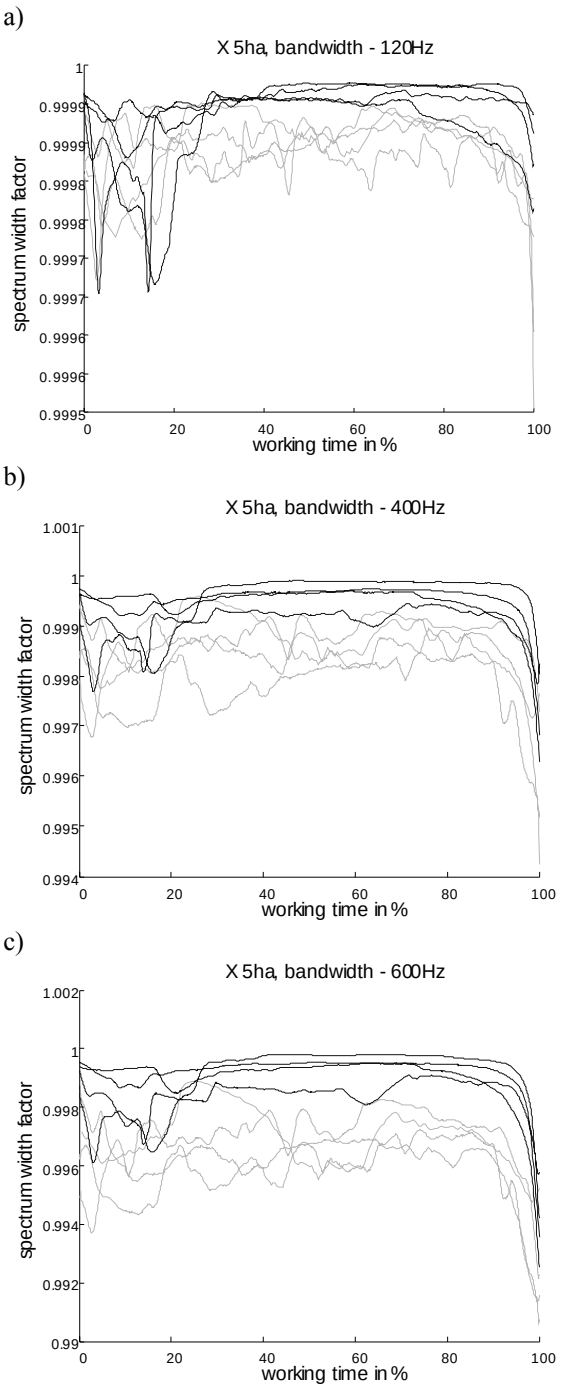

Fig. 9. Spectrum width factor of signal vibration acceleration in direction X in the bandwidth surrounding the fifth harmonic frequency with widths of: a) 120Hz, b) 400Hz, c) 600Hz

The above presented diagnostic parameters enable diagnosis of rigidity of the shafts which were used. Attention should be drawn to the fact that information on rigidity of shafts is hidden in various frequency ranges, however the bandwidth surrounding the fifth harmonic frequency of meshing, with width of 600 Hz in direction X, seems to have the biggest information value. The above presented property results in a situation that the spectrum width factor, determined in relevant bands, can be used for detecting shaft defects (the defects

which lead to changes of its rigidity). The relation between effectiveness of separation and bandwidth points to big influence of torsional rigidity of shafts in toothed gears on tooth contact conditions, and in the case of wheels with spur wheel - on the conditions of mating along the contact line. At the same time, the above means that the phenomenon of frequency modulation is the most appropriate model for the purpose of qualitative and then quantitative description of the influence of the shafts' torsional rigidity on contact conditions. The results of analysis of various widths of the examined spectrum surrounding the same carrier frequency, as presented in Fig. 9, enable such a conclusion to be formulated.

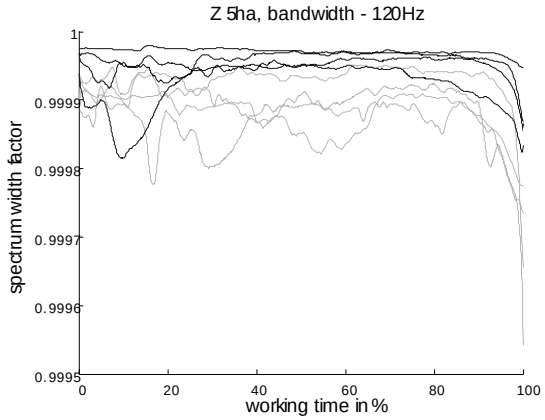

Fig. 10. Spectrum width factor of signal vibration acceleration in direction Z in the bandwidth surrounding the first harmonic frequency with width of 120Hz

5. CONCLUSIONS

The conducted research demonstrates usefulness of spectrum width factor in diagnosis of pitting in toothed wheels. In addition, the parameter is sensitive to the rigidity of the shafts used, thanks to which it can be used for diagnosing these elements. It is particularly interesting to examine the sensitivity of spectrum width factor to other system variables in the context of the factor's sensitivity to change of shafts' rigidity. This means an attempt of obtaining the answer to the following question: Will the change of the shafts' torsional rigidity, caused by defect, lead in addition to any qualitative change in the phenomenon-oriented measures which register disturbance of conditions of mating of specific kinematic nodes of the monitored system, other than changes in the structure of harmonic frequencies of meshing?

Acknowledgments

The paper was prepared on the basis of researches conducted within a project „Monitoring of Technical State of Construction and Evaluation of its Lifespan" (MONIT). Project is co-financed by the European Regional Development Fund in the Operational Programme Innovative Economy (PO IG 1.2)

6. BIBLIOGRAPHY

[1] Cempel Cz., (1982) *Podstawy wibroakustycznej diagnostyki maszyn*, WNT, Warszawa;
[2] Dybała J., Mączak J., Radkowski S., (2006): *Wykorzystanie sygnału wibroakustycznego w analizie ryzyka technicznego (Use of vibroacoustic signals in technical risk analysis*), ITE Warszawa – Radom 2006;
[3] Dziama A., Michniewicz M., Niedźwiedzki A.: (1995) *Przekładnie zębate (Toothed gears*), PWN Warszawa.
[4] Gienkin M. D., Sokołowa A. G.: (1987) *Wibroakusticzeskaja diagnostika maszin i mechanizmów, Maszinostrojenije*, Moskwa.
[5] Lawrowski Z.: (1993) *Tribologia – tarcie i smarowanie (Tribology – friction and lubrication),* W.N. PWN Warszawa.
[6] Muschaweck F.: (1988), *Untersuchengen zur Klassifikation von Fehler- und Schadenbedingten Betriebzuständen an einstufigen Stirnradgetrieben,* rozpr. dok., RWTH Achen.
[7] Nadolny K.: (1998) *Tribologia kół zębatych, Zagadnienie trwałości i niezawodności (Tribology of toothed wheels. Durability and reliability*), ITE Radom.
[8] Niemann G., Winter H.: (1983) *Machinenelemente Band II. Getriebe allgemein, Zahnradgetriebe – Grundlagen*, Stirnradgetriebe, Springer-Verlag, Berlin.
[9] Pytko S., Szczerek M.: (1993*) Pitting – forma niszczenia elementów tocznych (Pitting – a form of wear of rolling elements*), Tribologia no. 4/5.
[10] Radkowski S.: (2002) *Wibroakustyczna diagnostyka uszkodzeń niskoenergetycznych (Vibroacoustic diagnosis of low-energy defects*), Instytut Technologii Eksploatacji, Warszawa-Radom.

Prof. **Stanisław RADKOWSKI,** a professor in the Institute of Automotive Engineering of Warsaw University of Technology, manager of the Technical Diagnosis and Risk Analysis scientific team.
In his scientific work he deals with vibroacoustic diagnosis and technical risk analysis.

Robert GUMIŃSKI, M.Sc. - studying for Ph.D. at the Faculty of Automotive and Construction Machinery Engineering at Warsaw University of Technology.
Scientific interests: safety of technical systems, technical risk.

ANALIZA DYNAMIKI WENTYLATORA PROMIENIOWEGO W WARUNKACH NIEWSPÓŁOSIOWOŚCI WAŁÓW WIRNIKA I SILNIKA

Janusz ZACHWIEJA

Uniwersytet Technologiczno-Przyrodniczy w Bydgoszczy, Zakład Mechaniki Stosowanej,
Bydgoszcz, ul. S. Kaliskiego 7.

Streszczenie

Istotnym problemem jaki występuje w diagnozowaniu maszyn wirnikowych jest poprawna identyfikacja symptomów ich uszkodzeń. W przypadku grupy maszyn przepływowych, do której należą przemysłowe wentylatory promieniowe, najczęściej występującymi uszkodzeniami są: niewyważenie wirnika, defekty łożysk oraz niewspółosiowość wałów. Tryb pracy ciągłej urządzeń powoduje, że często niemożliwe jest wyłączenie maszyny i bezpośredni pomiar wartości równoległego przesunięcia i względnego kąta obrotu osi wałów. Dlatego rzeczą istotną staje się poszukiwanie symptomów tego typu uszkodzenia metodami pośrednimi, dającymi duży stopień pewności w przewidywaniu wpływu niewspółosiowości wałów na dynamikę pracy wentylatora. Zagadnienia te zostały omówione w artykule.

Słowa kluczowe: niewspółosiowość równoległa i kątowa osi, holospectrum, ekscentryczność orbity.

ANALYSIS OF CENTRIFUGAL FAN'S DYNAMICS IN CONDITIONS OF ROTOR AND MOTOR SHAFTS' MISALIGNMENT

Summary

An important problem connected with turbomachine diagnostics is identifying its failure symptoms. In case of the fluid-flow machines, which include industrial centrifugal fans, the most common failures are: a rotor's unbalance, bearings defect and a shaft misalignment. Continuous operation mode results in a fact that it is often impossible to disengage the machine and take a direct measurement of the translation and shaft axes' angle of relative revolution. Therefore an important thing is to determine the symptoms of a failure using indirect methods and a possibility to predict the influence of shafts misalignment on fan operation dynamics. These problems were discussed in this article.

Keywords: parallel misalignment, angular misalignment, holospectrum, orbit excentricyty.

1. WSTĘP

Układ przenoszenia napędu większości maszyn wirnikowych, składa się z szeregu elementów, w tym wałów: czynnego i biernego, połączonych określonym rodzajem sprzęgła.

W zależności od konstrukcji, sprzęgła mogą być sztywne, podatne lub zębate. Sprzęgła podatne dopuszczają niewspółosiowość łączonych wałów w dość szerokich granicach. Nie ma wątpliwości, że niewspółosiowość wałów jest źródłem drgań. Diagnozowanie niewspółosiowości na podstawie analizy sygnału będącego zapisem przebiegu drgań wirnika napotyka na pewne trudności związane z niejednoznacznością symptomów uszkodzenia. Dominujące wartości amplitud parametrów drgań w częstotliwości synchronicznej (1x) oraz wyższej harmonicznej (2x) są zazwyczaj uznawane jako oznaki braku współosiowości układu, choć co do tego nie ma pełnej zgodności badaczy.

Ogólnie definiuje się dwa typy niewspółosiowości łączonych wałów: równoległą i kątową. Najczęściej spotykaną w maszynach jest kombinacja wymienionych rodzajów. W takich przypadkach występowanie dużych wartości amplitud parametrów drgań jest trudne do wyjaśnienia. Szersze rozpoznanie tego problemu dałaby analiza numeryczna dynamiki wirnika uwzględniająca różne własności połączenia wałów. Zastosowanie metody elementów skończonych nie zawsze to umożliwia. Sporym problemem staje się chociażby sposób modelowania sprzęgła.

Przez wiele lat traktowano połączenie jako dodatkowy człon masowy, stopniowo przypisując mu cechy sprężyste i własności tłumienia drgań. Lorenzen, Niederman oraz Wattinger [1] porównali prędkość krytyczną wysokoobrotowego kompresora wyposażonego w alternatywne rodzaje sprzęgła: sztywne, podatne i zębate dowodząc tezy, że połączenie sztywne, w pewnych przypadkach może korzystnie wpływać na stabilność drgań wirnika. Sikhar i Prabhu[2] wyjaśnili dlaczego rodzaj i miejsce usytuowania sprzęgła wywiera znaczący wpływ na poziom wibracji wirnika.

Teoretyczny model sprzęgła podatnego, łączącego silnik z wirnikiem został zaprezentowany przez Xu i Marangoni [3, 4]. Doświadczalne badanie efektu niewspółosiowości wałów podpartych

w łożyskach walcowych, przeprowadził Prabhu [5]. Autor, wykazał, że zwiększanie kąta skoszenia, powoduje zmianę drugiej harmonicznej w odpowiedzi układu. Simon[6], modelował zachowanie dużego turbogeneratora w warunkach niewyważenia i niewspółosiowości. Dewell i Mitchell [7] określili dominujące częstotliwości drgań połączonych elastycznie tarcz, spowodowane kątową niewspółosiowością jako (2x) i (4x) częstotliwości obrotowej. Rosenberg [8] rozważał dynamikę wirującego wału, napędzanego poprzez sprzęgło, w zakresie prędkości krytycznych. Pokazał przy tym możliwość wystąpienia w modelowanych układach niestabilność drgań przy subharmonicznych prędkości krytycznej. Saigo [9] badał niestabilność układu wirnikowego spowodowaną tarciem coulombowskim w sprzęgle. Okazuje się, że zmniejszenie wartości siły tarcia, powoduje korzystną stabilizację układu. Sheu [10], analizując odpowiedź zespołu napędowego z dwoma sprzęgłami sprawdzał relacje pomiędzy skoszeniem osi wałów oraz tarciem w ich połączeniu. Udokumentował przy tym duży wpływ niewspółosiowości kątowej na zmienność prędkości wyjściowej. Hudson [11] pokazał, że wzbudzenie skrętne może powodować promieniowe drgania wirnika.

2. BADANIA DRGAŃ ŁOŻYSK WIRNIKA PRZY PRZESUNIĘTYCH RÓWNOLEGLE OSIACH WAŁÓW I ICH WZGLĘDNYM OBROCIE

Zamiarem autora było zbadanie wpływu niewspółosiowości wałów czynnego i biernego na dynamikę ruchu wirnika wentylatora promieniowego. W tym celu analizowano charakter drgań łożysk wirnika w warunkach dużej wartości przesunięcia równoległego osi wałów (1.15mm w płaszczyźnie pionowej) oraz ich względnego przemieszczenia kątowego (0.378% w płaszczyźnie pionowej i 0.240% w płaszczyźnie poziomej).

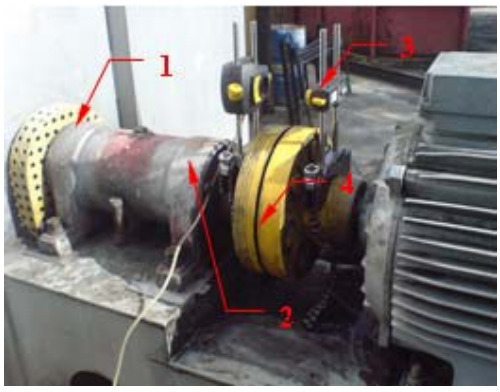

Rys. 1. Sposób osiowania silnika przy pomocy instrumentu laserowego:
1. łożysko bliskie tarczy wirnika, 2. łożysko bliskie sprzęgła, 3. instrument laserowy do osiowania wałów, 4. tarcze sprzęgła

Dla sprzęgła tarczowego ze szpilkami i tulejami gumowymi nie spotyka się w praktyce większych błędów względnego ustawienia elementów łańcucha kinematycznego napędu od wymuszonych w trakcie eksperymentu.

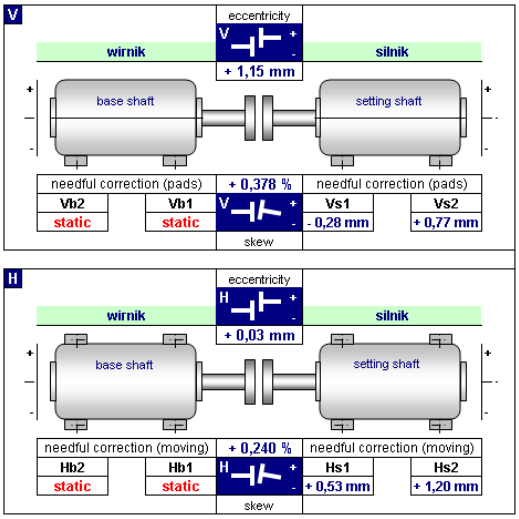

Rys. 2. Wyniki pomiaru względnego położenia osi wirnika i silnika

Rysunek 1 przedstawia sposób pomiaru odchyłki współosiowości wałów wirnika i silnika napędu wentylatora promieniowego. Na jednym z nich osadzony jest emiter-detektor wiązki laserowej odbijanej przez lustro montowane na drugim wale. Urządzenie jest w stanie określić względne położenie osi po obrocie wałów o kąt 60^0. Wynikiem pomiaru są wartości błędu usytuowania elementu wybranego jako aktywny (regulowany) w stosunku do pasywnego (stały). Jako stan wzorcowy uznaje się współliniowość osi obrotu elementów ruchomych. W szczególnym przypadku obydwa elementy łańcucha kinematycznego napędu mogą być traktowane jako aktywne.

Pomiary parametrów drgań łożysk wirnika wentylatora przeprowadzono przy prędkości znamionowej - 1500obr/min. Odpowiadająca tej prędkości częstotliwość drgań synchronicznych wynosi 25Hz. Sprawdzono również, poprzez wyznaczenie krzywej rezonansowej drgań łożysk, że eksploatacyjna prędkość obrotowa wirnika nie znajduje się w obszarze rezonansu (Rys. 3).

Obrazem drgań łożysk jest pokazane na Rys. 4. trójwymiarowe holospectrum [14] z zaznaczonymi wektorami początku fazy (IPV). Trójwymiarowość jest tutaj rozumiana jako zestawienie orbit holospectrum w płaszczyznach kilku łożysk jednocześnie. Pozwala to na określenie różnicy kątów fazowych w kierunkach poziomym i pionowym osobno dla każdego podparcia, jak też pomiędzy łożyskami.

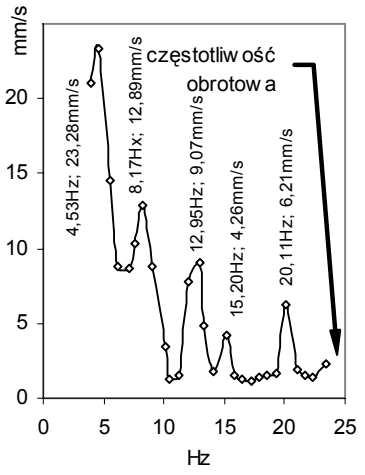

(a) (b)

Rys. 3. Kształt krzywej rezonansowej prędkości drgań wirnika wyznaczony podczas wybiegu

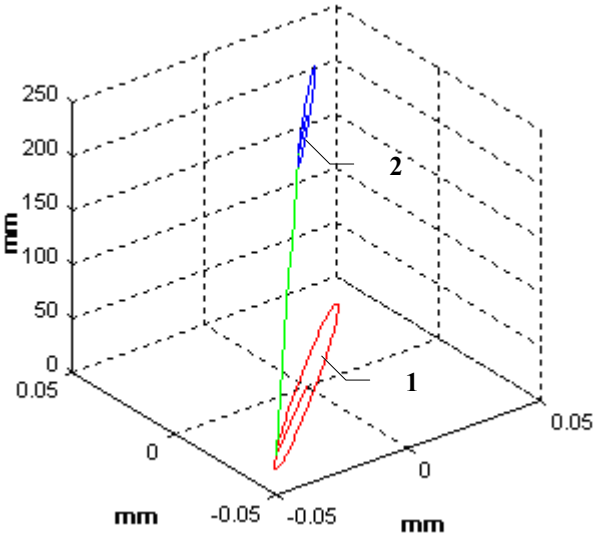

Rys. 4. Holospectrum (1x) drgań łożysk wirnika: 1. orbita w płaszczyźnie **1** położonej bliżej tarczy wirnika: IPV - $0.044.9e^{i221^0}$, 2. orbita w płaszczyźnie **2** położonej bliżej sprzęgła: IPV - $0.024.6e^{i227^0}$

Z uwagi na mniejszą sztywność posadowienia wentylatora w kierunku poziomym amplituda przemieszczenia w tym kierunku, łożyska usytuowanego blisko tarczy, jest największa. Choć na widmie prędkości drgań pojawiają się ultra-harmoniczne częstotliwości obrotowej, to można powiedzieć, że charakter widma jest znamienny dla wirnika z niewyważoną tarczą (Rys. 5a). Widmo prędkości drgań w kierunku pionowym (Rys. 5b), czyli w płaszczyźnie występowania większej niewspółosiowości wałów, zawiera kolejne ultra-harmoniczne prędkości obrotowej wirnika (2x),(3x),(4x).

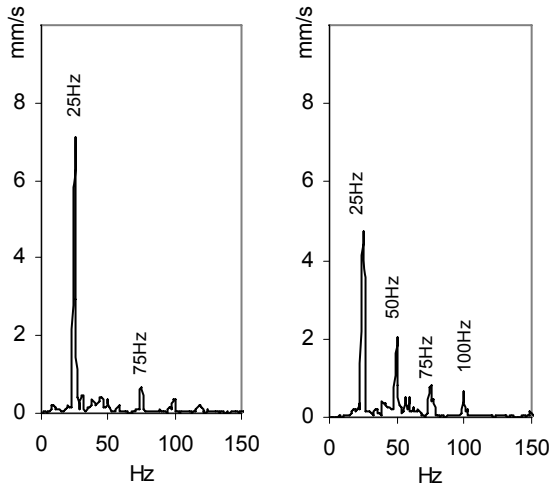

(a) (b)

Rys. 5. Charakterystyki amplitudowo-częstotliwościowe prędkości drgań łożyska bliższego tarczy w kierunku: (a) poziomym, (b) pionowym, przed wyważaniem i osiowaniem wirnika

Na widmie prędkości drgań łożyska położonego bliżej sprzęgła składowe ultra-harmoniczne są zaznaczone wyraźniej niż to ma miejsce dla łożyska położonego bliżej tarczy wirnika (Rys. 6).

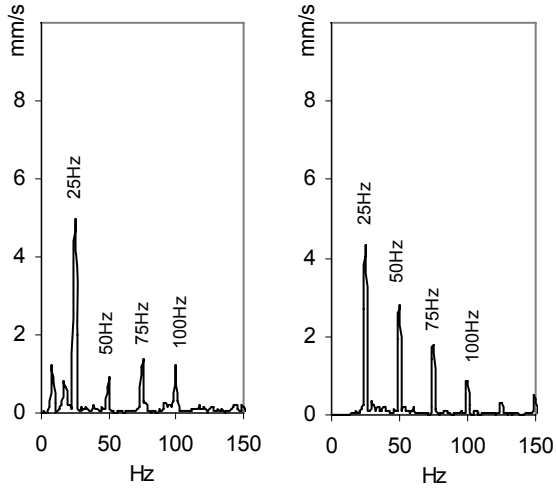

(a) (b)

Rys. 6. Charakterystyki amplitudowo-częstotliwościowe prędkości drgań łożyska bliższego sprzęgła w kierunku: (a) poziomym, (b) pionowym, przed wyważaniem i osiowaniem wirnika

Obecność wyższych harmonicznych zaznacza się wyraźnie w kierunku pionowym, a więc w płaszczyźnie występowania kątowej nierównoległości osi.

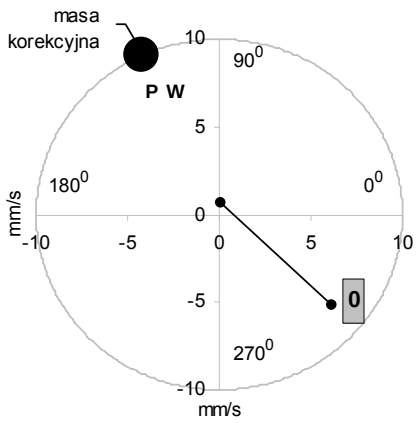

Rys. 7. Przebieg wyważania wirnika w klasie G.2.5 1. amplituda początkowa – 8.08 mm/s, 2. faza początkowa - 320^0, 3. masa korekcyjna – 12.5g, 4. pozycja masy - 115^0, 5. amplituda końcowa – 0.71 mm/s, 6. faza końcowa - 81^0; dobroć wyważania 2.403

Istotną ze względów technicznych kwestią, jest efektywność wyważania wirnika w sytuacji, gdy oprócz siły odśrodkowej wywołanej niewyważeniem na wirnik działają również wymuszenia spowodowane niewspółosiowością wałów. Miejscem przyłożenia tych sił i momentów zginających wał wirnika jest sprzęgło.

Wyważanie przeprowadzono w jednej płaszczyźnie korekcji, przy czym płaszczyzna pomiarowa przechodziła przez pierścień łożyska, prostopadle do jego osi. Prędkość drgań i kąt fazowy mierzono w kierunku poziomym. Do tego celu użyto wyważarki z opcją automatycznego wyznaczania masy próbnej. Jej dobór okazał się wysoce poprawny, zapewniając osiągnięcie zakładanej klasy wyważenia G2.5 przy jednym tylko uruchomieniu.

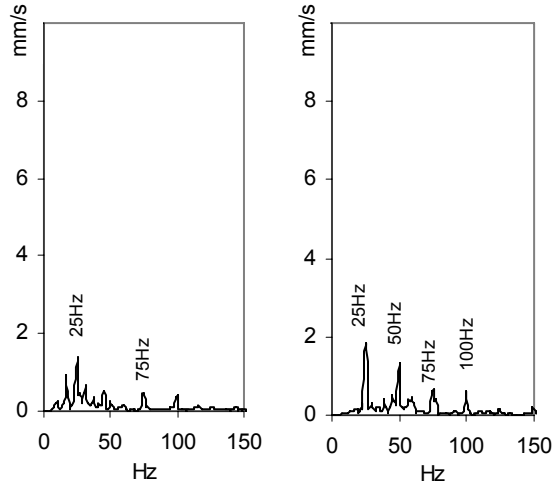

Rys. 8. Charakterystyki amplitudowo-częstotliwościowe prędkości drgań łożyska bliższego tarczy w kierunku: (a) poziomym, (b) pionowym, po wyważaniu wirnika

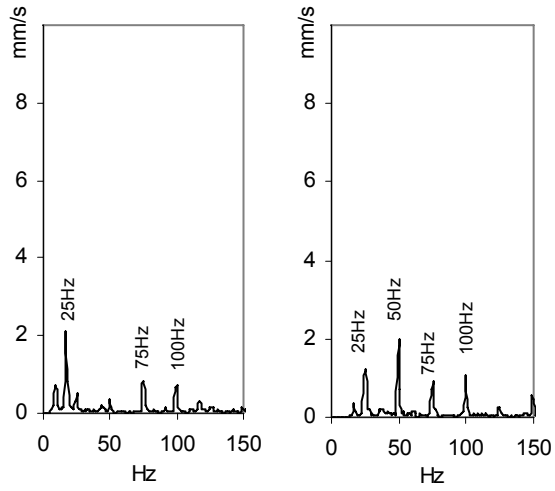

Rys. 9. Charakterystyki amplitudowo-częstotliwościowe prędkości drgań łożyska bliższego sprzęgła w kierunku: (a) poziomym, (b) pionowym, po wyważaniu wirnika

Efektem wyważania było zmniejszenie amplitud prędkości drgań łożysk wirnika tak w kierunku poziomym jak i pionowym (Rys. 8-9), przy czym najlepszy skutek osiągnięto w płaszczyźnie i kierunku mierzonych drgań (Rys. 8a). Widmo prędkości drgań uzyskane po wyważaniu zawiera nadal składowe ultra-harmoniczne częstotliwości synchronicznej.

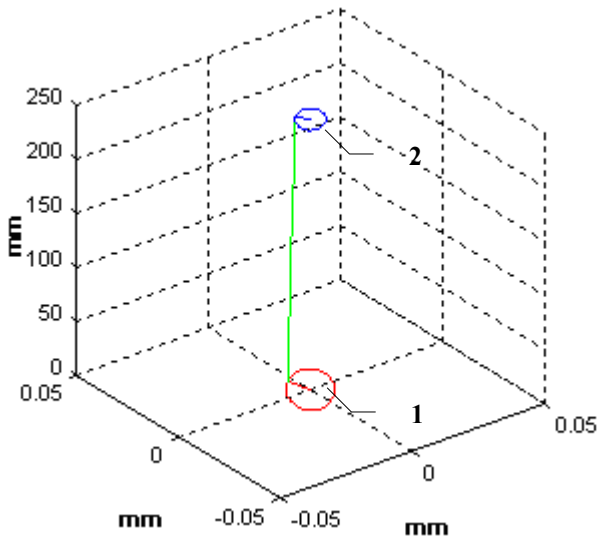

Rys. 10. Holospectrum (1x) drgań łożysk wirnika po wyważaniu:
1. orbita w płaszczyźnie **1** położonej bliżej tarczy wirnika: IPV - $0.0141e^{i66^0}$,
2. orbita w płaszczyźnie **2** położonej bliżej sprzęgła: IPV -. $0.0076e^{i90^0}$

Osiągnąwszy klasę dobroci wyważenia G2.5 można uznać, że widma prezentowane na Rys. 8-9 są odzwierciedleniem stanu, w którym dominującym wymuszeniem są oddziaływania, mające źródło w niewspółosiowości wałów.

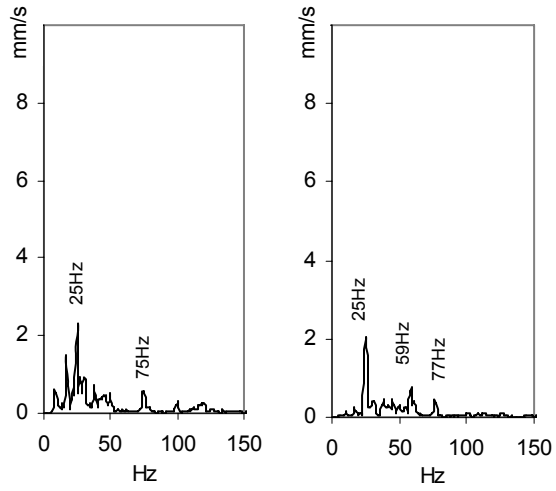

Rys. 11. Charakterystyki amplitudowo-częstotliwościowe prędkości drgań łożyska bliższego tarczy w kierunku: (a) poziomym, (b) pionowym, po wyważaniu i osiowaniu wirnika

Przeprowadzone po wyważaniu tarczy wirnika osiowanie zespołu wirnik-silnik powoduje zanik w widmie amplitud odpowiadających ultra-harmonicznym częstotliwości obrotowej. Efekt ten najsilniej występuje w płaszczyźnie pionowej łożyska bliskiego tarczy sprzęgła.

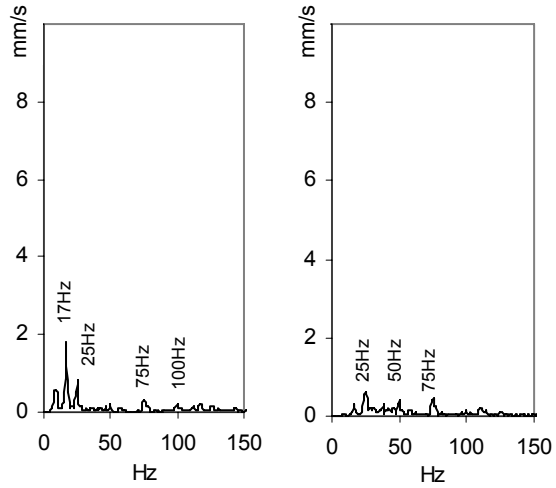

Rys. 12. Charakterystyki amplitudowo-częstotliwościowe prędkości drgań łożyska bliższego sprzęgła w kierunku: (a) poziomym, (b) pionowym, po wyważaniu i osiowaniu wirnika

Jest rzeczą charakterystyczną, że w wyniku osiowania wartość amplitudy drgań w częstotliwości obrotowej nie uległa zasadniczemu zmniejszeniu. Co więcej nastąpił jej wzrost w płaszczyźnie i kierunku pomiarowym przyjętym do wyważania.

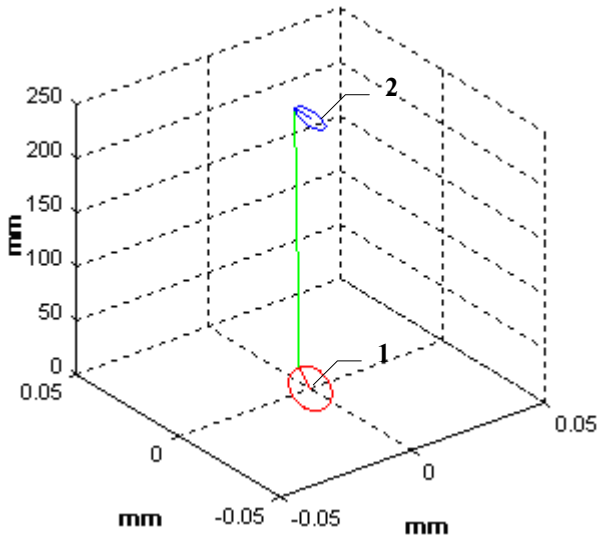

Rys. 13. Holospectrum (1x) drgań łożysk wirnika po wyważaniu:
1. orbita w płaszczyźnie **1** położonej bliżej tarczy wirnika: IPV - $0.0085e^{i107^0}$,
2. orbita w płaszczyźnie **2** położonej bliżej sprzęgła: IPV -. $0.0048e^{i127^0}$

Uszkodzeniom maszyn wirnikowych takim jak: niewyważenie wirnika, pęknięcie wału, niewspółosiowość wałów czynnego i biernego, tarcie między elementami ruchomymi i stałymi, luzy itp. towarzyszą określone symptomy nie tylko w widmie amplitudowo-częstotliwościowym lecz również w widmach fazowych. Skuteczna metoda diagnozowania uszkodzeń powinna –uwzględniając ten fakt- opierać się na analizie drgań układu w dwóch prostopadłych kierunkach. Taki sposób postępowania wyznacza technika holospectrum [15].

Uszkodzenie wirnika typu niewyważenie powoduje, że częstotliwość obrotowa f_1 (1x) staje się dominująca i przy tej częstotliwości różnica kątów fazowych powinna być bliska 90^0. Analizy Chena i jego współpracowników potwierdziły, że w przypadku niewspółosiowości wałów, która występuje w pewnym zakresie kąta wirnika, częstotliwościami charakterystycznymi są: f_1 f_2 i f_4 (f_2 jest dominującą). Różnica kątów fazowych pomiędzy sygnałami mierzonymi w kierunku poziomym i pionowym maleje i przy częstotliwości f_2 jest mniejsza niż dla częstotliwości f_4 oraz f_1 tj. $\Delta f_2 < \Delta f_4 < \Delta f_1$. Rysunki 14 i 15 przedstawiają wykresy zmian kątów fazowych przy częstotliwościach 25Hz(a), 50Hz(b), 75Hz(c), 100Hz(d). Różnice kątów fazowych między kierunkiem poziomym i pionowym dla tych częstotliwości zestawiono w tabelkach pod wykresami. W rozważanym przypadku mamy:
- dla łożyska bliżej tarczy: $6.63^0 < 82^0.15 < 123.06^0$
- dla łożyska bliżej sprzęgła: $48.5^0 < 51.2^0 < 80^0$.

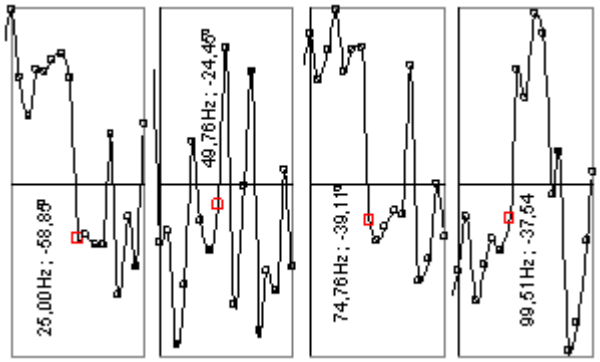

(a) (b) (c) (d)

kierunek poziomy

	faza(1x)	faza(2x)	faza(3x)	faza(4x)
poziom	-58.85	-24.45	-39.54	-37.54
pion	64.21	-17.82	-13.76	44.61
zmiana	**123.06**	**6.63**	**25.78**	**82.15**

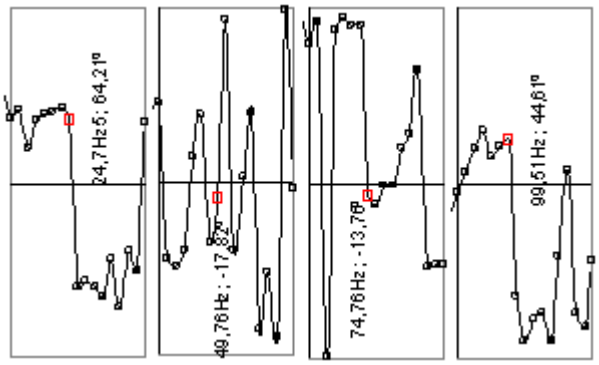

(a) (b) (c) (d)

kierunek pionowy

Rys. 14. Różnica faz pomiędzy prędkością drgań w kierunku poziomym i pionowym dla łożyska bliżej tarczy

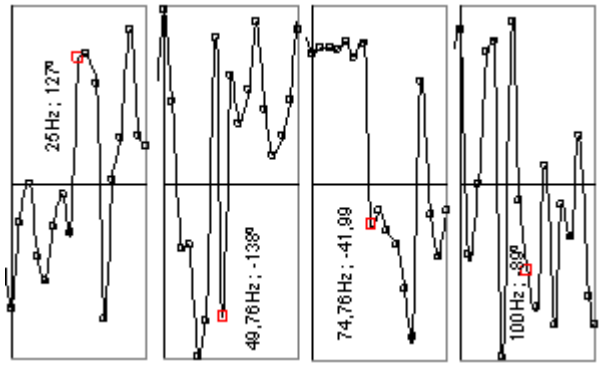

(a) (b) (c) (d)

kierunek poziomy

	faza(1x)	faza(2x)	faza(3x)	faza(4x)
poziom	127	-136	-41.99	-89
pion	47	-89.5	-80	-140.4
zmiana	**80**	**48.5**	**38.2**	**51.2**

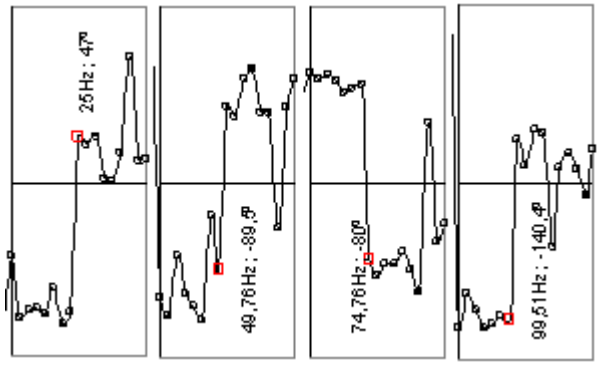

(a) (b) (c) (d)

kierunek pionowy

Rys. 15. Różnica faz pomiędzy prędkością drgań w kierunku poziomym i pionowym dla łożyska bliżej sprzęgła

Używając holospectrum powinniśmy obserwować symptom niewspółosiowości wałów jako wzrost długości głównej półosi elips w częstotliwościach (2x), (4x), (1x) czyli $a_2 > a_4 > a_1$ oraz zmniejszenie ich ekscentryczności w porządku: $e_2 < e_4 < e_1$. W badaniu stwierdzono:

- dla łożyska bliżej tarczy: $a(1x)$=14,43μm, $a(2x)$=16,24μm, $a(4x)$=18,30μm, oraz $e(1x)$=0,903, $e(2x)$=0,999, $e(4x)$=0,825.

Pomiędzy długościami większych półosi elips holospectrum zachodzi nierówność $a_1<a_2<a_4$, natomiast ich ekscentryczność określa relacja $e_2>e_1>e_4$,

- dla łożyska bliżej sprzęgła $a(1x)$= 8,35μm, $a(2x)$=25,58μm, $a(4x)$=35,63μm, oraz $e(1x)$=0,944, $e(2x)$= 0,992, $e(4x)$= 0,920.

Relacje $a_1<a_2<a_4$ oraz $e_2<e_1<e_4$ dla holospectrum drgań łożyska nie spełniają ściśle warunku określonego przez Chena. Przyczyną tego stanu rzeczy może być fakt, że nie możemy tutaj mówić o występowaniu czystej niewspółosiowości. Spełnione są natomiast w odniesieniu do obydwu łożysk zależności: $a(2x)>a(1x)$ oraz $e(2x)<e(1x)$, co osłabia kryterium Chena do przesłanki, że niewspółosiowość wałów powoduje zwiększenie w częstotliwości podwójnej harmonicznej długości głównej półosi elipsy holospectrum oraz zmniejszenie jej ekscentryczności w stosunku do wartości tych parametrów wyznaczonych dla częstotliwości obrotowej.

3. MODELOWANIE SPRZĘGŁA

Matematyczny opis ruchu układu dwóch niewspółosiowych wirników został przedstawiony w pracy [16]. Związki tam zamieszczone są wynikiem analizy równań wyrażających bilans energii potencjalnej i kinetycznej wirników oraz

łącznika posiadającego sztywność poprzeczną i skrętną. Tłumienie w układzie jest pomijane.

Rozwiązanie równań ruchu dało rezultat nieoczekiwany dla samych autorów. Wyznaczone bowiem charakterystyki amplitudowo–częstotliwościowe drgań układu nie zawierają znaczących amplitud drgań w częstotliwości (2x), co pozostaje w sprzeczności z dotychczasowymi ustaleniami innych badaczy.

W pracy [2] został pokazany sposób modelowania wirnika metodą FEM uwzględniający niewspółosiowość. Do węzła, w miejscu usytuowania sprzęgła, wprowadzono siłę oraz moment o wartości wynikającej z założonej niewspółosiowości równoległej ~2mm i nierównoległości kątowej w granicach 0^0-0.6^0. Rozwiązanie ograniczono do aspektów związanych z występowaniem w odpowiedzi układu członów periodycznych (1x), oraz (2x) częstotliwości obrotowej.

W dynamice maszyn w zależności od wymaganego stopnia uogólnienia wykorzystuje się kilka modeli opisujących własności połączenia. Model Kramera [3] pierwszego rodzaju (Rys. 16a) nie uwzględnia innych efektów niż bezwładnościowe. Sprzęgło jest w tym przypadku traktowane jako połączenie sztywne dwóch tarcz o określonej masie i momencie bezwładności.

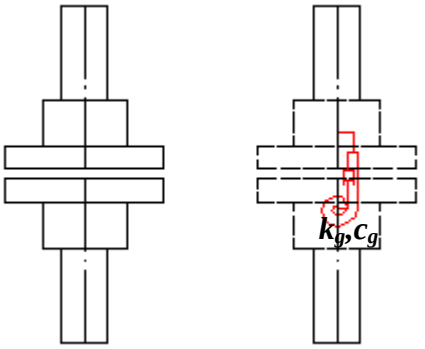

(a) (b)

Rys. 16. Modele Kramera: (a) pierwszego rodzaju, (b) drugiego rodzaju

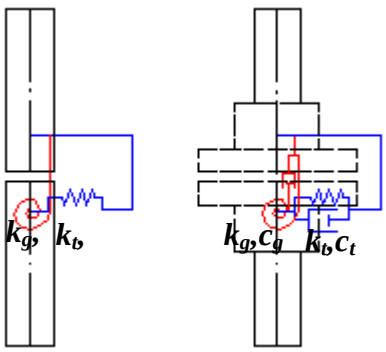

(a) (b)

Rys. 17. Modele Nelsona-Crandalla: (a) pierwszego rodzaju, (b) drugiego rodzaju

W modelu Kramera drugiego rodzaju (Rys. 16b), kątowa nierównoległość osi wałów powoduje zginanie elementu sprężystego w trakcie obrotu tarcz.

Pierwsze uproszczenie Nelsona-Crandala [5] (Rys. 17a) polega na zaniedbaniu bezwładności sprzęgła, podobnie jak i zdolności do tłumienia drgań. Model uwypukla jednie cechy sprężyste przy zginaniu elastycznej części sprzęgła w warunkach niewspółosiowości kątowej i równoległej osi wałów.

Najbardziej ogólnym modelem jest model Nelsona-Crandalla drugiego rodzaju (Rys. 17b), w którym uwzględniono sztywności związane z względnymi przemieszczeniami: translacyjnym oraz kątowym tarcz.

To krótkie wprowadzenie do zagadnienia modelowania niewspółosiowości wałów pokazuje złożoność problemu, z którym mierzyło się dotąd niewielu badaczy, dochodząc często do sprzecznych wniosków.

W diagnostyce „warsztatowej" panuje od lat utarty pogląd, że dominująca wartość amplitudy o częstotliwości (2x) stanowi rozstrzygające kryterium występowania niewspółosiowości w układzie. Przedstawione wyniki badań wskazują, że jest to warunek konieczny, lecz niewystarczający. Aby móc formułować wnioski oparte o powtarzalne i do końca znane warunki analizy, racjonalnym wydaje się rozważenie zagadnienia na drodze numerycznej.

Obliczenia przeprowadzono w oparciu o metody dynamiki układów wieloczłonowych przyjmując, co ze względu na konstrukcję i warunki pracy wirnika wentylatora nie jest specjalnie skomplikowane, cechy tarczy i wału jako ciał sztywnych [13]. Model sprzęgła jest identyczny z założeniami Nelsona-Crandalla drugiego rodzaju o sztywności i tłumieniu zestawionych w Tab.1. Konweniują one z danymi przyjętymi w pracy [12].

Tabela 1. Parametry sztywności i tłumienia modelu sprzęgła przyjęte do analizy [12]

oś →	**X**	**Y**	**Z**
sztywność translacyjna (poprzeczna) N/m	$1.2 \cdot 10^9$	$1.2 \cdot 10^9$	$1.2 \cdot 10^9$
tłumienie translacyjne (poprzeczne) Ns/m	11.3	11.3	11.3
sztywność obrotowa Nm/rad	$1.36 \cdot 10^6$	$1.36 \cdot 10^6$	$1.36 \cdot 10^6$
tłumienie obrotowe Nms/rad	11.3	11.3	11.3

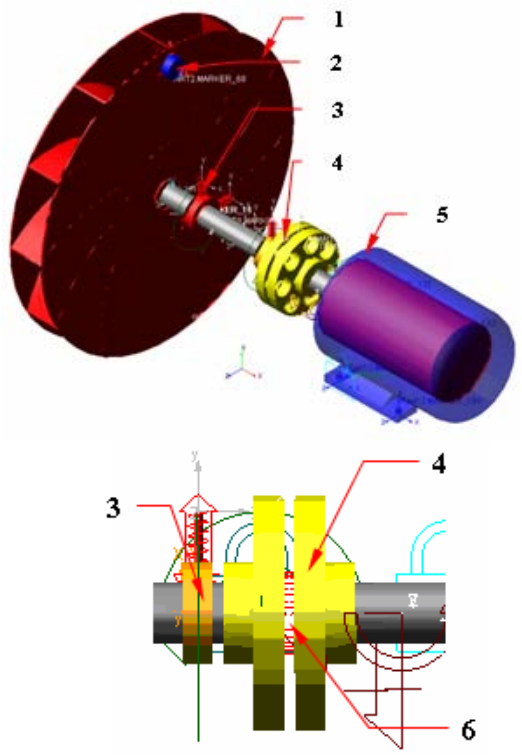

Rys. 18. Model wirnika przyjęty do analizy: 1. tarcza, 2. niewyważenie, 3. łożysko, 4. sprzęgło, 5. silnik, 6. człon sprężysto-tłumiący

Założono niewspółosiowość wirnika i silnika o charakterze kątowym i wartości 0.52% bez wyraźnej ekscentryczności (Rys. 19).

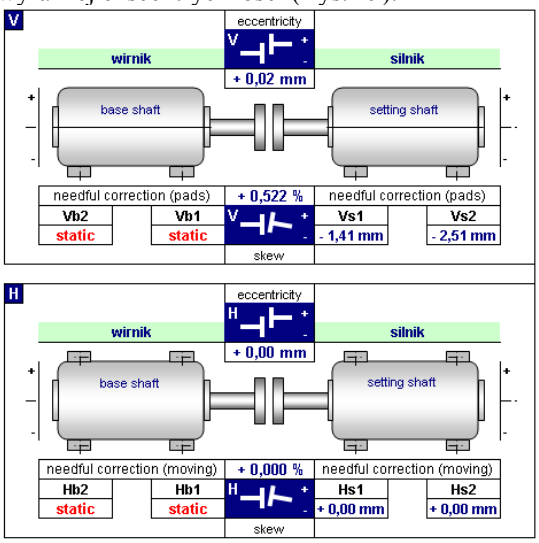

Rys. 19. Względne położenia osi wirnika i silnika w badanym modelu

Tarczę wirnika w traktowano w obliczeniach jako dokładnie wyważoną (umowna masa niewyważenia $m = 0$). Sztywność i tłumienie łożysk (Tab.2) przyjęto analogicznie jak w pracach [2, 17].

Umownie rozpędzano wirnik w czasie 5s do prędkości obrotowej 1500obr/min. Odpowiedź układu na wymuszenie wywołane niewspółosiowością jest przedstawiona w postaci charakterystyki Bodego (Rys. 20).

Tabela 2. Parametry sztywności i tłumienia modelu łożyska przyjęte do analizy[2, 17]

oś →	X	Y	Z
sztywność translacyjna (poprzeczna) N/m	10^9	10^9	10^9
tłumienie translacyjne (poprzeczne) Ns/m	10^3	10^3	10^3

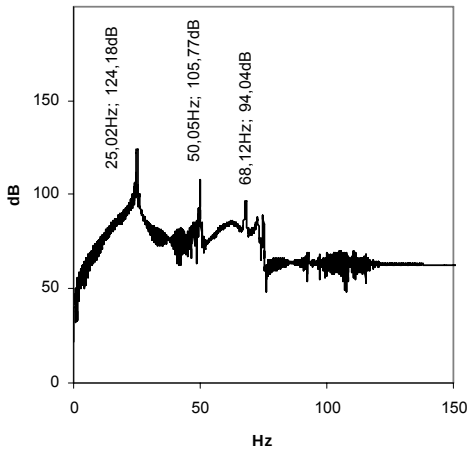

Rys. 20. Charakterystyka Bodego prędkości drgań wirnika

Na wykresie, oprócz amplitudy w częstotliwości 25Hz zauważalna jest ultraharmoniczna (2x) oraz amplituda prędkości drgań własnych ~68Hz. Śmiało więc można przyjąć, że drgania wirnika w częstotliwości obrotowej nie mogą mieć charakteru rezonansowego.

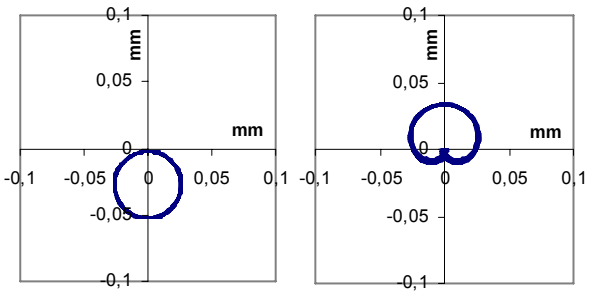

(a) (b)

Rys. 21. Kształt orbity nie filtrowanej: (a) łożysko bliżej tarczy, (b) łożysko bliżej sprzęgła

Ciężar wirnika oraz przewyższenie osi silnika w stosunku do osi wirnika powoduje, że trajektoria ruchu geometrycznego środków przekroju wału wirnika w płaszczyźnie łożysk są położone tak jak pokazuje Rys.21. Dominująca wartość amplitudy w częstotliwości (2x) czyni, że kształt orbity łożyska usytuowanego blisko sprzęgła jest „jabłkowaty".

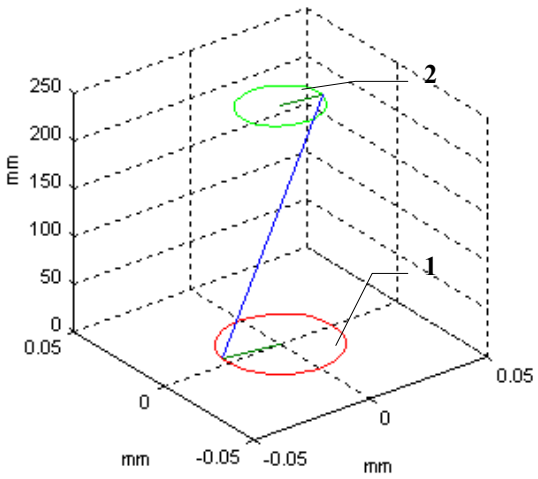

Rys. 22. Holospectrum (1x) przemieszczeń łożysk w modelu wirnika:
1. orbita w płaszczyźnie **1** położonej bliżej tarczy wirnika: IPV - $0.0236e^{i175^0}$,
2. orbita w płaszczyźnie **2** położonej bliżej sprzęgła: IPV -. $0.0170e^{i355^0}$

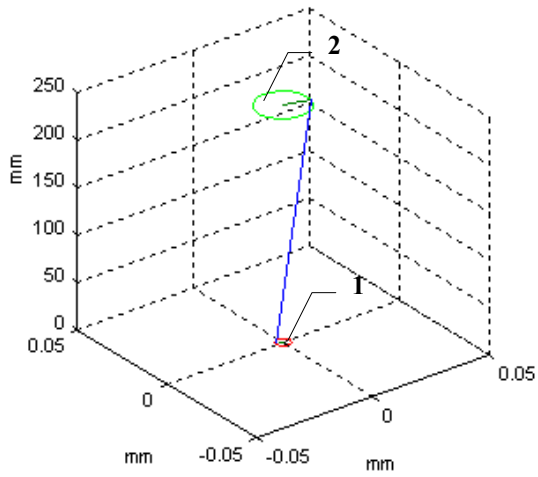

Rys. 23. Holospectrum (2x) przemieszczeń łożysk w modelu wirnika:
1. orbita w płaszczyźnie **1** położonej bliżej tarczy wirnika: IPV - $0.0031e^{i171^0}$,
2. orbita w płaszczyźnie **2** położonej bliżej sprzęgła: IPV -. $0.0108e^{i349^0}$

Orbity holospectrum łożyska przy sprzęgle spełniają warunek Chena: $a_2>a_1$ oraz $e_2<e_1$. Rozwiązanie wskazuje, podobnie jak to ma miejsce w badanym układzie rzeczywistym, możliwość występowania w widmie drgań (Rys.24-25) amplitud odpowiadających wyższym harmonicznym. Ich wartości zależą od wielkości niewspółosiowości a także sztywności i tłumienia nie tylko sprzęgła ale również łożysk. W pewnych przypadkach harmoniczne (4x), (3x) a nawet (2x) mogą być na tyle małe, że stają się niezauważalne.

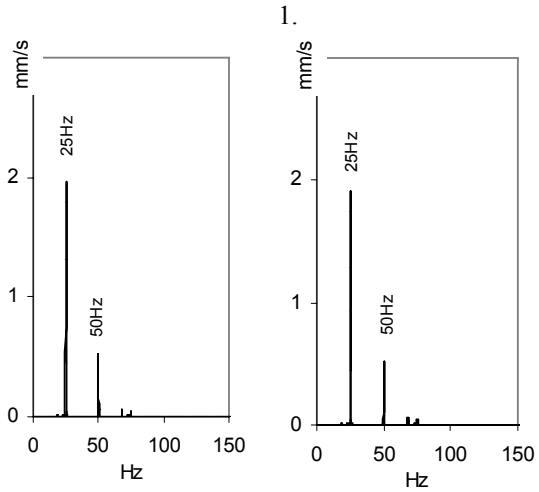

Rys. 24. Charakterystyki amplitudowo-częstotliwościowe prędkości drgań łożyska bliższego tarczy w kierunku: (a) poziomym, (b) pionowym

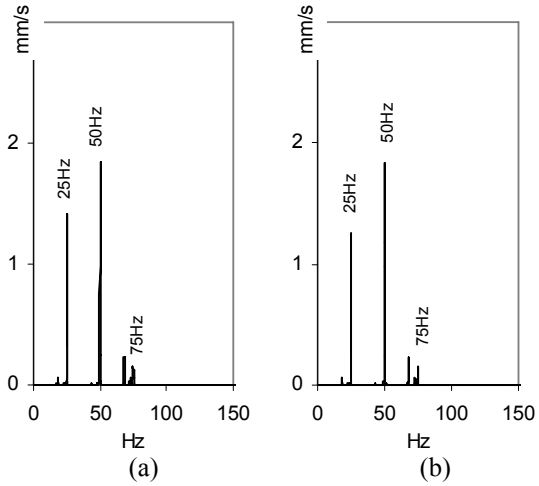

Rys. 25. Charakterystyki amplitudowo-częstotliwościowe prędkości drgań łożyska bliższego sprzęgła w kierunku: (a) poziomym, (b) pionowym

4. WNIOSKI

Oddziaływania sił i momentów w połączeniu wałów silnika i wirnika przy ich niewspółosiowości nie wpływa na zmianę częstotliwości drgań własnych układu. W trakcie przeprowadzonego eksperymentu nie stwierdzono, aby niewspółosiowość wirnika i silnika utrudniała wyważenie zespołu.

Przesunięcie równoległe i kątowe osi wałów prowadzi do cyklicznego zginania elastycznych elementów sprzęgła. Zginanie w częstotliwości synchronicznej (1x) prędkości obrotowej wirnika ma wpływ na zmianę amplitudy drgań. Niewspółosiowość w układzie jest zazwyczaj kompensowana przez podatność i tłumienie części elastycznych sprzęgła na tyle, że w praktyce nie obserwuje się aby drgania wentylatora promieniowego osiągały wartości niedopuszczalne

tylko z powodu niewspółosiowości wałów. Dowiodły tego badania, w których dopuszczono znaczne przemieszczenie równoległe i kątowe osi, a mimo to wartość amplitudy prędkości drgań nie zmieniła się znacząco.

Odpowiedź układu w częstotliwości ultra-harmonicznej (2x) i wyższych jest charakterystyczną cechą nieprawidłowej współosiowości wałów. Dominacji drgań w podwójnej harmonicznej częstotliwości obrotowej wirnika może sprzyjać lokalizacja sprzęgła i kształt postaci drgań własnych wirnika. Ponieważ łożyska charakteryzują się określoną podatnością, postać modalna, przy której następuje zmiana kąta fazowego przed i za sprzęgłem, sprzyja występowaniu drgań w częstotliwości (2x).

Przedstawione w pracy kryteria diagnozowania niewspółosiowości, oparte na analizie zmian kątów fazowych czy też holospectrum nie należy pojedynczo traktować jako rozstrzygające, choć rozosiowanie wirnika w wielu przypadkach powoduje jasne i wyraźne symptomy w postaci właśnie składowych 2x a także zmian charakterystyk modalnych. Uwagę tę można odnieść zwłaszcza do sprzęgieł o większej sztywności. Ogólnie należy jednak przyjąć, że dopiero zespół kilku cech charakterystycznych występujących łącznie może stanowić podstawę do formułowania wniosków odnośnie występowania niewspółosiowości w układzie.

LITERATURA

[1] Lorenzen H, E. A. Niederman E. A., Wattinger W.: *Solid couplings with flexible intermediate shafts for high speed turbo compressor trains*. Proceedings of the 18th Turbomachinery Symposium, Dallas, TX,USA. 101-110, 1991.

[2] Sekhar A. S., Prabhu B. S.: *Effects of coupling misalignment on vibrations of rotating machinery*. Journal of Sound and Vibration 185, 1995, 655-671.

[3] Xu M., Maragoni R. D.: *Vibration analysis of a motor-flexible coupling-rotor system subject to misalignment and unbalance*. Part I: theoretical model analysis. Journal of Sound and Vibration, 176, 1994, 663-679.

[4] Xu M., Maragoni R. D.: *Vibration analysis of a motor-flexible coupling-rotor system subject to misalignment and unbalance*. Part II: experimental validation. Journal of Sound and Vibration, 176, 1994, 681-691.

[5] B. S. Prabhu B. S.: *An experimental investigation on the misalignment effects in journal bearings*. STLE Tribology Transactions, 40, 1997, 235-242.

[6] G. Simon G.: *Prediction of vibration of large turbo-machinery on elastic foundation due to unbalance and coupling misalignment*. Proceedings of the Institution of Mechanical Engineers, 206, 1992, 29-39.

[7] Dewell D. L., Mitchell L. D.: *Detection of a misaligned disk coupling using spectrum analysis. Journal of Vibration*, Acoustics, Stress, and Reliability in Design, 106, 1984, 9-16.

[8] Rosenberg R. M.: *On the dynamical behavior of rotating shafts driven by universal (Hooke) coupling*. Journal of Applied Mechanics 25, 1958, 47-51.

[9] Saigo M., Okada Y., Ono K.: *Self-excited vibration caused by internal friction in universal joints and its stabilizing method*. Journal of Vibration and Acoustics 119, 1997, 221-229

[10] Sheu P. P., Chieng W. H., Lee A. C., *Modeling and analysis of the intermediate shaft between two universal joints*. Journal of Vibrations and Acoustics 118, 88-99.

[11] Hudson J. H.: *Lateral vibration created by torsional coupling of centrifugal compressor system driven by a current source drive for a variable speed induction motor*. Proceedings of the 21st Turbomachinery Symposium, Texas A&M 113-123.

[12] Tadeo A. T., Cavalca K. L.: *A Comparison of flexible coupling models for updating in rotating machinery response*, J. of the Braz. Soc. of Mech. Sci. & Eng. July-September, Vol. XXV, No. 3 , 2003, 235-246.

[13] Qu L., Chen Y., Liu X.: *A new approach to computer aided vibration surveillance of rotating machinery,* International Journal of Computer Applications in Technology, 2, pp. 108-117, 1989.

[14] Qu L., Liu X., Peyronne G., Chen Y.: *The holospectrum: a new method for rotor surveillance and diagnosis*, Mechanical Systems and Signal Processing, 3, pp. 255-267, 1989.

[15] Chen Y. D., Du R., Qu L. S.: *Fault features of large rotating machinery and diagnostic using sensor fusion,* Journal of Sound and Vibration, 188(2), pp. 227-242, 1995.

[16] Al-Hussain K. M., Redmond I., *Dynamic response of two rotors connected by rigid mechanical coupling with parallel misaligment*, Journal of Sound and Vibration, 249(3), pp. 483-498, 2002.

[17] Šarenac M.: *Stiffness of machine tool spindle as a main factor for treatment accuracy*, University of Niš. Facta Universitatis, Mechanical Engineering 1(6), pp. 665 – 674, 1999.

Dr inż. **Janusz ZACHWIEJA** jest adiunktem w Zakładzie Mechaniki Stosowanej Uniwersytetu Techniczno-Przyrodniczego w Bydgoszczy. Zajmuje się zagadnieniami z obszaru dynamiki układów mechanicznych oraz mechaniki płynów.

PRÓBKOWANIE SYGNAŁÓW DIAGNOSTYCZNYCH CZĘŚĆ IV PRÓBKOWANIE SYGNAŁÓW W PRZESTRZENI BERNSTEINA I PALEYA - WIENERA

Zenon SYROKA

Uniwersytet Warmińsko – Mazurski, Wydział Nauk Technicznych
Ul. Oczapowskiego 11, 10 –717 Olsztyn

Streszczenie

W pracy przedstawiono matematyczny opis sygnałów diagnostycznych przestrzeni Bernsteina i Paleya- Wienera oraz sposób konstrukcji tej przestrzeni. Podano matematyczną teorię w zastosowaniu do próbkowania sygnałów diagnostycznych w tych przestrzeniach.

Słowa kluczowe: próbkowanie sygnałów, przestrzenie sygnałów, przestrzeń Bernsteina, przestrzeń Paleya-Wienera.

SAMPLING OF THE DIAGNOSTIC SIGNALS
PART IV
SIGNAL SAMPLING IN THE BERENSTEIN AND PALEY-WINER SPACE

Summary

In this article are defined the diagnostic signals in the Berenstein and Paley-Wiener space and the way this space is constructed. The mathematical theory in the application of the diagnostic sampling signal is presented.

Keywords: sampling signals, signals space, Berenstein space, Paley-Wiener space.

1. WPROWADZENIE

Sygnały należące do przestrzeni Bernsteina B_σ^p i Paley – Winera PW_σ^p, $\sigma > 0$, $1 \le p \le \infty$, są szczególnie ważne ze względu na właściwości ich opisu za pomocą szeregów kardynalnych. Nadają się one bardzo dobrze do opisu **próbkowania regularnego**.

W próbkowaniu regularnym, momenty próbkowania sygnałów są od siebie równo odległe, sygnały próbkowane są dolnopasmowe i mają jednowymiarową dziedzinę położoną centralnie względem początku układu (względem zera).

2. SZEREG FOURIERA W PRZESTRZENIACH FUNKCYJNYCH

Niech N, N_o, Z oznaczają odpowiednio zbiór liczb naturalnych, zbiór nieujemnych liczb całkowitych, zbiór wszystkich liczb całkowitych, a R, R_+, C, zbiór liczb rzeczywistych, dodatnich rzeczywistych i zespolonych.

W szczególności R^n jest n – wymiarową przestrzenią eukildesową z normą w postaci:

$$\|u\|_2 := \left(u_1^2 + ... + u_n^2\right)^{1/2}, \qquad (1)$$

gdzie $u = (u_1,.....,u_n)$, $u_j \in R$, $j \in \{1,2,.....,n\}$.

Iloczyn skalarny $u, v \in R^n$ dany jest wzorem:

$$uv := \sum_{j=1}^{n} u_j v_j \ . \qquad (2)$$

Przez u/v oznaczymy wektor $\left(u_1/v_1,....., u_n/v_n\right)$, a przez u^{-1} wektor $\left(1/u_1,..... 1/u_n\right)$. Podobnie $\lfloor u \rfloor$ oznacza wektor $(\lfloor u_1 \rfloor.....,\lfloor u_n \rfloor)$, gdzie $\lfloor u_n \rfloor$ oznacza największą liczbę całkowitą nie większą niż u_n.

Przez $[a,b]$, $a,b \in R^n$, oznaczymy n – wymiarowy przedział zawierający wszystkie wektory $u \in R^n$, spełniające warunek $a \le u \le b$ (porządek po współrzędnych).

Dla $k \in N_0^n$, $u \in R^n$, określimy następujące wielkości:
$|k| := k_1 + ... + k_n$.

$u^k := u_1^{k_1} .....u_n^{k_n}$.

$k!:= k_1!.....k_n!$.

Dla funkcji $s: R^n \to C$ wielkość $D^k s$ określimy wzorem:

$$D^k s := \frac{\delta^{|k|}}{\delta u^k} s := \frac{\delta^{|k|}}{\delta u_1^{k_1} .....\delta u_n^{k_n}} s \ , \ \left(|k| = r\right). \tag{3}$$

Niech $C\left(R^n\right)$ będzie przestrzenią wszystkich jednostajnie ciągłych i ograniczonych funkcji $s: R^n \to C$, wyposażonych w normę supremum $\|s\|_c$ i niech

$C^r\left(R^n\right) := \left\{s \in C\left(R^n\right), \quad D^k s \in C\left(R^n\right) \quad \forall \quad |k| \le r\right\}$

$r \in N_o$, będzie przestrzenią funkcji ciągłych r - krotnie różniczkowalnych w sposób ciągły.

$L^p\left(R^n\right)$ oznacza przestrzeń wszystkich mierzalnych funkcji $s: R^n \to C$, dla których normy

$$\|s\|_{L^p} := \left\{\frac{1}{\left(\sqrt{2\Pi}\right)^n} \int_{R^n} |s(u)|^p \, du\right\}^{1/p},$$

$$\left(1 \le p < \infty\right). \tag{4}$$

$$\|s\|_{L^\infty} := ess \sup_{u \in R^n} |s(u)|, \tag{5}$$

są skończone.

L_λ^p, $\lambda \in R_+^n$, $\left(1 \le p \le \infty\right)$ jest przestrzenią λ - okresowych mierzalnych funkcji $s: R^n \to C$, które są całkowalne w p – tej potędze w przedziale $(0, \lambda)$ z normą

$$\|s\|_{L_\lambda^p} = \left\{\left(\prod_{j=1}^n \lambda_j\right)^{-1} \int_{(0,\lambda)} |s(u)|^p \, du\right\}^{1/p} \tag{6}$$

Transformata Fouriera $\hat{s}$ funkcji $s \in L^1\left(R^n\right)$ jest zdefiniowana wzorem:

$$\hat{s}(v) := \frac{1}{\left(\sqrt{2\Pi}\right)^n} \int_{R^n} s(u) e^{ivu} \, du \ , \ \left(v \in R^n\right). \tag{7}$$

Transformata Fouriera – Plancherela funkcji $s \in L^p\left(R^n\right)$, $1 < p \le 2$, jest określona jako funkcja $\hat{s}: R^n \to C$, która spełnia zależność:

$$\lim_{\rho \to \infty} \left\| \frac{1}{\left(\sqrt{2\Pi}\right)^n} \int_{K_\rho(0)} s(u) e^{-iuv} - \hat{s}(v) \right\|_{L^q} = 0 \, , \tag{8}$$

gdzie $K_\rho(0) \subset R^n$ jest kulą o środku w punkcie 0 i promieniu $\rho > 0$, i $\frac{1}{p} + \frac{1}{q} = 1$.

K – ty współczynnik Fouriera sygnału $s \in L_\lambda^1$ jest zdefiniowany jako:

$$[s]_\lambda^\wedge(k) := \left(\prod_{j=1}^n \lambda_j\right)^{-1} \int_{(0,\lambda)} s(u) e^{-i2\Pi k \frac{u}{\lambda}} du \ ,$$

$$\left(k \in Z^n\right), \tag{9}$$

a odpowiadający powyższej transformacie szereg Fouriera dany jest w postaci:

$$s(t) \sim \sum_{k \in Z^n} [f]_\lambda^\wedge(k) e^{i2\Pi k \frac{t}{\lambda}} \ , \ \left(t \in R^n\right). \tag{10}$$

W ogólności $\sum_{k \in Z^n}$ jest wartością granicy

$$\lim_{N \to \infty} \sum_{k_1=-N}^{N} ..... \sum_{k_n=-N}^{N} .$$

Związek pomiędzy transformatą Fouriera sygnału $s \in L^1\left(R^n\right)$ i sygnałem $s \in L_\lambda^1$ określa twierdzenie Poissona.

Jeżeli $s \in L^1\left(R^n\right)$, to szereg:

$$s_\lambda^*(t) := \frac{\prod_{j=1}^n \lambda_j}{\left(\sqrt{2\Pi}\right)^n} \sum_{k \in Z^n} s(t + \lambda k), \left(t \in R^n\right), \tag{11}$$

jest zbieżny bezwzględnie prawie wszędzie. Zdefiniujemy sygnał $s_\lambda^* \in L_\lambda^1$ taki, że

dla każdego $g \in L_\lambda^\infty$. (12)

bierając w szczególności

$$g(u) = e^{\left(-i2\Pi \frac{u}{\lambda}\right)}, \tag{13}$$

otrzymamy:

$$\hat{s}_\lambda^*(k) = \hat{s}\left(\frac{2\Pi k}{\lambda}\right), \qquad \left(k \in Z^n\right). \tag{14}$$

W powyższym wyrażeniu lewa strona wyznacza współczynniki Fouriera λ - okresowego sygnału s_λ^* zdefiniowanego za pomocą (9), a prawa strona jest transformatą Fouriera sygnału $s \in L^1\left(R^n\right)$ zdefiniowanego za pomocą (7).

Sygnał s_λ^* można rozwinąć w szereg Fouriera:

$$s_\lambda^*(t) = \frac{\prod_{j=1}^n \lambda_j}{\left(\sqrt{2\Pi}\right)^n} \sum_{k \in Z^n} s(t + \lambda k) \sim \sum_{k \in Z^n} \hat{s}\left(\frac{2\Pi k}{\lambda}\right) e^{i2\Pi k \frac{t}{\lambda}} \tag{15}$$

Jeżeli obydwa szeregi występujące w wyrażeniu (15) są jednostajnie zbieżne w zwartych podzbiorach R^n, to znak „~" zastąpiony może być przez „=".

Splot sygnałów $s_1 * s_2$, $s_1, s_2 : R^n \to C$ jest zdefiniowany wzorem:

$$(s_1 * s_2)(t) = (2\Pi)^{-n/2} \int_{R^n} s_1(u) s_2(t-u) du \,, \tag{16}$$

jeśli tylko całka istnieje.

Jeżeli $s_1 \in L^1(R^n)$ i $s_2 \in L^p(R^n)$, $1 \le p \le \infty$, to $(s_1 * s_2) \in L^p(R^n)$.

Jeżeli $s_1 \in L^1(R^n)$ i $s_2 \in C(R^n)$, to $(s_1 * s_2) \in C(R^n)$.

Dla powyższych warunków zachodzą związki:

$$\|s_1 * s_2\|_{L^p} \le \|s_1\|_{L^1} \|s_2\|_{L^p} \,. \tag{17}$$

$$\|s_1 * s_2\|_C \le \|s_1\|_{L^1} \|s_2\|_C \,.$$

Dla $1 \le p \le 2$ zachodzi dodatkowo:

$$\left(s_1 \hat{*} s_2\right)(v) = \hat{s}_1(v) \hat{s}_2(v). \tag{19}$$

3. OPIS SYGNAŁÓW DIAGNOSTYCZNYCH W PRZESTRZENI BERNSTEINA

Przestrzenie Bernsteina są dogodnym narzędziem do opisu problemów przetwarzania analogowo – cyfrowego. Szczególnie są przydatne do opisu procesu próbkowania, gdyż analiza tego problemu znacznie upraszcza się w tych przestrzeniach

Sygnał nazywamy całkowitym, jeżeli jest holomorficzny na zbiorze C.

Sygnał całkowity jest typu wykładniczego jeżeli istnieją dodatnie stałe A i B takie, że

$$|s(z)| \le A e^{B|z|}, \quad z \in C \,. \tag{20}$$

Z sygnałem typu wykładniczego stowarzyszona jest liczba σ, nazywana typem wykładniczym, określona jako:

$$\sigma = \limsup_{r \to \infty} \frac{\log M(r)}{r}, \tag{21}$$

gdzie $M(r)$ oznacza maksymalny moduł sygnału s w okręgu $|z| = r$.

Przez E_σ oznaczamy sygnały całkowite typu wykładniczego mniejszego lub równego σ.

Definicja 1

Przestrzeń Bernsteina B_σ^p ***składa się z sygnałów, które należą do*** E_σ***, a po ograniczeniu do R należą do*** $L^p(R)$***. Normę na*** B_σ^p ***określamy jako normę z*** $L^p(R)$.

Dla sygnałów w przestrzeni Bernsteina zachodzi związek:

$$B_\sigma^1 \subset B_\sigma^p \subset B_\sigma^r \subset B_\sigma^\infty \text{ dla } 1 \le p \le r \le \infty \,. \tag{22}$$

Ponadto, jeśli $\frac{1}{p} + \frac{1}{q} = 1$ oraz $s_1 \in B_\sigma^p$ i $s_2 \in B_\sigma^q$, to $s_1 s_2 \in B_{2\sigma}^1$.

Dla każdego sygnału $s \in B_\sigma^p$, $r \in N$ i $p \ge 1$ zachodzi:

$$\left\|s^{(r)}\right\|_p \le \sigma^r \|s\|_p \,. \tag{23}$$

Nierówność Nikolskiego przyjmie następującą postać: (18)

Niech $1 \le p \le \infty$. *Wtedy dla każdego sygnału* $s \in B_\sigma^p$, i $h > 0$ *mamy:*

$$\|s\|_p \le \sup_{u \in R} \left\{ h \sum_{n \in Z} |s(u - hn)|^p \right\}^{1/p} \le (1 + h\sigma) \|s\|_p \tag{24}$$

Kryterium zwartości w przestrzeni Bernsteina. Niech $1 \le p \le \infty$, i niech (s_n), $n \in N$ będzie ograniczonym w normie ciągiem sygnałów z przestrzeni B_σ^p. Niech C_o będzie zwartym podzbiorem płaszczyzny zespolonej C. Wówczas istnieje podciąg (s_{n_k}) ciągu (s_n), który jest zbieżny jednostajnie na C_o.

Wniosek 2

Przestrzeń Bernsteina jest zupełna, jest więc przestrzenią Banacha.

Dla $\sigma \in R_+^n$ *i* $1 \le p \le \infty$, B_σ^p *będzie przestrzenią sygnałów całkowitych na* C^n*, typu wykładniczego* σ*, spełniających warunek:*

$$|s(z)| \le \|s\|_{C(R^n)} \exp\left\{ \sum_{j=1}^n \sigma_j |y_j| \right\}, \quad (z \in C^n),$$

gdzie:

$$z = (z_1 .....z_n), \quad z_j = x_j + i y_j \,,$$

należą do $L^p(R^n)$.

Dla każdego $h \in R_+^n$ i sygnałów z przestrzeni Bernsteina zachodzi:

$$\|s\|_{L^p} \le \sup_{u\in R^n}\left\{\frac{\prod_{j=1}^{n} h_j}{\left(\sqrt{2\Pi}\right)^n}\sum_{k\in Z^n}|s(u+hk)|^p\right\}^{1/p} \le \prod_{j=1}^{n}\left(1+\sigma_j h_j\right)\|s\|_{L^p},$$

Jest to nierówność Nikolskiego dla przestrzeni C^n.

W przestrzeni B_σ^p, $1 \le p \le 2$, transformata Fouriera określona jest poprzez twierdzenie Paleya – Wienera.

Twierdzenie 3 Twierdzenie Paleya- Wienera

Załóżmy, że $\hat{s} \in L^2(R)$. $\hat{s}$ *jest transformatą Fouriera sygnału s zanikającego na zewnątrz przedziału* $[-\sigma,\sigma]$, *wtedy i tylko wtedy gdy sygnał s po ograniczeniu do R, należy do* E_σ.

Twierdzenie 4

Załóżmy, że $s \in L^p(R^n)$, $1 \le p \le 2$. *Jeżeli jego transformata* $\hat{s}$ *zanika prawie wszędzie na zewnątrz przedziału* $[-\sigma,\sigma]$, *to sygnał s ma rozszerzenie na cały zbiór* C^n *jako element* B_σ^p *i można go zapisać w postaci:*

$$s(t) = \frac{1}{\left(\sqrt{2\Pi}\right)^n}\int_{(-\sigma,\sigma)} \hat{s}(v)e^{ivt}dv, \quad (t \in R^n).$$

(27)

4. OPIS SYGNAŁÓW DIAGNOSTYCZNYCH W PRZESTRZENI PALEYA- WINERA

Niech $m(B)$ oznacza n- wymiarową miarę Lebesguea zbioru $B \subset R^n$, i niech B składa się z M rozłącznych składników B_j, $j = 1,.....M$ takich, że dla każdego j, $0 < m(B_j) < \infty$. Zbiór B jest fizycznie interpretowany jako pasmo sygnału.

Definicja 5

Przestrzeń Paleya - Wienera PW_B *jest zdefiniowana jako*:

$$PW_B := \left\{s : s \in L^2(R^n) \cap C(R^n),\ \operatorname{supp}\hat{s} \subseteq B\right\}$$

(28)

Jeżeli B jest pojedynczym przedziałem $[-\Pi B, \Pi B] \subset R$, to przestrzeń oznaczamy $PW_{\Pi B}$.

Jeżeli zbiór B składa się z więcej niż jednego rozłącznych składników, elementy przestrzeni PW_B nazywamy sygnałem wielopasmowym.

Poniższa definicja określa przestrzeń sygnałów Paleya – Wienera PW_σ^p.

$$\left(\hat{s} \doteq B_\sigma^p\right). \quad (26)$$

Definicja 6 [1]

Dla $\sigma > 0$ *i* $1 \le p \le \infty$ *sygnał* $s(t)$ *należy do przestrzeni Paleya – Wiennera* PW_σ^p, *jeśli można go przedstawić w postaci:*

$$s(r) = \int_{-\sigma}^{\sigma} g(u)e^{izu}du, \qquad (z \in C), \qquad (29)$$

dla $g \in L^p(-\sigma,\sigma)$ *i* $\sigma = \Pi B$.

Przestrzeń PW_σ^p jest podzbiorem E_σ, ponieważ każdy element PW_σ^p jest homologiczny z C, a także ma miejsce związek :

$$|s(z)| \le \int_{-\sigma}^{\sigma} |g(u)|e^{-u\operatorname{Im} z}du \le e^{\sigma|z|}\|g\|_1. \quad (30)$$

Zachodzi inkluzja :

$$PW_\sigma^r \subset PW_\sigma^p,\ r > p \ge 1, \qquad (31)$$

która jest konsekwencją nierówności Höldera.

Odwzorowanie (transformata Fouriera) $F : s \to \hat{s}$ jest ograniczoną liniową transformacją $L^p(R)$ w $L^q(R)$ gdy $1 < p \le 2$.

W szczególności, jeżeli $1 < p \le 2$, to założenie $s \in PW_\sigma^p$ implikuje, $s \in B_\sigma^q$, a więc zachodzi:

$$PW_\sigma^p \subset B_\sigma^q. \qquad (32)$$

Poniższy zestaw twierdzeń daje warunki dostateczne, aby sygnał φ należał do przestrzeni Paleya – Wienera.

Twierdzenie 7 Paleya – Wienera

Jeżeli $s \in L^2(R)$, *to s ma analityczne rozszerzenie do C które należy do* E_σ, *wtedy i tylko wtedy jeżeli* $\operatorname{supp}\hat{s} \subseteq [-\sigma,\sigma]$.

W przypadku gdy $p = q = 2$ *, z powyższego twierdzenia wynika, iż*

$$PW_\sigma^2 \equiv B_\sigma^2. \qquad (33)$$

Twierdzenie 8 [1] Paleya – Wienera (wersja L^P)

1. Jeżeli sygnał s należy do E_σ *a po ograniczeniu do R należy do* $L^p(R)$, $1 < p < 2$, *to istnieje* $\varphi \in L^q(-\sigma,\sigma)$, $q = \frac{p}{p-1}$ *takie, że:*

$$s(z)=\int_{-\sigma}^{\sigma}\varphi(u)e^{iuz}du\,. \tag{34}$$

2.Jeżeli $\varphi\in L^p(-\sigma,\sigma)$, $1<p<2$, *i*

$$s(z)=\int_{-\sigma}^{\sigma}\varphi(u)e^{iuz}du\,,$$

to sygnał s należy do E_σ *a po ograniczeniu do R należy do* $L^p(R)$.

Dla $p>2$ zachodzi relacja:

$$PW_{\Pi B}^{p}\subset PW_{\Pi B}^{2}\,. \tag{35}$$

Twierdzenie 9 Paleya – Wienera (wersja L^1)

Sygnał s należy do E_σ *a po ograniczeniu do R należy do* $L^1(R)$, *wtedy i tylko wtedy gdy można go przedstawić w postaci:*

$$s(z)=\int_{-\sigma}^{\sigma}\varphi(u)e^{iuz}du\,, \tag{36}$$

gdzie $\varphi(\sigma)=\varphi(-\sigma)=0$, *i* φ *rozszerzone na zewnątrz przedziału* $(-\sigma,\sigma)$ *posiada absolutnie zbieżny szereg Fouriera w przedziale* $(-\sigma-\delta,\sigma+\delta)$, $\delta>0$.

Sygnały należące do przestrzeni Paleya – Wienera są pasmowo ograniczone lub dolnopasmowe, początek (zero) zawarte jest w środku przedziału (w środku pasma) przedziału częstotliwości lub czasu. Widmo takiego sygnału jest zawarte w przedziale $[-\Pi B,\Pi B]$.

5. PRÓBKOWANIE SYGNAŁÓW W PRZESTRZENI BERNSTEINA

Podstawą rozważań próbkowania sygnałów w przestrzeni Bernsteina są następujące fakty łączące splot dyskretny ze splotem ciągłym.

Jeżeli $s_1\in B_\sigma^p$ i $s_2\in B_\sigma^q$, $1\le p\le\infty$, oraz q jest sprzężone z p, i $\sigma=\Pi B$, wtedy zachodzi związek*:*

$$\sum_{n\in Z}s_1\left(\frac{n}{B}\right)s_2\left(t-\frac{n}{B}\right)=B\int_R s_1(u)s_2(t-u)du$$

Wobec powyższego można wyciągnąć wniosek, iż splot w przestrzeni Bernsteina jest równy pewnemu splotowi dyskretnemu.

Lemat 10

Niech $s_1\in B_{\Pi B}^p$, $s_2\in B_{\Pi B}^q$, *dla* $B\in R_+^n$, $1\le p\le\infty$, $\dfrac{1}{p}+\dfrac{1}{q}=1$, *wtedy:*

$$(s_1*s_2)(t)=\frac{1}{\left(\sqrt{2\Pi}\right)^n\prod_{j=1}^{n}B_j}\sum_{k\in Z^n}s_1\left(\frac{k}{B}\right)s_2\left(t-\frac{k}{B}\right),\quad \left(t\in R^n\right), \tag{38}$$

jest szeregiem absolutnie i jednostajnie zbieżnym w R^n.

W oparciu o lemat (10) można łatwo udowodnić klasyczne twierdzenie o próbkowaniu Shannona. Niech bowiem $s\in B_{\Pi B}^p$, $1\le p\le\infty$, $\prod_{j=1}^{n}\operatorname{sinc}(k_j)\in B_{\Pi B}^q$, $1<q\le\infty$. Z lematu (20) otrzymamy:

$$\sum_{k\in Z^n}s\left(\frac{k}{B}\right)\prod_{j=1}^{n}\operatorname{sinc}\left(B_j\left(t_j-\frac{k_j}{B_j}\right)\right)=.$$

$$\sum_{k\in Z^n}s\left(t-\frac{k}{B}\right)\prod_{j=1}^{n}\operatorname{sinc}(k_j)=s(t) \tag{39}$$

Twierdzenie. 11 **O próbkowaniu w przestrzeni Bernsteina**

Jeżeli sygnał $s\in B_{\Pi B}^p$, $1\le p\le\infty$, to *możemy go przedstawić w postaci szeregu:*

$$s(t)=\sum_{n\in Z}s\left(\frac{n}{B}\right)\operatorname{sinc}(Bt-n). \tag{40}$$

Szereg ten jest absolutnie i jednostajnie zbieżny na zbiorach zwartych.

W przestrzeni Bernsteina zachodzi

Twierdzenie 12

Dla każdego sygnału $s\in B_{\Pi B}^p$, $1\le p\le\infty$, $r\in N$ *mamy:*

$$s^{(r)}(t)=\sum_{n\in Z}s\left(\frac{n}{B}\right)\left(\frac{d}{dt}\right)^r\operatorname{sinc}(Bt-n). \tag{41}$$

Szereg ten jest absolutnie i jednostajnie zbieżny na zbiorach zwartych.

Powyższe twierdzenie będzie potrzebne do analizy próbkowania za pomocą nieklasycznych jąder.

6. PRÓBKOWANIE W PRZESTRZENI PALEYA – WIENERA

Podstawą analizy próbkowania w przestrzeni $PW_{\Pi B}^p$ jest poniższe twierdzenie:

Twierdzenie 13 **O próbkowaniu w przestrzeni Paleya - Wienera**

Jeżeli $s\in PW_{\Pi B}^p$, $1\le p\le\infty$, *wtedy s można przedstawić w postaci szeregu:*

$$s(t)=\sum_{n\in Z}s\left(\frac{n}{B}\right)\operatorname{sinc}(Bt-n) \tag{42}$$

jednostajnie zbieżnego na zwartych podzbiorach C. Jeżeli $p>1$, *to zbieżność jest absolutna. W przypadku* $p=1$, *zbieżność nie jest absolutna, lecz może być, jeżeli g w definicji (15) należy do* $\Re eH^1$.

Przestrzeń Hardy'ego H^1 stanowią sygnały s analityczne w dysku jednostkowym $D=\{z\in C:|z|<1\}$, dla których:

$$\sup_{0\le r<1}\int_{-\Pi}^{\Pi}\left|s\left(re^{j\theta}\right)\right|d\theta<\infty. \qquad (43)$$

Przestrzeń $\Re eH^1$ jest ograniczoną do części rzeczywistej przestrzenią H^1, innymi słowy, jeżeli $s\in H^1$, wtedy

$$s(\theta)=\lim_{\substack{r\to 1\\ r<1}}\Re es\left(re^{j\theta}\right), \qquad (44)$$

należy do $\Re eH^1$.
Zachodzi relacja :

$$L^p(-\Pi,\Pi)\subset \Re eH^1\subset L^1(-\Pi,\Pi). \qquad (45)$$

Poniżej zostały przedstawione własności przestrzeni Paleya – Wienera, szczególnie przydatne w teorii próbkowania sygnałów

1. Przestrzeń Paleya – Wienera $PW_{\Pi B}$ jest przestrzenią Hilberta z reprodukującym jądrem równym:
$$B\operatorname{sinc}B(s-t),\ (s,t)\in R\times R. \qquad (46)$$
Sygnał $s\in PW_{\Pi B}$ można zapisać w postaci :
$$s(t)=\int_R s\left(\frac{v}{B}\right)\operatorname{sinc}(Bt-v)dv \qquad (47)$$
2. Jeżeli $s\in PW_{\Pi B}$, to zachodzi:
$$s(t)=\frac{2}{\sqrt{2\Pi}}\int_{-\Pi B}^{\Pi B}\hat{s}(x)e^{ixt}dx.$$
Sygnał s jest ograniczony do R, i $s(t)\to 0$ gdy $t\to\pm\infty$.
3. Zbiór $\left\{\sqrt{B}\operatorname{sinc}(Bt-n)\right\}$, $n\in Z$, jest ortonormalną bazą dla $PW_{\Pi B}$, przy czym n – ty współczynnik szeregu Fouriera wynosi:
$$c_c=\left(\frac{1}{\sqrt{B}}\right)s\left(\frac{n}{B}\right).$$
Poniższy szereg dla $s\in PW_{\Pi B}$ jest szeregiem ortogonalnym
$$s(t)=\sum_{n\in Z}s\left(\frac{n}{B}\right)\operatorname{sinc}(Bt-v),$$
który jest zbieżny w normie $PW_{\Pi B}$ absolutnie i jednostajnie na całym R.
4. Zależność Parsevala dla $s\in PW_{\Pi B}$ przyjmuje postać:
$$\|s\|^2=\frac{1}{B}\sum_{n\in Z}\left|s\left(\frac{n}{B}\right)\right|^2.$$

Opis procesu próbkowania w oparciu o przestrzenie Paleya – Wienera czyni klasyczną teorię Shannona – Nyquista bardziej przejrzystą.

BIBLIOGRAFIA

[1] Higgins J. R.: *Sampling Theory in Fourier and Signal Analysis* - Foundations. Clarendon Press, Oxford 1996.
[2] Kufner A., Kadlec J.: *Fourier Series*, Academia Prague 1971.
[3] Lieb E. H., Loss M.: *Analysis, Graduate Studies in Mathematics*, American Mathenatical Society, 1998.
[4] Stein E. M., Weiss G.: *Fourier Analysis on Euclidean Spaces*. Princeton University Press 1971.
[5] Syroka Z.: *Próbkowanie sygnałów diagnostycznych. Cz. I. Próbkowanie w przestrzeni Hilberta z reprodukującym jądrem Shanona.* Diagnostyka Nr 2(42)/2007,s. 19-26.
[6] Syroka Z:. *Próbkowanie sygnałów diagnostycznych. Cz. II. Próbkowanie w przestrzeni Hilberta z bazami harmonicznymi za pomocą nieklasycznych jąder.* Diagnostyka Nr 2(42)/2007, s. 27-34.
[7] Syroka Z.: *Próbkowanie sygnałów diagnostycznych. Cz. III. Próbkowanie w przestrzeni Hilberta z bazami wielomianowymi za pomocą nieklasycznych jąder.* Diagnostyka Nr 2 (42)/2007, s. 35-41.

Nadanie "Medalu im. Profesora Stefana Ziemby"
Prof. dr. hab. inż. Wojciechowi CHOLEWIE

W imieniu członków Zespołu Diagnostyki Sekcji Podstaw Eksploatacji Komitetu Budowy Maszyn PAN, a także bardzo licznej grupy uczniów, przyjaciół i współpracowników, oraz członków Zarządu Polskiego Towarzystwa Diagnostyki Technicznej, **zawnioskowałem o nadanie Medalu im. Prof. Ziemby Panu Profesorowi Wojciechowi Cholewie za całokształt Jego dorobku w zakresie wprowadzenia do dziedziny budowy i eksploatacji maszyn metod i technik sztucznej inteligencji, co znalazło szczególny wyraz w opublikowaniu w roku 2008 serii monografii pt.:**

1. **W. Cholewa, T. Rogala, „Modele odwrotne i modelowanie diagnostyczne", Zeszyty Naukowe Katedry Podstaw Konstrukcji Maszyn, Zeszyt 136 (73 s.), Gliwice 2008.**
2. **W. Cholewa (red.), „Szkieletowy System Doradczy DIADYN", Zeszyty Naukowe Katedry Podstaw Konstrukcji Maszyn, Zeszyt 137 (158 s.), Gliwice 2008.**
3. **W. Cholewa, K. T. Kosmowski, S. Radkowski (red.), „Modele systemów oceny ryzyka i diagnostyki technicznej", Zeszyty Naukowe Katedry Podstaw Konstrukcji Maszyn, Zeszyt 138 (177 s.), Gliwice 2008.**

Wojciech CHOLEWA, profesor zwyczajny, dr hab. inż., od ukończenia studiów w r. 1971 nieprzerwanie pracuje na Politechnice Śląskiej w Gliwicach. Jest absolwentem Wydziału Mechanicznego Energetycznego Politechniki Śląskiej. Działalność naukowo-dydaktyczną rozpoczął w r.1971. Przeszedł kolejno wszystkie stanowiska aż do stanowiska profesora zwyczajnego, które objął w r. 1995. **Jest autorem lub współautorem ponad 250 publikacji naukowych i naukowo-technicznych, w tym ponad 15 monografii i podręczników.** Szczególne znaczenie mają monografie: „Metoda diagnozowania maszyn z zastosowaniem zbiorów rozmytych" (1983), „Diagnostyka procesów. Metody, modele sztucznej inteligencji, zastosowania" (2002). Wypromował ok. 150 magistrów inżynierów mechaników, był promotorem 16 prac doktorskich, recenzował wiele rozpraw doktorskich, ponad 15 rozpraw habilitacyjnych i ponad 10 wniosków na tytuł profesora. Kilku Jego wychowanków uzyskało stopień doktora habilitowanego oraz tytuł profesora.

Profesor Cholewa pełnił i pełni wiele odpowiedzialnych funkcji, wśród których należy wymienić: zastępcę dyrektora Instytutu Podstaw Konstrukcji Maszyn, kierownika Katedry Podstaw Konstrukcji Maszyn Wydziału Mechanicznego Technologicznego Politechniki Śląskiej, dziekana Wydziału Mechanicznego Technologicznego (2 kadencje), prorektora Politechniki Śląskiej ds. Organizacji i Rozwoju (2 kadencje), członka Senatu Politechniki Śląskiej przez wiele kadencji, członka Komitetu Budowy Maszyn PAN, członka Zarządu Polskiego Towarzystwa Diagnostyki Technicznej (przez dwie kadencje) i wiele innych.

Profesor Cholewa wielokrotnie organizował krajowe i międzynarodowe sympozja i konferencje naukowe. Był współorganizatorem I Kongresu Diagnostyki Technicznej w Gdańsku w 1996r. Jest współtwórcą Sympozjów AI-MECH/AI-METH zastosowań metod sztucznej inteligencji. Jest powoływany do komitetów naukowych wielu konferencji z zakresu podstaw konstrukcji maszyn, sztucznej inteligencji, diagnostyki technicznej maszyn i procesów. Współpracował i współpracuje z wieloma ośrodkami naukowymi całego świata.

Prof. Cholewa bierze udział w pracach redakcyjnych czasopism naukowych. Jest członkiem Rady Redakcyjnej Mechanical Systems and Signal Processing (Elsevier), członkiem Rady Naukowej czasopisma „Diagnostyka" i wielu innych.

Prof. W. Cholewa ma duże zasługi w tworzeniu zaplecza naukowo-badawczego. Był inicjatorem i organizatorem budowy Laboratorium Badań Wibroakustycznych Instytutu Mechaniki i Podstaw Konstrukcji Maszyn Politechniki Śląskiej w Gliwicach. Jest współzałożycielem Centrum Doskonałości AI-METH Zastosowań Metod Sztucznej Inteligencji. Działalność naukowa przyniosła mu uznanie w postaci członkostwa w organizacjach i instytucjach naukowych m.in. Akademii Inżynierskiej w Polsce.

Twórcze dokonania Profesora W. Cholewy obejmują następujące działy dyscypliny „Budowa i eksploatacja maszyn": podstawy konstrukcji maszyn, komputerowe wspomaganie projektowania, eksploatacja maszyn, diagnostyka techniczna maszyn i procesów, a także dyscypliny „Automatyka

i Robotyka”, zwłaszcza w zakresie pomiaru, przetwarzania i analizy sygnałów oraz rozwoju zintegrowanych i rozproszonych systemów pomiarowych i diagnostycznych, a także z dyscypliny „Informatyka”, zwłaszcza zagadnienia związane z rozwojem systemów programów diagnostycznych, systemów baz danych i zastosowań sztucznej inteligencji. Inicjatywa i prace W. Cholewy zapoczątkowały z początkiem lat osiemdziesiątych ubiegłego stulecia wprowadzanie do diagnostyki technicznej nowoczesnych metod sztucznej inteligencji oraz szeroko rozumianej informatyki. Profesor Cholewa jest autorem pojęcia „System doradczy”, który odpowiada angielskiemu „Expert system”. Zaprojektował, kierował wdrożeniami i osobiście uczestniczył w budowie wielu systemów diagnostycznych, począwszy od Programowanych Analizatorów Sygnałów (PAS-3 do PAS-7), poprzez diagnostyczny system doradczy DT-200 (wdrożony na bloku nr 7 Elektrowni Kozienice), system K-015 bazujący na zastosowaniu sieci przekonań, system Diadyn diagnostyki maszyn krytycznych. Obecnie Profesor kieruje zespołem wykonującym moduły systemu DiaSter diagnostyki i sterowania procesów. Wszystkie wymienione powyżej działy wchodzą w zakres dyscypliny „Budowa i eksploatacja maszyn”.

Profesor Wojciech Cholewa jest autorem wielu metod, koncepcji i systemów, które zostały skutecznie wdrożone w zakresie diagnostyki maszyn i procesów. Wprowadził metody zbiorów rozmytych do diagnostyki technicznej. Wprowadził do diagnostyki technicznej i spopularyzował systemy doradcze oraz inżynierię wiedzy. Jest głównym autorem koncepcji i projektu Systemu DT-200 diagnostyki turbozespołów energetycznych 200 MW, który stanowił jeden z przełomowych projektów wdrożeniowych w zakresie diagnostyki technicznej w latach 1995-98. Jest autorem koncepcji modeli odwrotnych, które znalazły zastosowanie w diagnostyce maszyn krytycznych. Od kilku lat propaguje zastosowanie sieci przekonań (Bayesa) w diagnostyce technicznej, np. do diagnozowania reaktorów jądrowych (wspólne prace z Królewskim Instytutem Technologicznym w Sztokholmie). Ze względu na posiadaną przez siebie bardzo szeroką wiedzę jest zapraszany do recenzowania wielu prac naukowych i projektów. Jest uczestnikiem wielu opiniotwórczych gremiów, które inicjują nowe trendy w dziedzinie diagnostyki technicznej maszyn i procesów. Jego prace mają charakter integrujący obie gałęzie diagnostyki – diagnostykę maszyn i diagnostykę procesów. Dowodem na docenienie Jego szczególnej roli w zakresie integracji obu tych gałęzi było zaproszenie Go przez J. Korbicza, J. M. Kościelnego i Z. Kowalczuka do współredagowania fundamentalnej monografii „Diagnostyka procesów. Modele, metody sztucznej inteligencji, zastosowania” (WNT Warszawa, 2002), a potem do współredagowania angielskojęzycznej wersji tej monografii pt. „*Fault Diagnosis. Models, Artificial Intelligence, Applications”* (Berlin Heidelberg: Springer -Verlag, 2004).

Nadanie medalu Prof. S. Ziemby Panu Profesorowi Wojciechowi Cholewie jest realizacją życzenia całego środowiska naukowego i praktyków zajmujących się diagnostyką techniczną maszyn i procesów, środowiska, którego Profesor jest jednym z najwybitniejszych Twórców, a także wybitnym członkiem.

Prof. Wojciech Moczulski
Zespół Diagnostyki
Sekcja Podstaw Eksploatacji
Komitet Budowy Maszyn PAN

IX Międzynarodowa Konferencja Naukowo-Techniczna *Diagnostyka Procesów i Systemów DPS'2009* Gdańsk-Jelitkowo

W dniach 7-9 września 2009 roku odbyła się w Gdańsku Jelitkowie na terenie Dworu Prawdzica *dziewiąta Międzynarodowa Konferencja Naukowo-Techniczna Diagnostyka Procesów i Systemów DPS'2009*, która ma już trzynastoletnią tradycję. Konferencja organizowana jest cyklicznie począwszy od 1996 roku przez trzy ośrodki akademickie Politechnikę Gdańską (Wydział Elektroniki Telekomunikacji i Informatyki), Politechnikę Warszawską (Instytut Automatyki i Robotyki) oraz Uniwersytet Zielonogórski (Instytut Sterowania i Systemów Informatycznych). Były to początkowo coroczne zjazdy naukowe, które od 1999 roku odbywają się w cyklu dwuletnim.

Niniejsza konferencja stanowiła IX edycję Konferencji, która początkowo nosiła nazwę „Diagnostyka Procesów Przemysłowych". Począwszy od roku 2007 zakres tematyczny Konferencji rozszerzono i zmieniono jej tytułu na „Diagnostyka Procesów i Systemów".

Patronat nad konferencją w Gdańsku objął **Komitet Automatyki i Robotyki Polskiej Akademii Nauk**, **Komitet Automatyki Polskiego Stowarzyszenia Pomiarów Automatyki i Robotyki (PolSPAR)**, oraz **Towarzystwo Konsultantów Polskich**. Bezpośrednim patronat nad konferencją roztoczył J.M. Rektor Politechniki Gdańskiej prof. dr hab. inż. Henryk Krawczyk.

Nad jakością recenzowanych i prezentowanych prac sprawował pieczę Międzynarodowy Komitet Naukowy złożony z 75 profesorów: Zdzisław Kowalczuk, (Przewodniczący) Józef Korbicz, Jan Maciej Kościelny (Współprzewodniczący), oraz Stanisław Bańka (Szczecin, PL), Michele Basseville (Rennes, F), Morgens Blanke (Lyngby, DK), Piotr Bielawski (Szczecin, PL), Mieczysław Brdyś (Birmingham, UK), Liliana Byczkowska-Lipińska (Łódź, PL), Eduardo Camacho (Sevilla, ESP), Wojciech Cholewa (Gliwice, PL), Fahmida N. Chowdhury (Lafayette, US), Steven Ding (Duisburg, D), Jan Duda (Kraków, PL), Andrzej Dyka (Gdańsk, PL), Andras Edelmayer (Budapest, H), Sylviane Gentil (Grenoble, F), Janos Gertler (Fairfax, US), Krzysztof Janiszowski (Warszawa, PL), Wojciech Jędruch (Gdańsk, PL), Ireneusz Jóźwiak (Wrocław, PL), Andrzej Kasiński (Poznań, PL), Jacek Kluska (Rzeszów, PL), Edward Jezierski (Łódź, PL), Witold Kosiński (Warszawa, PL), Kazimierz Kosmowski (Gdańsk, PL), Krzysztof Kozłowski (Poznań, PL), Andrzej Królikowski (Poznań, PL), Marek Kurzyński (Wrocław, PL), Jerzy Kurek (Warszawa, PL), Piotr Kulczycki (Warszawa, PL), Antoni Ligęza (Kraków, PL), Jan Lunze (Bochum, D), Jan M. Maciejowski (Cambrigde, UK), Krzysztof Malinowski (Warszawa, PL), Andre Manitius (Fairfax, US), Wojciech Moczulski (Gliwice, PL), Henrik Niemann (Lyngby, DK), Mariusz Nieniewski (Warszawa, PL), Cezary Orłowski (Gdańsk, PL), Romeo Ortega (Gif, F), Ronald J. Patton (Hull, UK), Witold Pedrycz (Edmonton, CDN), Andrzej Pieczyński (Zielona Góra, PL), Marios Polycarpou (Cincinnati, US), Vicenc Puig (Barcelona, ESP), Stanisław Radkowski (Warszawa, PL), Ewaryst Rafajłowicz (Wrocław, PL), Ryszard Rojek (Opole, PL), Leszek Rutkowski (Częstochowa, PL), Jose Sá da Costa (Lisbon, P), Dominique Sauter (Nancy, F), Alexey Shumsky (Vladivostok, RUS), Sivio Simani (Ferrara, I), Jan Sokołowski (Nancy, F), Janusz Sosnowski (Warszawa, PL), Marcel Staroswiecki (Lille, F), Jakob Stoustrup (Aalborg, DK), Piotr Szczepaniak (Łódź, PL), Andrzej Świerniak (Gliwice, PL), Roman Śmierzchalski (Gdynia, PL), Mirosław Świercz (Białystok, PL), Ryszard Tadeusiewicz (Kraków, PL), Piotr Tatjewski (Warszawa, PL), Krzysztof Tchoń (Wrocław, PL), Didier Theilliol (Nancy, F), Leszek Trybus (Rzeszów, PL), Dariusz Uciński (Zielona Góra, PL), Tadeusz Uhl (Kraków, PL), Wiesław Wajs (Kraków, PL), Bogdan Wiszniewski (Gdańsk, PL), Marcin Witczak (Zielona Góra, PL), Marian Wysocki (Rzeszów, PL), Marek Zaremba (Hull, CDN), Youmin Zhang (Montreal, CDN), Jacek M. Żurada (Louisville, US).

Naukowcy ci specjalizują się w różnych dziedzinach teorii i zastosowań diagnostyki, reprezentując uczelnie techniczne z 11 krajów świata. Lokalnym organizatorem konferencji była Politechnika Gdańska, Wydział Elektroniki Telekomunikacji i Informatyki oraz Towarzystwo Konsultantów Polskich Oddział Gdańsk. Współprzewodniczącymi Komitetu Organizacyjnego byli dr inż. H. Kormański i dr P. Raczyński z Wydziału ETI Politechniki Gdańskiej.

Konferencja DPS, zbliżona tematycznie do serii międzynarodowych sympozjów nt. „Fault Detection, Supervision and Safety for Technical Processes – SAFEPROCESS" organizowanych pod auspicjami IFAC, skupia się zatem na rozwiązywaniu naukowych i technicznych problemów związanych z diagnostyką procesów przemysłowych opartą na matematycznych i inżynierskich metodach i technikach. W obecnej postaci realizuje zadanie międzynarodowego forum wymiany informacji naukowej i technicznej w kraju oraz doświadczeń inżynierskich w zakresie diagnostyki, która znajduje się na styku automatyki, pomiarów i przetwarzania sygnałów, oraz sieci komputerowych, zwłaszcza tam, gdzie stosuje się matematyczne teorie oraz narzędzia modelowania i identyfikacji, informatyki i sztucznej inteligencji.

Głównym celem konferencji jest połączenie tych dziedzin systemowej i inżynierskiej wiedzy dla szeroko pojmowanej diagnostyki i jej praktycznych zastosowań, w tym detekcji, izolacji, lokalizacji,

identyfikacji, diagnozy, rekonfiguracji i sterowania. Zadaniem tego forum było również umożliwienie efektywnej integracji środowisk naukowych z inżynierami, technologami pracującymi w różnych gałęziach przemysłu i usług (energetyki, chemii, przemysłu maszynowego, spożywczego, medycyny, biotechnologii, ochrony środowiska, etc.), jak również z producentami sprzętu i oprogramowania komputerowych systemów sterowania i diagnostyki.

Konferencji DPS Gdańsk'2009 zgromadziła 113 uczestników, którzy w trakcie trzech dni obrad wysłuchali 68 referatów. Szczególną wartość stanowiło sześć niżej wymienionych referatów plenarnych wygłoszonych przez zaproszonych gości:

- Michele Basseville (IRISA/CNRS, Rennes), "On statistical change detection for FDI"
- Eduardo F. Camacho (Universidad de Sevilla), "Fault tolerant model predictive control"
- Steven X. Ding (University of Duisburg-Essen) "Integrated design of wireless fault tolerant networked control systems"
- Jan Maciejowski (Cambridge University) "Fault tolerant control - is it possible?"
- Jakob Stoustrup (Aalborg University) "Fault diagnosis and fault tolerant control - an optimization based approach"
- Antoni Nowakowski (Gdansk University of Technology) "Advances of thermal IR-diagnostics in medicine".

Pozostałe referaty skupiały się wokół takich tematów jak: modelowanie oraz symulacja uszkodzeń i relacji symptomy-uszkodzenia; metody detekcji i lokalizacji uszkodzeń oparte na różnych technikach i narzędziach modelowania; systemy diagnostyczne i ich zastosowania praktyczne w różnych dziedzinach gospodarki; oraz problemy bezpieczeństwa procesów przemysłowych, kontroli jakości, niezawodności oprogramowania i inne.

Organizatorzy dołożyli wszelkich starań, aby zapewnić sprawny i atrakcyjny przebieg konferencji, a specjalną wagę przyłożyli do udziału młodych kadr naukowych, zwłaszcza doktorantów, którym uzyskali starano się zapewnić jak najbardziej sprzyjającą atmosferę.

W kuluarowych opiniach uczestników DPS widać było bardzo wysoką ocenę konferencji i jej kształtu. Szczególnym zainteresowaniem cieszyły się wykłady plenarne oraz zagadnienia związane z metodologią diagnostyki, systemami doradczymi, oraz zastosowaniami metod sztucznej inteligencji. Według uczestników DPS'2009 warto poszerzać tematykę konferencji na inne obszary diagnostyki (np. medycynę i informatykę).

Zbiór referatów konferencyjnych, w postaci dwóch książek grupujących osobno referaty w języku angielskim i w języku polskim liczący łącznie prawie **700** strony został wydany pod redakcją prof. Z. Kowalczuka w postaci książek „**Systemy wykrywające, analizujące i tolerujące usterki**" ISBN 978-83-926806-2-8 oraz „**Diagnosis of Processes and Systems**" ISBN 978-83-926806-3-5 przez Pomorskie Wydawnictwo Naukowo-Techniczne (http://www.konsulting.gda.pl/pwnt) w Gdańsku.

Dla skupienia uwagi Czytelnika zawartość merytoryczna pierwszej książki została podzielona na osiem sekcji: modelowanie i sterowanie; diagnostyka przemysłowa; modelowanie diagnostyczne; decyzje diagnostyczne; monitoring przemysłowy; technologie informacyjne, zastosowania diagnostyki; systemy przemysłowe.

W drugiej książce zawarta jest część plenarna (fault diagnosis and fault-tolerant control) oraz pięć sekcji technicznych (fault-tolerant control systems; estimation and identification methods; optimal and active sensor designs; fault diagnosis of industrial processes; soft computing approaches).

Obie książki (dostępne pod internetowym adresem: http://konsulting.gda.pl/pwnt) powinny zainteresować inżynierów i technologów, jak również naukowców i pracowników instytucji naukowych, którzy pragną pogłębiać zagadnienia niezawodności i detekcji błędów w systemach i procesach przemysłowych, zwłaszcza tych krytycznych pod względem bezpieczeństwa.

Pamiątkowe zdjęcie uczestników Konferencji DPS'2009 w Gdańsku na tle sterowca „SCIenter" (Politechnika Gdańska, WETI-KSD).

Pozostałe informacje oraz zdjęcia (fot. M. Domżalski) z przebiegu konferencji można obejrzeć na stronie domowej Konferencji: http://www.konsulting.gda.pl/dps09.

prof. dr hab. inż.
Zdzisław Kowalczuk
Przewodniczący IX MKNT DPS'2009

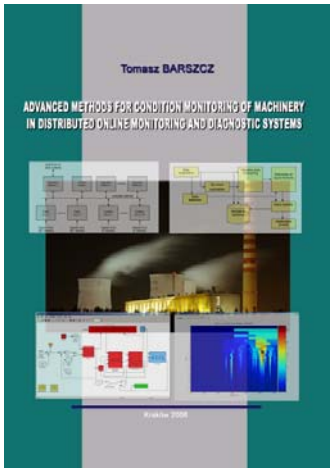

Informacja o rozprawie habilitacyjnej Tomasza BARSZCZA pt. „Advanced methods for condition monitoring of machinery in distributed online monitoring and diagnostic systems" („Zaawansowane metody oceny stanu maszyn w rozproszonych systemach ciągłego monitorowania i diagnostyki")

Zasadniczą tematyką rozprawy habilitacyjnej są architektury rozproszonych systemów ciągłego monitorowania i diagnostyki oraz metody oceny stanu dostosowane do tych architektur. W pierwszych częściach pracy przeprowadzono analizę stanu rozwoju maszyn, na przykładzie maszyn energetycznych: bloku parowo – gazowego, turbiny wiatrowej i nowoczesnego bloku parowego. W dalszej kolejności przedstawiono bieżący stan wiedzy w dziedzinie. W rozprawie przedstawiono bieżący stan kluczowych technologii z zakresu systemów monitorowania i diagnostyki. Fundamentalne problemy badawcze przedstawione w rozprawie to:

- opracowanie rozproszonej i otwartej architektury systemu
- opracowanie metod diagnostyki maszyn, dostosowanych do zaproponowanej architektury
- demonstracja słuszności podejścia na dużej instalacji (Wirtualna Elektrownia)

W książce przedstawiono prace badawcze, które koncentrowały się nie na propozycji podziału zadań pomiędzy komponenty sprzętowe i programowe oraz na badaniach i propozycji technologii wymiany i przechowywania danych. W rezultacie opracowano szczegółowe specyfikacje i projekty poszczególnych komponentów systemu.

Opracowane algorytmy diagnostyczne prezentują możliwości zastosowań algorytmów z różnych grup. Dla każdej z metod przedstawiono algorytm, warunki jego stosowalności oraz sposób integracji z zaproponowaną architekturą systemu. Szczególnym osiągnięciem jest Wirtualna Elektrownia, w której zastosowano zaproponowaną rozproszoną architekturę do zamodelowania elementów całego bloku energetycznego. Opracowano architekturę rozwiązania, która posiada szczególną cechę dwóch baz danych oraz dwóch interfejsów użytkownika, dzięki czemu możliwe jest zastosowanie rozwiązania do zaawansowanych analiz diagnostycznych oraz do szkolenia operatorów i analiz bieżących danych. Ważnym osiągnięciem jest też możliwość stosowania wariantowych modeli komponentów bloku energetycznego.

Należy podkreślić, że opracowane metody zostały zaimplementowane i zweryfikowane w praktyce na kilkuset instalacjach pracujących w wielu krajach. Większość przedstawionych metod została wdrożona do systemów monitorowania i diagnostyki. Doświadczenia zebrane podczas prac badawczych i doświadczeń eksploatacyjnych potwierdziło poprawność przyjętych rozwiązań. Otrzymane i zaprezentowane wyniki są ważne zarówno z naukowego, jak i praktycznego punktu widzenia.

Z uwagi na szeroki zakres problematyki poruszanej w rozprawie, równie szeroki jest zakres potencjalnych dalszych badań. Najistotniejsze z nich to: analiza i adaptacja nowych technologii informacyjnych do systemów monitorowania i diagnostyki oraz zautomatyzowane metody analizy danych zbieranych przez tzw. centra diagnostyczne.

Diagnostyka

Obszar zainteresowania czasopisma to:
- ogólna teoria diagnostyki technicznej
- eksperymentalne badania diagnostyczne procesów i obiektów technicznych;
- modele analityczne, symptomowe, symulacyjne obiektów technicznych;
- algorytmy, metody i urządzenia diagnozowania, prognozowania i genezowania stanów obiektów technicznych;
- metody detekcji, lokalizacji i identyfikacji uszkodzeń obiektów technicznych;
- sztuczna inteligencja w diagnostyce: sieci neuronowe, systemy rozmyte, algorytmy genetyczne, systemy ekspertowe;
- diagnostyka energetyczna systemów technicznych;
- diagnostyka systemów mechatronicznych i antropotechnicznych;
- diagnostyka procesów przemysłowych;
- diagnostyczne systemy utrzymania ruchu maszyn;
- ekonomiczne aspekty zastosowania diagnostyki technicznej;
- analiza i przetwarzanie sygnałów.

Topics discussed in the journal:
- General theory of the technical diagnostics,
- Experimental diagnostic research of processes, objects and systems,
- Analytical, symptom and simulation models of technical objects,
- Algorithms, methods and devices for diagnosing, prognosis and genesis of condition of technical objects,
- Methods for detection, localization and identification of damages of technical objects,
- Artificial intelligence in diagnostics, neural nets, fuzzy systems, genetic algorithms, expert systems,
- Power energy diagnostics of technical systems,
- Diagnostics of mechatronic and antropotechnic systems,
- Diagnostics of industrial processes,
- Diagnostic systems of machine maintenance,
- Economic aspects of technical diagnostics,
- Analysis and signal processing.

Wszystkie opublikowane artykuły uzyskały pozytywne recenzje wykonane przez niezależnych recenzentów.

All the published papers were reviewed positively by the independent reviewers.

Druk:
Centrum Graficzne „GRYF”, ul. Pieniężnego 13/2, 10-003 Olsztyn, tel. / fax: 089–527–24–30

Oprawa:
Zakład Poligraficzny, UWM Olsztyn, ul. Heweliusza 3, 10-724 Olsztyn
tel. 089-523-45-06, fax: 089-523-47-37

IMEKO TC
11th Workshop on Smart Diagnostics of Structures, Kraków, Poland

Kraków, October 18-20, 2010

Sponsors:

International Measurement Confederation

The Polish Academy of Science Committee on Machine Building

POLISH ASSOCIATION OF DIAGNOSTIC ENGINEERING

University of Science and Technology- AGH, Kraków, Poland

www.innowacjapolska.pl

Wszystkie opublikowane w czasopiśmie artykuły uzyskały pozytywne recenzje, wykonane przez niezależnych recenzentów.
Redakcja zastrzega sobie prawo korekty nadesłanych artykułów.
Kolejność umieszczenia prac w czasopiśmie zależy od terminu ich nadesłania i otrzymania ostatecznej, pozytywnej recenzji.
Wytyczne do publikowania w DIAGNOSTYCE można znaleźć na stronie internetowej:
http://www.uwm.edu.pl/wnt/diagnostyka

Redakcja informuje, że istnieje możliwość zamieszczania w DIAGNOSTYCE ogłoszeń i reklam.
Jednocześnie prosimy czytelników o nadsyłanie uwag i propozycji dotyczących formy i treści naszego czasopisma.
Zachęcamy również wszystkich do czynnego udziału w jego kształtowaniu poprzez nadsyłanie własnych opracowań związanych z problematyką diagnostyki technicznej. Zwracamy się z prośbą o nadsyłanie informacji o wydanych własnych pracach nt. diagnostyki technicznej oraz innych pracach wartych przeczytania, dostępnych zarówno w kraju jak i zagranicą.